九州大学学術情報リポジトリ
Kyushu University Institutional Repository

Shallow crack effect in residual tensile strength evaluation of finite-sized structures made of ductile materials

劉, 何

https://hdl.handle.net/2324/4110414

出版情報：Kyushu University, 2020, 博士（工学）, 課程博士
バージョン：
権利関係：

Shallow crack effect in residual tensile strength evaluation of finite-sized structures made of ductile materials

A dissertation submitted to

Graduate School of Engineering, Kyushu University, Japan

for the degree of Doctor of Philosophy in Hydrogen Energy System

Presented by

LIU HE

April 2020

Index

Abstract

Residual strength, which reflects the practical load-carrying capacity of pre-damaged structures, is a critical concern in fail-safe design. As a representative case of local stress intensifiers, pre-existing cracks (pre-cracks) in engineering structures have attracted the most attention of residual strength investigations. Conventionally, residual strength issues of pre-cracked structures are solved by fracture mechanics with a presumption of the unstable crack propagation dominating the loss of load-carrying capacity. That is, fracture instability characterized by fracture instability toughness is regarded as the physical meaning of residual strength. With the joint efforts of mechanical and material researchers, however, the pre-cracks are becoming mechanically shallower, and the materials are becoming stronger and tougher, resulting in an extremely high fracture instability toughness that makes the unstable crack propagation hardly occur. Hence, as plasticity develops with loading, if plastic instability, such as the necking, instead of fracture instability dominating residual strength of shallow pre-cracked structures, most previous studies probably become invalid.

Moreover, the plastic instability dominating residual strength can challenge the general viewpoint of engineering that cracks weaken structures. First, as an extreme case of the notch that the notch root radius approaches to zero, crack is widely considered to have no strengthening effect, such as notch strengthening, because unstable crack propagation is believed to occur at low stress. However, this situation will be changed if plastic instability can dominate the residual strength of shallow pre-cracked structures because plastic strain localization induced by crack can resist the general yielding and plastic instability. Second, the extremely high fracture toughness of shallow cracks may make the factors that can enhance the plastic strain localization in the pre-cracked cross-section favorable for residual strength, such as the increase of pre-crack depth within a certain range or the change in the plasticity property of the material. These assumptions are necessary to be verified due to the insufficient investigation of residual strength in the presence of shallow pre-cracks.

Based on the above, this dissertation focused on the residual tensile strength of shallow pre-cracked structure made of interstitial-free (IF) steel. In order to guarantee the symmetry of pre-crack

shape, measurability of pre-crack depth and constrained pre-strain in specimen, the shallow crack-like notch was adopted, and the identification criterion of shallow crack-like notches in the case of plastic instability prevailing was proposed initially. Then, the trends, physical meanings, and corresponding damage characteristics of residual strength responding to the pre-crack depth were clarified. Meanwhile, the concept of shallow crack was redefined for residual strength issues, and the mechanism of shallow crack effect on residual strength was explained by analyzing whether the plastic strain localization induced by pre-crack positively or negatively affects the load-carrying abilities in different imaginary partitions of pre-cracked cross-sections. After that, the qualitative and quantitative predictions of the residual strength in the presence of shallow cracks were preliminarily explored. Qualitative prediction focused on the trend analysis of residual strength from the perspective of plastic strain localization, while quantitative prediction focused on the necessary considerations for correctly predicting residual strength values and corresponding damage characteristics. Eventually, the concept of shallow cark effect was applied to the hydrogen environment, in which the magnitude of plastic strain localization can be dramatically raised. Aforementioned work extent residual strength theory into the field of shallow cracks.

In addition, the redefinition of shallow crack for residual strength issue, a novel failure-assessment diagram, and the subdivision of hydrogen-embrittlement susceptibilities in this study were expected to help identify and analyze the shallow crack effect in practical applications related to residual strength.

List of abbreviations

EBSD	Electron backscatter diffraction
EPFM	Elastic-plastic fracture mechanics
FAD	Failure assessment diagram
FEA	Finite element analysis
FSY	Full-scale yielding
HAC	Hydrogen-assisted cracking
HE	Hydrogen embrittlement
HEDE	Hydrogen-enhanced decohesion
HELP	Hydrogen-enhanced localized plasticity
KAM	Kernel average misorientation
LEFM	Linear elastic fracture mechanics
LSY	Large-scale yielding
SEM	Scanning electron microscope
SSY	Small-scale yielding
MSC	Material selection chart
UTS	Ultimate tensile strength

Nomenclature

A^{int}	Initial area of intact cross-section	α	Notch opening angle
A^{net}	Initial area of net cross-section reduced by the presence of notch/crack	ε_e, ε_t	Engineering and true strain
E	Young's modulus	ε_{ij}^{p}	Plastic strain tensor
e_{ij}^{p}	Plastic strain deviator tensor	ε_{ii}^{pl}: ε_{xx}^{pl}, ε_{yy}^{pl}, ε_{zz}^{pl}	Normal coordinate plastic strains (x, y-direction) and tangential (z-direction) plastic strain
H	Gage length	$\bar{\varepsilon}_{ii}^{pl}$: $\bar{\varepsilon}_{xx}^{pl}$, $\bar{\varepsilon}_{yy}^{pl}$, $\bar{\varepsilon}_{zz}^{pl}$	Uniform (averaged) normal coordinate plastic strains (x, y-direction) and tangential (z-direction) plastic strain
K_{t}	Stress concentration factor	η	Stress triaxiality
k	Yield stress in pure shear	λ	Elongation in gage length
l	Ligament size of notch/pre-cracked cross-section	π	Circumference ratio
P	Applied load	ρ	Notch root radius
r	Radius of intact cross-section	σ_{Y}	Yield strength (0.2% offset yield strength)
S	Distance from crack tip along crack plane	σ_1, σ_2, σ_3	Principal stresses, $\sigma_1 > \sigma_2 > \sigma_3$
s_{ij}	Stress deviator tensor	σ_e, σ_t	Engineering and true stress
t	Notch/pre-crack depth	σ_{eq}	von Mises equivalent stress
Δt	Crack depth increment	σ_h	Hydrostatic stress
U_x, U_y	Normal coordinate displacements	σ_{ij}	Cauchy stress tensor
v	Poisson's ratio	σ_{ii}: σ_{xx}, σ_{yy}, σ_{zz}	Normal coordinate stresses (x, y-direction) and tangential (z-direction) stress
Y	Yield stress in uniaxial loading	σ_{R}	Residual strength based on intact cross-section
δ_{ij}	Kronecker delta	σ_b, σ_b^{net}	Tensile strength (or notch tensile strength) based on net cross-section

CHAPTER 1. General introduction

1. 1 Research background

1.1.1 Residual strength of pre-cracked structures

Residual strength reflects the maximal stress below which a defective structure can still carry without falling [1–4]. That is, it indicates the practical load-carrying capacity in the presence of flaws, which usually deviates from the designed structural strength. It is a consensus that achieving flawlessness is almost impracticable with present engineering technology. Various product quality deficiencies, such as cracks, punctures, and burrs, and service-induced damages, such as scratches, wear scars, and corrosion pits, widely exist in engineering structures. They are the source of local stress intensifications and are widely believed by engineers and scholars to herald degradations in load-carrying capacity [4–10]. Hence, to prevent unexpected failures, the residual strength evaluation is a crucial concern in fail-safe designs.

As a representative case of local stress intensifiers, pre-existing cracks (pre-cracks) in engineering structures have attracted the most attention of residual strength study [11–13]. The most direct and classical way to evaluate the residual strength of pre-cracked structures is replicating the identical working conditions through experiment. Naturally, it requires extensive experiments to deal with various cracks when engineers do not have a clear recognition of the underlying reasons for the loss of load-carrying capacity. With the developments of mechanical engineering and material science, many attempts have been made to find widely applicable tools to anticipate failures in advance. Especially the modern fracture mechanics, which was unveiled by Griffith

energy balance model proposed in 1920 [14] and matured by proposing concepts of stress intensity factor (usually written as K) for linear elastic fracture mechanics (LEFM) in 1957 [15] and J contour integral (usually written as J) for elastic-plastic fracture mechanics (EPFM) in 1968 [16], had significantly prompted the residual strength analysis of pre-cracked structures by correlating the allowable stress and crack depth with the fracture toughness [17–20]. The residual strength of pre-cracked structures can be derived based on the fracture mechanics approach [21,22], such as the failure assessment diagrams (FAD) shown in Fig. 1.1, the material selection charts (MSC) shown in Fig. 1.2, and a straightforward failure strength vs. crack depth relation in Fig. 1.3.

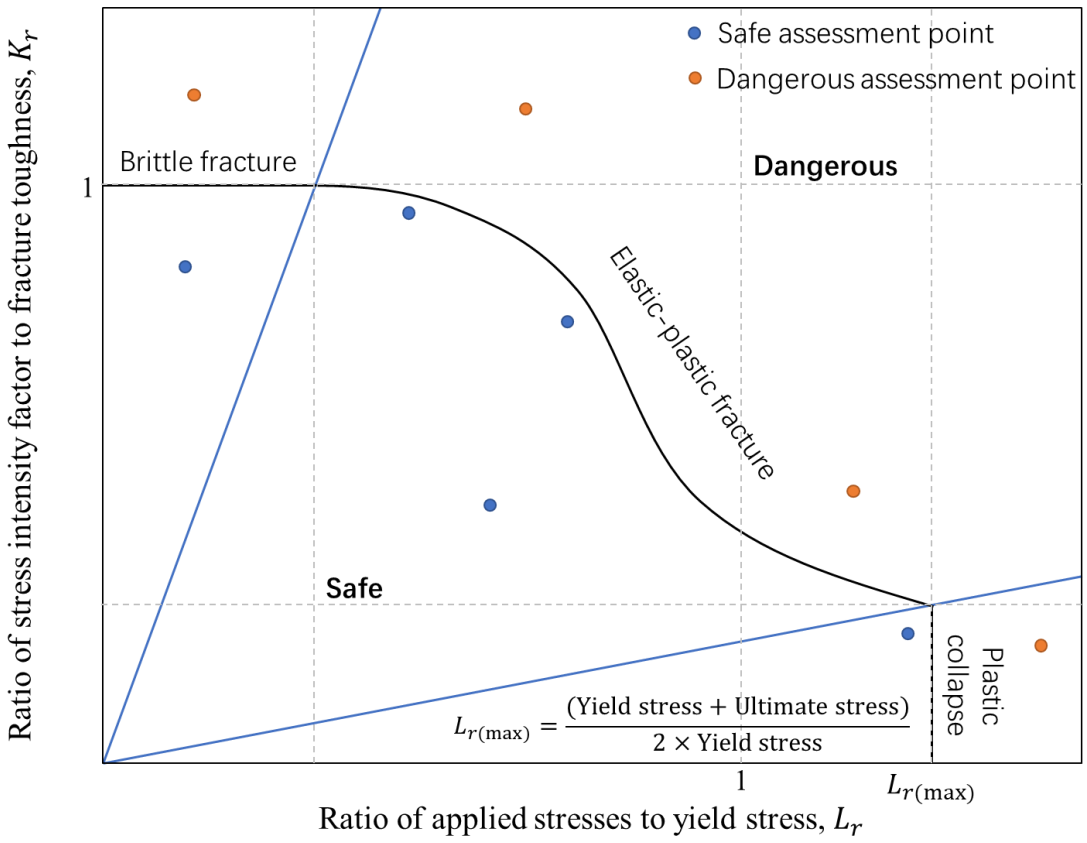

Fig. 1.1 Failure assessment diagram (FAD) covering fully brittle to fully ductile behavior [17,22,23].

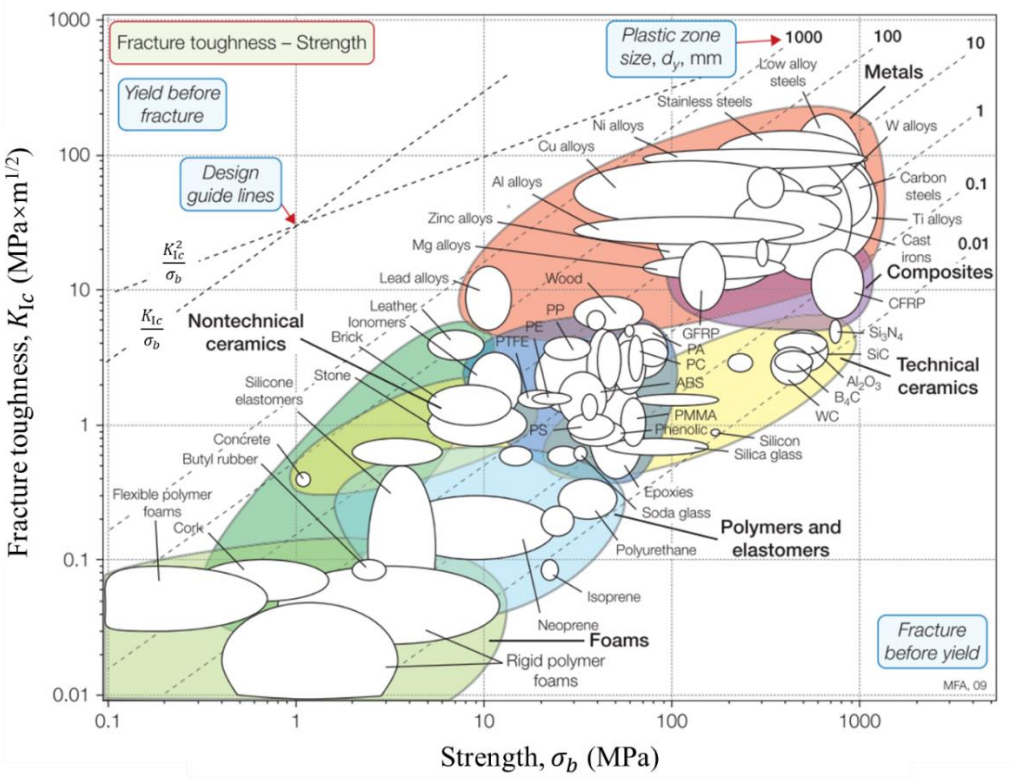

Fig. 1.2 Correlation map of fracture toughness vs. strength used in selecting material for damage-tolerant design [20].

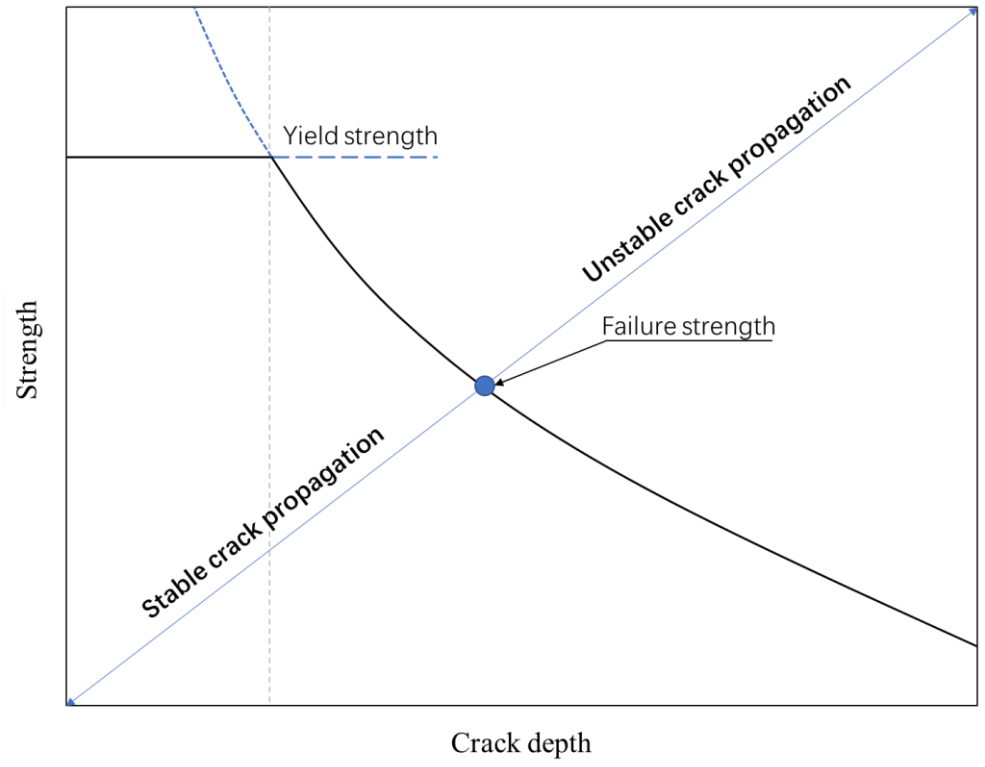

Fig. 1.3 Schematic of relationship between failure strength and crack depth (stable crack propagation includes non-propagating crack) [1,24].

Although fracture mechanics has been a primary means for residual strength issues, the theory of residual strength evaluation and prediction is still immature. The cracking behavior is the critical concern of fracture mechanics, while the onset of unstable crack propagation may not occur even applied stress approaching the allowable stress determined by the plastic flow property [25], such as the cut-off lines for fracture mechanics approach in Figs. 1.1 and 1.3. Beyond the scope of fracture mechanics, investigations are insufficient, so the evaluation of residual strength still mainly relies on the experiment and experience. Moreover, when fracture happens after the general yielding, the mixed-use of yield strength and ultimate strength to define the failure strength [24,26] in the fracture mechanics approach makes the determination of residual strength unclear. This further highlights that the research on residual strength should not be limited by fracture mechanics. The above problems of the present residual strength study are just the tips of the iceberg. Existing theories can be used to improve the research on residual strength, but they should not be the constraints. A new framework must be proposed for future investigations of residual strength.

In this study, residual strength is suggested to be identical to the ultimate structural strength regardless of the general yielding. The yield strength is critical for mechanical design because it guarantees the normal operation of machines. However, the onset of general yielding due to unreasonable loading can be avoided through sophisticated design. Meanwhile, as the concept of user-friendly becoming increasingly important in modern society, the idea of fail-safe design is changing from prioritizing the machine integrity to prioritizing personnel safety in emergencies, such as introducing crumple zones in automobile design [27]. The higher ultimate tensile or compressive strength can absorb more energy before losing the load-carrying capacity to protect the operator. Extensive vehicle crash tests, as shown in Fig. 1.4, have proven that a proper plastic

deformation can save lives in accidents [28]. In summary, the yield strength is for machine operation, and the residual strength is for personnel safety.

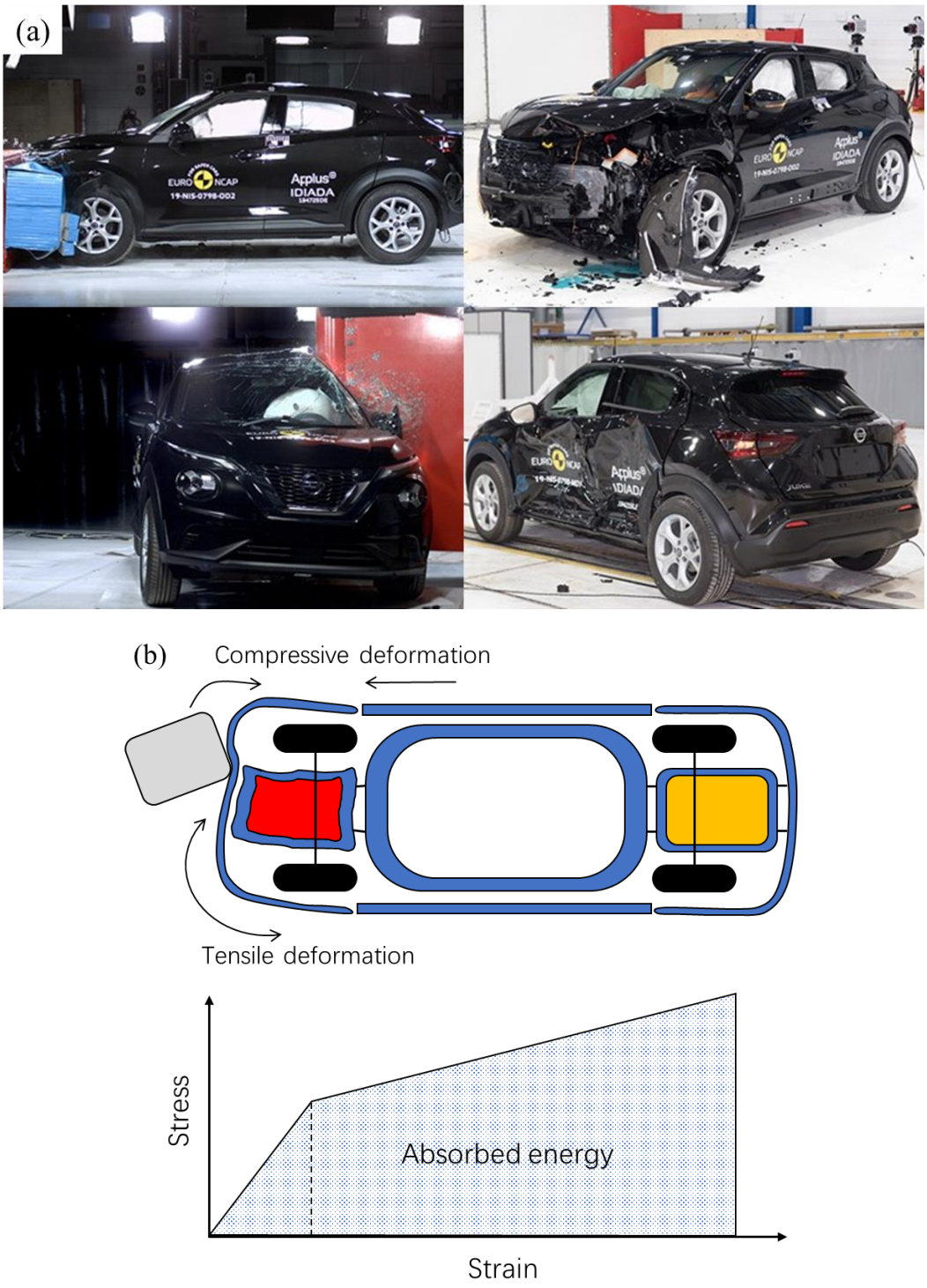

Fig. 1.4 (a) Vehicle crash test (Nissan Juke, DIG-T 117, N-Connecta, LHD [29]); (b) Cars with crumple zones help save lives in accidents through plastic deformation [28].

1.1.2 Physical meanings of residual strength

A variety of reasons can cause the loss of load-carrying capacity, that is, the physical meaning of residual strength various with practical working conditions. The physical meanings of residual strength can be summarized as fracture instability, plastic instability, and geometric instability [18]. Different physical meanings may compete with each other to dominate the residual strength in applications. Hence, understanding these physical meanings is a prerequisite for the in-depth study of residual strength.

1.1.2.1 Fracture instability

The onset of unstable crack propagation can limit the residual strength, whose critical condition is called 'fracture instability' [30]. It is the general consideration of residual strength evaluation according to the fracture mechanics approach. The crack propagation may become immediately unstable after brittle fracture initiation, or it may occur after a stable ductile tearing [17]. Hence, this critical condition can be determined by fracture initiation toughness of brittle fracture, or fracture instability toughness on a rising crack-extension resistance curve (R-curve) of ductile fracture [30,31]. When the driving force of crack propagation is always higher than the fracture toughness, the unstable crack propagation begins. For instance, as shown in Fig. 1.5, if the driving force of a crack is characteristic by energy release rate [32], $\mathcal{G}$, and R denotes the resistance, then the condition for stable crack propagation is

$$\mathcal{G} = R \tag{1-1}$$

for the case of brittle fracture shown in Fig. 1.5 (a), or

$$\frac{d\mathcal{G}}{da} \leq \frac{dR}{da} \tag{1-2}$$

for the case of ductile fracture shown in Fig. 1.5 (b). Correspondingly, the unstable crack propagation occurs when

$$\frac{d\mathcal{G}}{da} > \frac{dR}{da} \tag{1-3}$$

Therefore, the crack is non-propagating at σ_1 for both Figs. 1.5(a) and (b). As the applied stress increases, fracture initiates at σ_2, and this critical condition is called fracture initiation toughness. For brittle fracture shown in Fig. 1.5 (a), the fracture instability toughness coincides with fracture initiation toughness because the resistance is a fixed value. However, the ductile fracture will remain stable until applied stress increases to σ_4, that is, approaching fracture instability toughness. Although the fracture toughness for unstable crack propagation should be called fracture instability toughness, it is commonly referred to fracture initiation toughness in the case of Fig. 1.5 (a) and fracture instability toughness in the case of Fig. 1.5 (b) in fracture mechanics study to distinguish brittle and ductile fractures. However, in this study, the onset condition for unstable crack propagation will be collectively called fracture instability toughness to highlight the physical meaning of residual strength, namely, fracture instability.

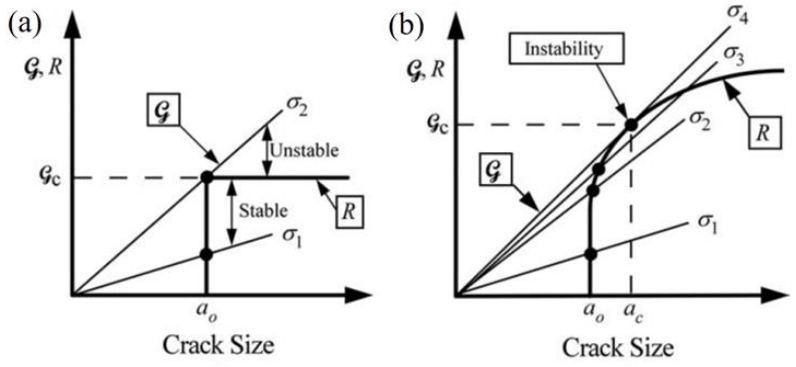

Fig. 1.5 Schematic driving force, $\mathcal{G}$, vs. *R*-curve diagrams (a_0 is pre-crack depth, a_c is critical crack depth at fracture instability and σ with subscript is applied stress, $\sigma_1 > \sigma_2 > \sigma_3 > \sigma_4$) [17]: (a) flat *R*-curve for brittle fracture and (b) rising *R*-curve for ductile fracture.

1.1.2.2 Plastic instability

The plastic instability [33–37] generated by the insufficient strain hardening offsetting the stress increment [38]. Typical physical phenomena, for instance, are known as necking and shear banding, as shown in Fig. 1.7. A classical mathematical solution for the onset of plastic instability by Considère [39] focuses on the critical condition of the true stress, σ_t, vs. true strain, ε_t, (or load vs. elongation) curve reaching a maximum value, as shown in Fig. 1.8. That is,

$$\frac{d\sigma_t}{d\varepsilon_t} = \sigma_t \tag{1-4}$$

This condition is special for very ductile pre-cracked structures, or pre-cracks are very shallow, so their fracture instability toughness may increase to an extremely high value with lowing plastic constraint [40]. Hence, the residual strength of pre-cracked structures also can be dominated by plastic instability.

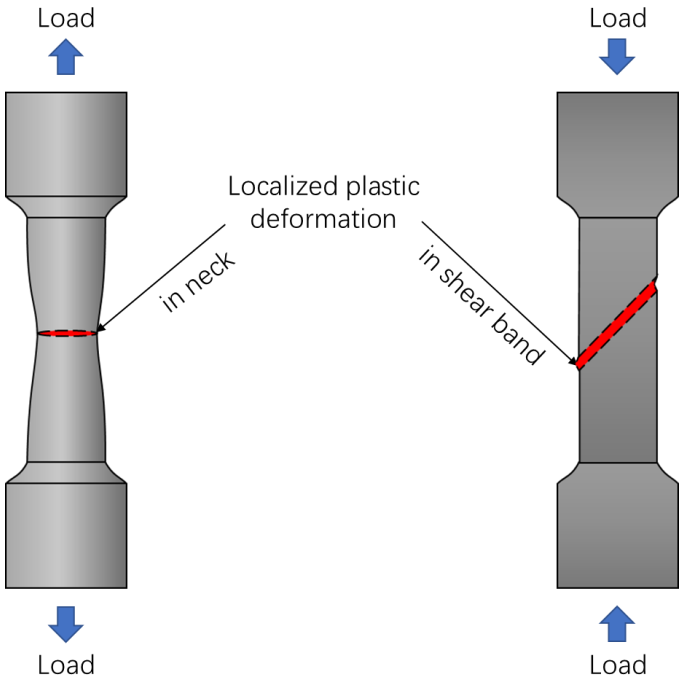

Fig. 1.7 Schematic necking and shear banding induced by plastic instability.

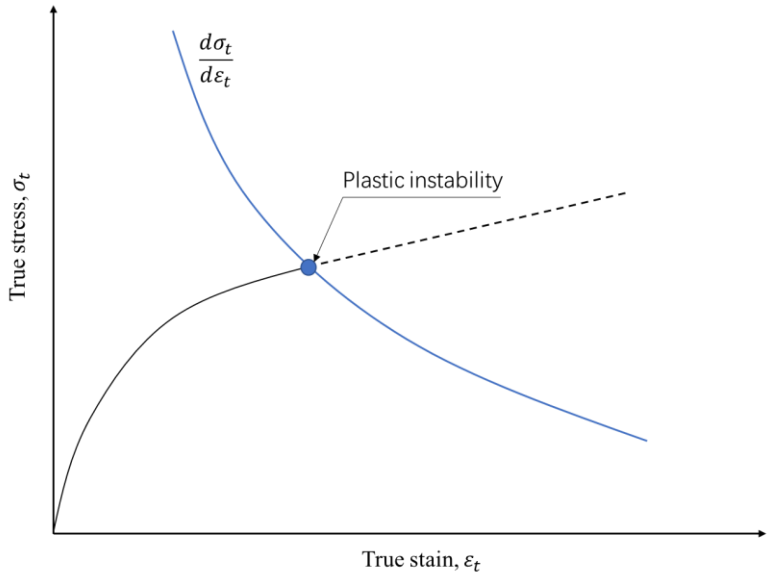

Fig. 1.8 Onset of plastic instability in true stress, σ_t, vs. true strain, ε_t, curves.

1.1.2.3 Geometric instability

Geometric instability limits the load-carrying capacity as a result of the dramatic geometric deflection deviating the deformation path from the original loading path. The typical physical phenomena are buckling and bulging [41–43], as shown in Fig, 1.9. Geometric instability is usually prohibited in the initial design, and it also rarely appears before the onset of fracture instability or plastic instability in pre-cracked structures. Hence, it is not a major consideration of this study. However, it should note that sometimes people confuse geometric instability with plastic instability because a considerable deflection may become plastic, and a dramatic geometric deflection also may happen after the onset of plastic instability. Here, we emphasize that the plasticity in geometric instability, if it has, is induced by geometric deflection with a significant variation in the loading path, while the plastic instability depends on the plastic flow property without a significant variation in the loading path. That is, geometric

deflection is the fundamental reason for geometric instability, and localized plastic deformation is responsible for plastic instability.

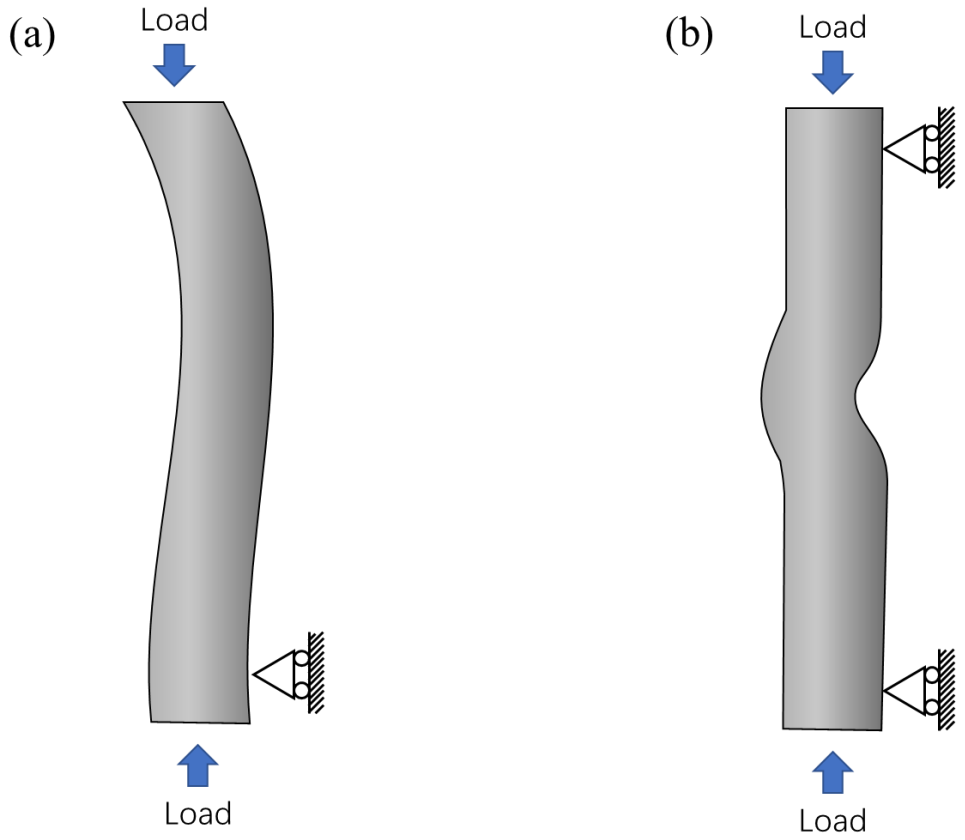

Fig. 1.9 Geometric instability due to large geometric deflection that deviates deformation path from original loading path: (a) buckling and (b) bulging.

1.1.3 Research gap in residual strength of shallow pre-cracked structures

With the assistance of fracture mechanics, general considerations of residual strength mainly focus on cracks deeply embedded in structures [2,3,7–12,44]. However, as technology advances, most pre-cracks in engineering structures nowadays become very shallow. Such shallow cracks [40] (mechanically shallow cracks), whose plastic zone

size is usually comparable to the crack depth or even structure dimensions [45,46], have been recognized to have distinct mechanical properties [47,48] and may result in anti-commonsense phenomena, such as the shallow (or short) crack problem in fatigue [49]. Nevertheless, previous studies have rarely involved the residual strength issue of shallow pre-cracked structures, neither the physical meaning of residual strength nor the corresponding damage characteristic has been clarified, let alone reasonable evaluations and predictions.

Experiences of addressing the residual strength of deep pre-cracked structures based on fracture mechanics [1,50] are occasionally invalid for shallow pre-cracked structures. Most previous studies [2,3,7–12,44], typically presupposing a small-scale yielding (SSY) [51–53] condition, implied the physical meaning of residual strength is fracture instability [10,12]. Hence, the residual strength is determined by fracture initiation toughness of brittle fracture or fracture instability toughness on a rising crack extension resistance curve (*R*-curve) of ductile fracture [30,31]. Both the former and latter are regarded as material intrinsic properties for deep pre-cracked structures, so the residual strength generally has a definite inverse relationship with the pre-crack depth. However, for shallow pre-cracked structures made of ductile metals, the stress triaxiality [54–56] is insufficient to confine plasticity, the *R*-curve thus becomes geometric dependent [17,30,57]. For instance, the shallower the crack, the steeper *R*-curve and the higher fracture instability toughness [17,30,31,58–61]. Furthermore, when shallow pre-crack in full-scale yielding (FSY) [47] (namely, the general yielding condition) owns a terrifically high fracture instability toughness, the plastic instability may compete with fracture instability to govern the residual strength. The above situations obscure the trends of residual strength with shallow pre-crack depth and doubt the applicability of fracture mechanics.

With further hypotheses, the notch strengthening phenomenon also impugns the commonsense of cracks weakening the structure because the crack is a particular case of the notch owning a minuscular root radius [17,62]. Even an atomically sharp crack can be blunted immediately with plasticity. Hence, a notch can be equivalent to a crack if its depth is the only influential factor of mechanical properties [63–65]. In turn, the crack may play a similar role as the notch in affecting the structural strength. Particularly notches with a moderate stress triaxiality can delay the yielding in notched cross-sections before stimulating the local failure (fracture) the notch roots, thereby resulting in notch strengthening phenomenon [54,66–68]. Identically, if the plastic instability, instead of fracture instability, dominates the residual strength, the commonsense of cracks weakening structures would be challenged. However, this assumption still requires laboratory verification because: 1. Notches are design parameters, so the notch strengthening generally is evaluated on net cross-sections rather than the intact cross-sections (gross area of cross-section without considering the presence of pre-crack) of residual strength evaluation; 2. Most conventional failure assessments are subject to yield strength [10,17] to avoid mechanical failure, so they are ineffective for residual strength of shallow pre-cracked structures that consider an extreme case of safety. Therefore, it is necessary to get rid of commonsense in engineering to investigate the ‘shallow crack effect on residual strength evaluation.’

1. 2 Purpose of this study

This study was motivated by the need for a better understanding of the trends, physical meanings, and corresponding damage characteristics of residual strength of shallow pre-cracked structures. With the joint efforts of mechanical and material

researchers, the pre-cracks are becoming mechanically shallower, and the materials are becoming stronger and tougher. Therefore, this study is considered prospective and necessary for the future fail-safe design.

The residual tensile strength (hereinafter shortened as ‘residual strength’) under plane strain loading was selected as the research object. Because both opening-mode (Mode-I) loading and the plane strain loading are relatively dangerous than other loading configurations in most cases [17]. Since the extensive plasticity was expected to obtain mechanically shallow cracks, interstitial-free (IF) steel (low strength grade with excellent ductility [69], as shown in Fig. 1.10) was used for machining specimens. Meanwhile, IF steel only consists of a single ferrite phase without a large number of interstitial atoms [70]. It thus supplied a fundamental representation of the mechanical properties of ductile ferrite steels. The entire research architecture was designed to get rid of the shackles of previous studies, so some original definitions and concepts were proposed in the following content. All novel definitions and concepts were inspired by deficiencies in present literature for residual strength study, verified by experimental and numerical results, and generalized by scientific discussion. In summary, this study sought to find answers to the following questions:

1. How to introduce shallow crack on laboratory specimens for the residual strength study?
2. What is the definition of shallow cracks in residual strength issues?
3. What are the shallow crack effects on the trends, physical meaning, and corresponding damage characteristics of residual strength?
4. How to predict the residual strength affected by shallow cracks?
5. What are the potential applications of this research?

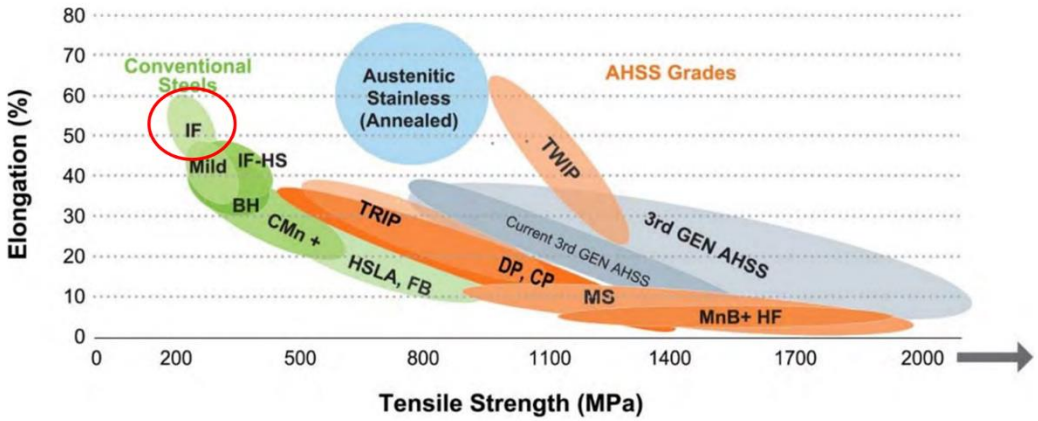

Fig. 1.10 Interstitial-free (IF) steel in steel strength vs. ductility diagram [69].

In this thesis:

Question 1 will be answered in CHAPTER 2.

Questions 2 and 3 will be answered in CHAPTER 3.

Question 4 will be answered in CHAPTER 4.

Question 5 will be partially answered in CHAPTER 5.

1. 3 Thesis outline

This thesis consists of 6 chapters. All chapters are arranged to serve the central theme of ‘shallow crack effect on residual tensile strength evaluation’. The thesis outline is as follows:

Chapter 1 described the general introduction of this study. The development and present level of residual strength study were briefly reviewed to propose a clear and unified definition of residual strength for this study. After indicating the potential

physical meanings of residual strength, the research gap in residual strength of shallow pre-cracked structures was pointed out. Then, the motivation of this study, namely, improving the residual strength theory in the case of shallow cracks, was formed. The main objectives and originalities of each part of this study were described.

Chapter 2 solved the prerequisite for investigating the residual strength of shallow pre-cracked structures, that is, the identification of shallow crack-like notches for structural failure. Introducing crack-like notches is essential for this study because fatigue pre-cracking fails to ensure geometric symmetry, pre-crack measurability, and restricted pre-strain of shallow pre-cracked structures under plane strain condition. However, the results obtained by previous studies related to crack-like notches under small-scale yielding are invalid for shallow notches with extensive plasticity, particularly when plastic instability instead of fracture instability governs the residual strength. From the perspective of asymptotic and phenomenological analysis, this chapter proposed a novel criterion for shallow crack-like notch identification.

Chapter 3 clarified the trends, physical meaning, and corresponding damage characteristics of residual strength with shallow pre-crack depth. Results showed that the residual strength of shallow pre-cracked specimens was preferentially governed by plastic instability instead of fracture instability. Furthermore, when shallow pre-crack depths were shorter than a critical value, the rupture occurred in the intact cross-section and the residual strength was identical to the tensile strength of smooth specimens. Such an anti-commonsense phenomenon was explained from the perspective of plastic strain localization. Finally, the ‘shallow crack effect’ special for residual strength issues was defined.

Chapter 4 focused on predicting the residual strength of shallow pre-cracked structures. The prediction was divided into a qualitative part and a quantitative part. A novel failure assessment diagram correlating to physical meanings of residual strength and damage characteristics was suggested for qualitative predicting the trends of residual strength from the perspective of plastic strain localization. Meanwhile, a new classification of pre-cracks was proposed according to the physical meaning and corresponding damage characteristics of residual strength. The quantitative prediction was expected to be numerical and phenomenological because engineers can easily find out when the prediction method fails. It was implemented by finite element analysis based on continuum mechanics. Then, we evaluated whether the local plastic flow property influenced by pre-cracks could influence the prediction results.

Chapter 5 considered an application of shallow crack effect to a typical case of plastic strain localization enhanced by the hydrogen. Hydrogen embrittlement (HE) is widely believed to be harmful to engineering structures made of ferritic steel, particularly in the presence of pre-cracks. This chapter proved the effectiveness of the shallow crack effect when the characteristic of plastic strain localization is changed. Additionally, this effect calls into question the general applicability of conventional investigation of HE susceptibility that mainly focuses on the variation of fracture characteristic, which is often defaulted to cause changes in mechanical properties. Hence, HE susceptibility is deduced to geometric HE susceptibility for shallow pre-cracked structures, while that for deep pre-cracked structures is metallurgic HE susceptibility.

Chapter 6 summarized the results and proposed the outlook.

CHAPTER 2. Equivalence between shallow notch and shallow crack in structural failure caused by plastic instability

Introduction

Artificial pre-cracks with various depths are suitable for the laboratory investigation of crack effects on mechanical properties. The familiar method of preparing pre-cracked specimens is fatigue cracking. However, this method may occasionally fail to ensure rigorous investigation conditions, such as the geometric symmetry, pre-crack measurability, and restricted pre-strain. An alternative method is introducing a crack-like notch to resemble a crack [64,71]. Hence, discussions on when a notch is equivalent to a crack have been presented in an extensive body of literature [72–77]. Most of these studies endeavored to achieve a unified criterion for reasonably and conveniently identifying crack-like notches in applications. The core idea of crack-like notch identification has been developed from the empirical correlation between the geometric configuration and damage initiation behavior [72] to the physical reasoning of a situation wherein the plasticity development dominating the fracture process is insensitive to geometric variation [62]. Conventional viewpoint with regard to crack-like notches in a finite-sized structure can be summarized as follows: (1) the plastic zone in front of the notch, which contains the fracture process zone, must not be too large (SSY) to ensure that the free surface has minor influence on the fracture process;

(2) the plastic zone size must be sufficiently larger than the notch root radius such that the disturbance of the notch root variation to the development of plasticity can be ignored; (3) the mechanical fields controlling the plastic zone in the notched structure must have a broad asymptotic convergence to that of a crack under the same boundary conditions. This criterion, for instance, contributes to correlating the crack and notch problems in laboratory studies [78] and obtaining geometric-independent fracture toughness [79] by the notches.

Nonetheless, regarding the investigation of the structural strength in the presence of artificial pre-cracks, the abovementioned criterion for crack-like notches sometimes may be invalid. The structural strength of a pre-cracked structure can be dominated not only by fracture instability [30], but also by plastic instability [25]. The latter readily occurs in a shallow pre-cracked structure made of a ductile material [38] owing to the low plastic constraint [17], and may have great importance for laboratory investigations and the future advanced design because, nowadays, most preexisting defects in engineering structures become minuscule with the development of processing and material technologies. Classical concepts of crack-like notches require the precondition of small-scale yielding and assume that the fracture progressing at the crack tip is always responsible for failure. Naturally, they cannot satisfy the case of plastic instability prevailing in shallow pre-cracked structures. Amongst small defects, shallow pre-crack is still a representative stress and strain concentrator. Therefore, it is necessary to extend the concept of crack-like notches to the investigations of shallow pre-cracked structures.

This study partially solved the issue of shallow crack-like notches subjected to monotonic tension by only focusing on the plastic instability occurring under plane

strain conditions without the assistance of pre-crack propagation. Based on finite element analysis (FEA), the boundary condition, geometric configuration, and elastoplastic fields dominating the overall work hardening in notched and pre-cracked cross-sections were considered. This paper proposes that if the structural strength and failure mode are independent of the notch geometry (except for the notch depth), and elastoplastic fields in notched and cracked cross-sections are broadly convergent by asymptotic analysis, then, a shallow notch is equivalent to a shallow crack. The underlying reason is that different elastoplastic field gradients close to the notch root or crack tip may still result in the same overall work hardening in notched and pre-cracked cross-sections. This concept was verified on interstitial-free (IF) steel, which is a typical strain hardening ferrite steel with excellent ductility and simple metallurgical microstructure [70,80]. Additionally, the generality of the identification method and the significance of the influential factors for shallow crack-like notches was discussed in this study.

It should be noted that the definition of tensile strength was based on the net cross-sectional stress because this definition usually is standard for notched specimens. After proving that notches are equivalent to cracks in a certain condition, the tensile strength can be easily transformed to residual strength, which is based on the intact cross-section.

2. 1 Methodology

2.2.1 Concept of shallow crack-like notch identification

When a pre-cracked specimen is subjected to monotonic tension, plastic instability typically occurs in the form of necking without (*Problem I*) or with (*Problem II*) the assistance of stable crack propagation, as shown in Fig. 2.1. Because shallow cracks with an extremely low plastic constraint condition can result in extremely high fracture toughness [30], they will probably not propagate until plastic instability occurs. Additionally, if a notch imitates *Problem II* with stable crack propagation in front of the notch root, the notch and stable crack would be equivalent to a crack with the sum of their total depth. Hence, this study focused on *Problem I*, and *Problem II* will be discussed in future works.

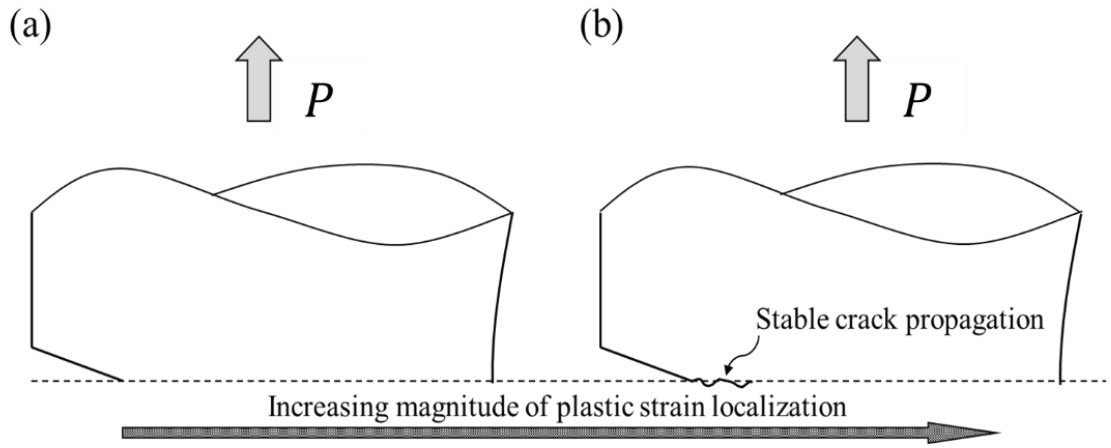

Fig. 2.1 Tensile static strength of shallow pre-cracked structures dominated by plastic instability (necking) occurring: (a) without crack propagation, and (b) with stable crack propagation.

Both a notch and a crack can cause a gradient distribution in elastoplastic fields. Hence, it can be easily perceived that if the elastoplastic fields in notched and pre-cracked cross-sections are entirely the same, then, plastic instability will occur under the same condition. However, this is impossible because the severity of stress

concentration varies with the geometric configurations, and notches and cracks will undoubtedly result in different gradients in elastoplastic fields, particularly close to the notch root and crack tip. In fact, plastic instability fundamentally depends on the overall work hardening in one cross-section, which may still be the same level even if the elastoplastic field have a slight difference in gradients between the notched and pre-cracked structures. First, if a shallow notched structure has a sufficient broad ligament, which makes the disturbance of the notch geometric variation insignificant, the remote elastoplastic fields of the notch root may be convergent to that of the crack tip over a wide range. Second, for most nonlinear power hardening materials, their strain hardening rate decreases as the increase of plastic deformation [54]. Hence, in practice, the increment of the local strain hardening varying with the different elastoplastic field gradients may result in the same load-carrying ability. Basing on this assumption, two requirements for crack-like notches can be derived: 1. The elastoplastic fields in a notched and a pre-cracked cross-section should be broadly convergent to each other such that the influence of the geometric configuration is insignificant. 2. The comparison of elastoplastic field convergence should be made under the same boundary conditions, one of which is at the same structural strength (or load-carrying capacity). These two requirements can ensure the similarity of the overall work hardening in the notched and pre-crack cross-sections, and they were verified initially by using FEA, and then experimentally verified using specimens made of IF steel.

It should be noted that the “broadly convergent” in the aforementioned first requirement means that the elastoplastic fields, which govern the overall work hardening condition of notched and pre-cracked cross-sections, should coincide with each other in a wide range of ligaments, and the differences of elastoplastic field gradients are only allowed in the vicinity of notch root or crack tip. Although the same

onset condition of plastic instability only requires the same overall work hardening condition in the yield cross-sections, “broadly convergent” is necessary because it not only limits the crack-like notch geometry but also indicates that identifying crack-like notches should be conducted with the unified structure size and preexisting defect configuration. For instance, comparing the similarity between a shallow notch located in the edge of small structures and a shallow crack embedded in large infrastructures is not recommended at present due to their different constraint state.

2.2.2 Implementations of finite element analysis and experimental verification

In this study, FEA was implemented using ANSYS Workbench (2019 R3) with the large deflection option [81] to compare the elastoplastic fields and critical condition for plastic instability. Because it was expected that the structural strength is independent of geometric configurations, the comparisons of elastoplastic fields were conducted under the maximum load. The base material model came from IF steel, whose grain size and hardness were respectively adjusted to 51.2 μm and 65 HV, respectively, by annealing at 750 °C for two hours and then cooling in air. For detailed information on initial microstructure observation and average grain size measurement, see Appendix A1. The chemical composition of IF steel is presented in Table 2.1.

Table 2.1 Chemical composition of Interstitial-free steel.

Element	C	N	Si	Mn	P	S	Ti	Al	O	Fe
Amount (wt. %)	0.0019	0.0008	0.009	≤ 0.003	≤ 0.002	≤ 0.003	0.029	0.028	0.0015	Bal.

The material modeling in this study was based on the conventional J_2 flow theory of plasticity [82], which consists of the von Mises yield criterion, associated flow rule, and nonlinear isotropic hardening law. Let σ_{ij} be the Cauchy stress tensor and σ_1, σ_2, and σ_3 be three principal stress. The hydrostatic stress can be written as

$$\sigma_h = \frac{1}{3} I_1 = \frac{1}{3}\sigma_{ii} = \frac{1}{3}(\sigma_1 + \sigma_2 + \sigma_3) \tag{2-1}$$

where I_1 is the first invariant of the stress tensor, and the repeated indices (ii) denote the Einstein summation convention. Let s_{ij} denotes the stress deviator tensor and its principal values be s_1, s_2, and s_3. The relation between σ_{ij} and s_{ij} is

$$s_{ij} = \sigma_{ij} - \sigma_h \delta_{ij} \tag{2-2}$$

where δ_{ij} denotes the Kronecker delta. Then, the second invariant of the deviatoric stress tensor, J_2, is written as

$$J_2 = \frac{1}{2} s_{ij} s_{ji} = -(s_1 s_2 + s_2 s_3 + s_3 s_1) = \frac{1}{6}[(\sigma_1 - \sigma_2)^2 + (\sigma_2 - \sigma_3)^2 + (\sigma_3 - \sigma_1)^2 - 2(\sigma_1 + \sigma_2 + \sigma_3)^2] \tag{2-3}$$

The von Mises yield criterion presumes that the yielding begins when J_2 reaches a critical value and the yield criterion is written as

$$f(J_2) = J_2 - k^2 = 0 \tag{2-4}$$

where f is the yield function, and k is the yield stress in pure shear, whose magnitude is $\sqrt{3}$ times lower than the yield stress under uniaxial loading, Y. Alternatively, Eq. (2-4) can be transformed into

$$f(J_2) = \sqrt{3J_2} - Y = \sigma_{eq} - Y = 0 \tag{2-5}$$

in which $\sqrt{3J_2}$ is defined as the equivalent stress, σ_{eq}, that is

$$\sigma_{\mathrm{eq}} = \sqrt{3J_2} = \sqrt{\frac{3}{2}s_{ij}s_{ji}} = \sqrt{\frac{(\sigma_1-\sigma_2)^2+(\sigma_2-\sigma_3)^2+(\sigma_3-\sigma_1)^2}{2}} \tag{2-6}$$

Corresponding to the definition of σ_{ij}, let ε_{ij}^{p} be plastic strain tensor obtained by subtracting the elastic part from the total strain tensor and e_{ij}^{p} be the plastic strain deviator tensor, the equivalent plastic strain, $\varepsilon_{\mathrm{eq}}^{p}$ dual to σ_{eq} is written as

$$\varepsilon_{eq}^{p} = \sqrt{\frac{2}{3}e_{ij}^{p}e_{ji}^{p}} = \sqrt{\frac{2\left[\left(\varepsilon_1^p-\varepsilon_2^p\right)^2+\left(\varepsilon_2^p-\varepsilon_3^p\right)^2+\left(\varepsilon_3^p-\varepsilon_1^p\right)^2\right]}{9}} \tag{2-7}$$

When material deforms isotropically, the plastic strain increment is normal to the yield surface, and the flow potential function is identical to f. Then, the associated flow rule is written as

$$d\varepsilon_{ij}^{p} = d\lambda\frac{\partial f(J_2)}{\partial\sigma_{ij}} \tag{2-8}$$

where $d\varepsilon_{ij}^{p}$ is the plastic strain increment and its magnitude is denoted as $d\lambda$, which is identical to the equivalent plastic strain increment, $d\varepsilon_{\mathrm{eq}}^{p}$, by solving Eq. (2-8).

Consider a nonlinear isotropic hardening condition, Y will depend on the history of $d\varepsilon_{\mathrm{eq}}^{p}$, that is

$$Y = \Phi(\int d\varepsilon_{\mathrm{eq}}^{p}) = \Phi(\varepsilon_{\mathrm{eq}}^{p}) \tag{2-9}$$

In uniaxial tension, the instantaneous value of Y and $\varepsilon_{\mathrm{eq}}^{p}$ are identical to true stress, σ_t, and true plastic strain, ε_t^{p}, respectively. ε_t^{p} can be extracted by subtracting the elastic part, ε_t^{e}, from the true strain, ε_t

$$\varepsilon_t^{p} = \varepsilon_t - \varepsilon_t^{e} = \varepsilon_t - \frac{\sigma_t}{E} \tag{2-10}$$

Therefore, the function Φ can be determined from the constitutive relationship of σ_t vs. ε_t obtained by experiment, which is described by Hollomon's equation [80] in this study, as follows:

$$\sigma_t = K\varepsilon_t^n \tag{2-11}$$

where σ_t is the true stress, ε_t is the true strain, K is the strength coefficient, and n is the strain-hardening exponent. The variables listed in Table 2.2 were obtained by stretching the smooth round bars made of IF steel according to the ASTM E8M standard [83]. Fig. 2.2 shows the design of smooth specimen, which is stretched on a precision universal tester (Shimadzu AG-5000A) with an extensometer (Shimadzu SG 50-50). The engineering stress-strain curve of the smooth specimen obtained by FEA agrees well to that obtained by experiment except the final part of post-necking elongation, as shown in Fig. 2.3. The difference the final part of post-necking elongation is probably due to the crack initiation and propagation that accelerate the decrease of load-carrying capacity. However, it has no fluence on determine structural failure by plastic instability.

Table 2.2 Mechanical property of Interstitial-free steel.

Young's Modulus E (GPa)	Poisson's ratio v	Yield strength σ_Y (MPa)	Tensile strength σ_b (MPa)	Strength coefficient K (MPa)	Strain-hardening exponent n
200.00	0.30	116.1	244.0	456.5	0.27

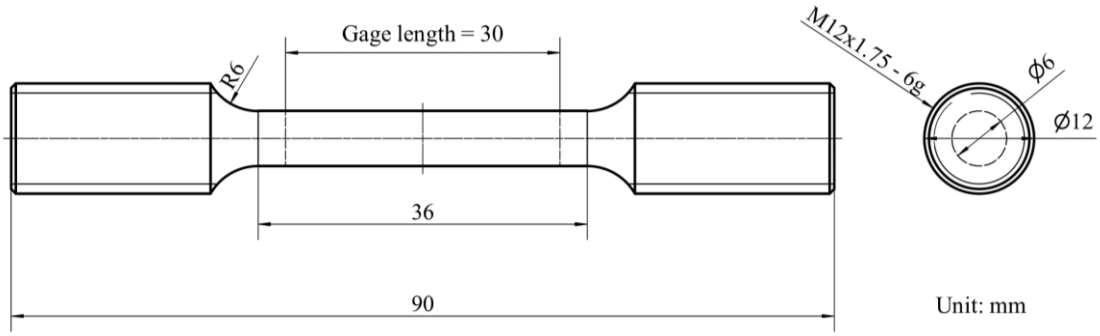

Fig. 2.2 Design of smooth specimen according to ASTM E8M: Small-size specimen with gage length five times gage diameter.

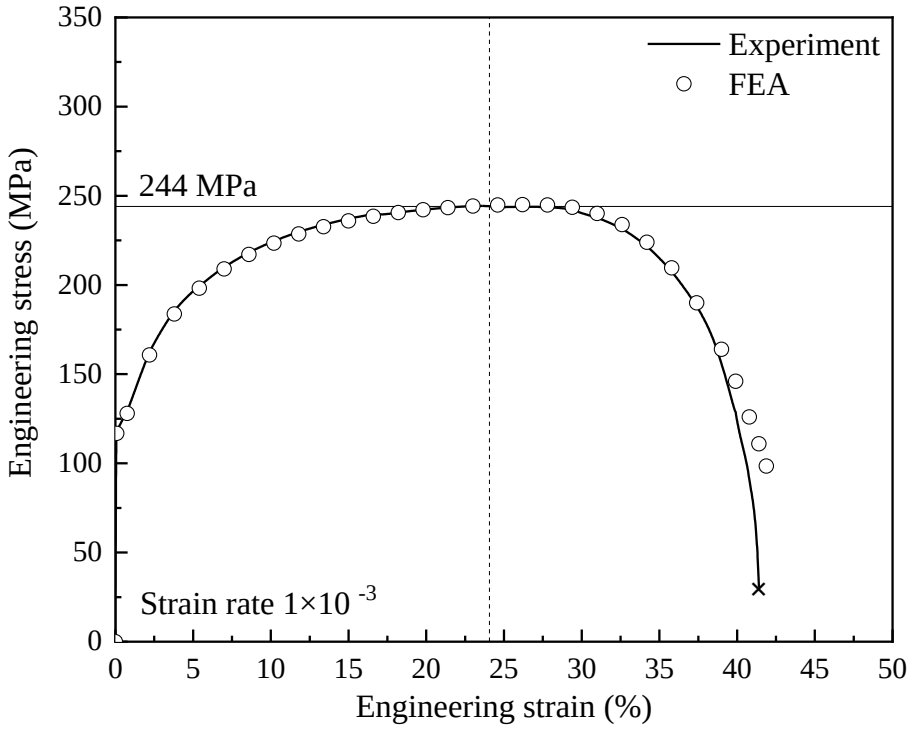

Fig. 2.3 Experimental and numerical results of engineering stress-strain curves of smooth specimen.

The round bar was simplified to an axisymmetric model, which is a quarter of the gage projected into a 2D Cartesian plane, as shown in Fig. 2.4(a). The circumferential notch and pre-crack were assumed to be introduced in the middle of the gage. The effects of three typical dimensions were considered, namely, the notch root radius, ρ, notch opening angle, α, and normalized notch or crack depth t/l. The former two factors are classical considerations (with SSY pre-condition) in crack-like notch discussions because if they do not affect structural failure, the notch depth will be the one and only influential factor, just like the crack depth. The y-axial displacement, U_{y}, of the notched or pre-cracked cross-section was fixed at 0. The value of the external load, P, was calculated by the force reaction to U_{y} at the top edge of the FEA model. Quadratic (PLANE183 [81] with axisymmetric option) dominant meshing was carried out with the refinements close to the notch root and crack tip, as shown in Fig. 2.4(b). The minimum element size decreased to 1 μm, which ensured that all flowing results

were independent of element size with a precision of two after the significant digits.

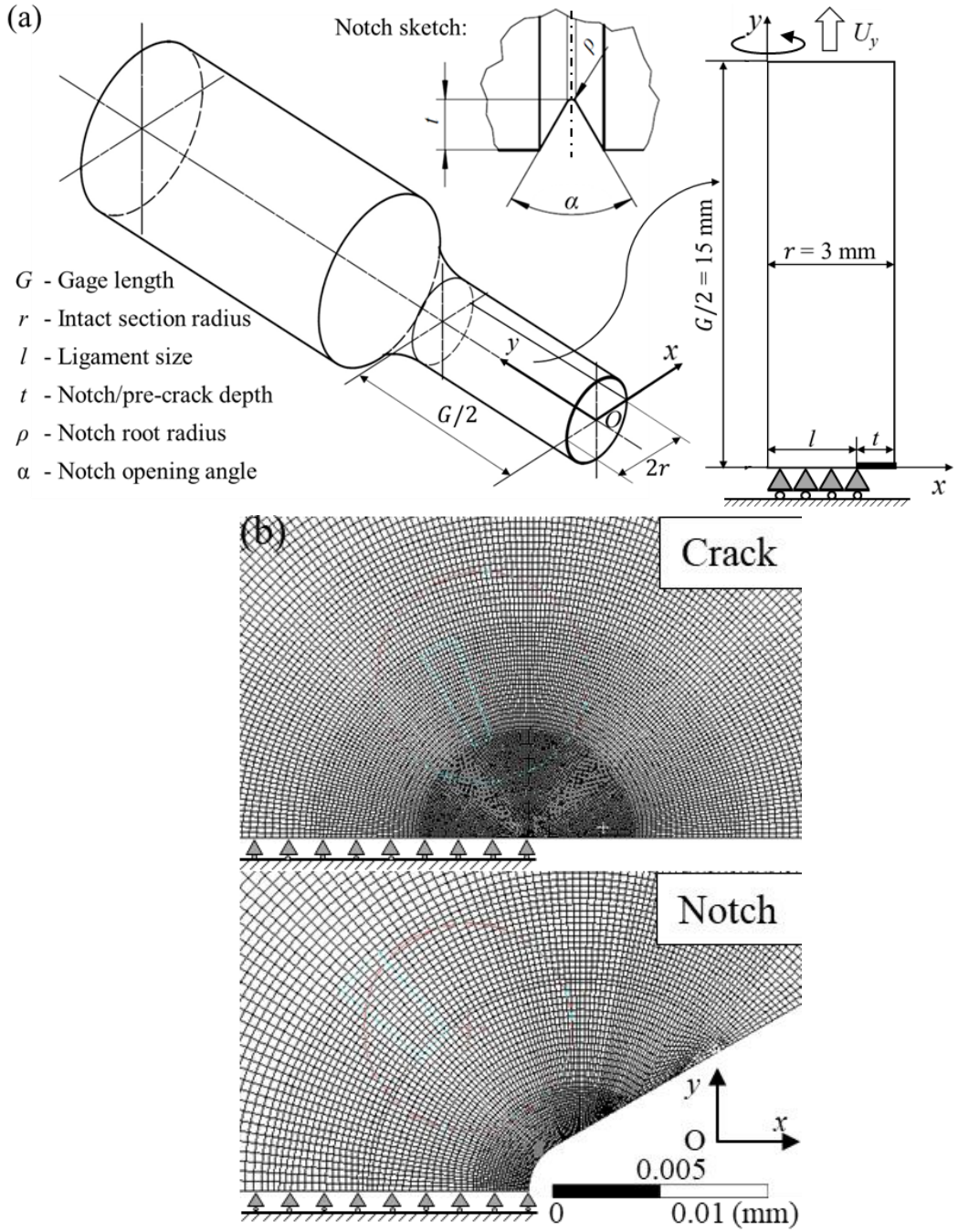

Fig. 2.4 Axisymmetric model for FEA: (a) Simplification, dimensions, and boundary conditions. (b) Meshing examples for crack and notch.

The distribution of σ_{eq} and $\varepsilon_{\mathrm{eq}}^{p}$ in notched and pre-cracked cross-sections were calculated using FEA to evaluate the elastoplastic field convergence. According to Fig. 2.4(a), the principal axes of σ_{ii} and ε_{ii}^{p} in the ligament were along the y-axis, the x-axis

and the circumferential direction of the axisymmetric model, respectively. The local strain hardening property can alter with the elastoplastic field gradients [54]. Hence, in this study, the gross amount of the work hardening condition in one cross-section was quantitively evaluated by averaging the integration of the local strain hardening modulus, as follows:

$$\overline{H} = \frac{\int_0^l H dl}{l} \tag{2-12}$$

where l is the ligament size; H is the local strain hardening modulus approximating the trend of the load-carrying ability varying with the strain increment, as follows:

$$H = \frac{1}{N}\sum_{i=1}^{N} \frac{\sigma_{\mathrm{eq}(i+1)} - \sigma_{\mathrm{eq}(i)}}{\varepsilon^{p}_{\mathrm{eq}(i+1)} - \varepsilon^{p}_{\mathrm{eq}(i)}} \tag{2-13}$$

where N is the number of loading steps in the plastic range, and the initial value of $\sigma_{\mathrm{eq}(i)}$ is determined at $\varepsilon^{p}_{\mathrm{eq}(0.2)}$ = 0.2%. The minimum value of N in this study is 500 steps to guarantee a precision of two after the significant digits for $\overline{H}$. Therefore, for a crack-like notch, the distributions of σ_{eq} and $\varepsilon^{p}_{\mathrm{eq}}$, and the value of $\overline{H}$ in the notched cross-section should be similar to those in the pre-cracked cross-section.

After identifying the crack-like notch by FEA, the experimental verification was carried using the notched specimens. The specimen dimensions were the same as those in the test for obtaining the base material model, as shown in Fig. 2.3. The notches were introduced in the longitudinal middle of the gage part and their dimensions are listed in Table. 2.3. For detailed information on the measurement of the notch dimensions, see Appendix A2. The tensile strength, σ_b, of the notched specimens is defined as the ratio of the maximum load, $P_{\max}$, to the initial net cross-sectional area, A_0^{net}. Microstructural observations were performed on a SEM at 15 kV to determine the damage as a response to the geometric configuration variation.

Table 2.3 Notch dimensions for experimental verification.

Designed dimensions		**Final dimensions after buff polish**				
t/l (%)	ρ (mm)	t/l (%)	ρ (mm)	t (mm)	r (mm)	α (°)
20.00	0.005	21%	0.005	0.52	3.01	60.6
	0.010	21%	0.010	0.52	3.02	60.1
	0.015	21%	0.013	0.51	2.99	60.8
	0.020	20%	0.021	0.51	3.11	60.4
	0.025	21%	0.025	0.52	2.93	60.1
40.00	0.005	39%	0.005	0.85	3.03	60.0
	0.010	40%	0.009	0.86	3.01	60.3
	0.015	40%	0.015	0.84	2.94	60.0

2. 2 Results

Fig. 2.5 shows that σ_b remained a constant approximately when $\rho \leq 0.25$ mm and $\alpha \leq 90°$. Moreover, the influence of α on σ_b was not dramatic compared with that of ρ particularly for $\alpha \leq 90°$. Hence, the distribution of σ_{eq} and $\varepsilon_{\mathrm{eq}}^{p}$ as a response to the variations of ρ with a fixed $\alpha = 60°$ were compared in Fig. 2.6 to investigate the potential cause of the crack-like notch. The distribution of σ_{eq} and $\varepsilon_{\mathrm{eq}}^{p}$ in the remote place of notch root were convergent to those of the pre-cracked section with a discrepancy of 5%. The discrepancy was obtained by calculating the percentage of elastoplastic fields difference between notched and pre-cracked cross-sections in the reference value of elastoplastic fields of pre-cracked cross-section. The distribution of σ_{eq} and $\varepsilon_{\mathrm{eq}}^{p}$ close to the notch root and crack tip had some differences compared with those close to the crack tip. However, these differences did not occupy most of the area in the notched cross-section. Furthermore, as shown in Fig. 2.6(a), the gradient distributions of σ_{eq} close to the notch root and crack tip crossed over each other, This suggests the possibility of an identical overall work hardening in the net cross-sections when ρ was smaller than a critical value, as illustrated in Fig. 2.7(a), which shows that the values of $\overline{H}$ in notched and pre-cracked sections were similar. The reason is

attributed to the local strain hardening increment changing with different elastoplastic field gradient distributions, and to the different triaxial stress states generated by notch geometric variation altering the local strain hardening property. Hence, as long as the elastoplastic fields were broadly convergent in notched and pre-cracked cross-sections, the disturbance from $\rho < 0.025$ mm could be ignored.

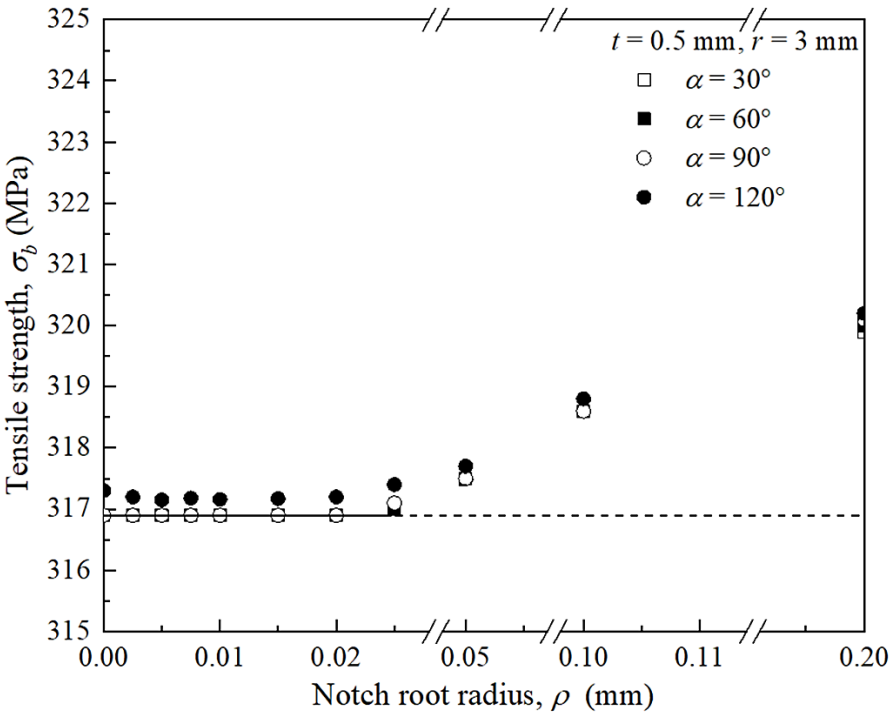

Fig. 2.5 Response of tensile strength, σ_b, to variations of notch root radius, ρ, and notch opening angle, α, at t/l = 20 % obtained by FEA.

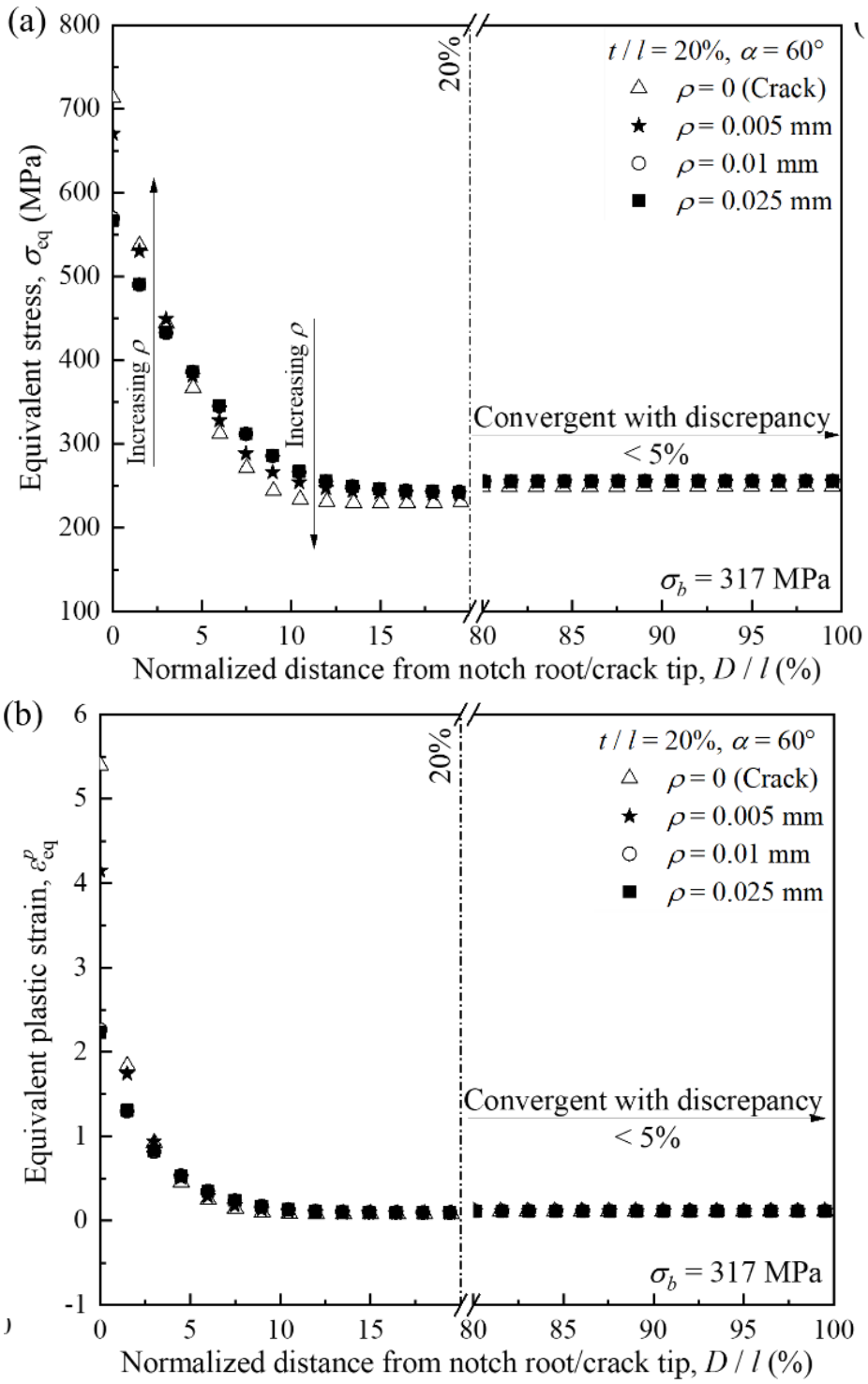

Fig. 2.6 Distributions of equivalent stress, σ_{eq}, and equivalent plastic strain, $\varepsilon^{p}_{\mathrm{eq}}$, responding to variations of notch root radius, ρ.

The experimental results are in good agreement with the results obtained by FEA. Fig. 2.7(b) shows the σ_b of the notched specimens plotted against the (elastic) stress concentration factor [84], K_{t}. Although K_{t} significantly varied with ρ, σ_b was

approximately a constant. The case of t/l = 20% was taken as a typical example to analyze in detail. The engineering stress-strain curves of these specimens also coincided with each other, as shown in Fig. 2.8. Some differences exist in the post-necking elongation are attributed to that the variation in notch root radius combined with the processing error that only has limited effect during the stage of damage accumulating massively. They are insignificant for determining whether plastic instability occurs under the same boundary conditions.

Moreover, the damage patterns of these specimens are similar, as shown in Fig. 2.9. The round dimples (indicated by the yellow line) located at the center of fracture surface are large in size and equiaxed in shape. Their appearance requires a circumstance that owns good ductility with the domination of normal strain [85,86]. Hence, these large equiaxed dimples were probably formed at the early stage of the post-necking elongation, where the ductility was not severely deteriorated by strain hardening and damage initiation, and the deformation path was not deflected significantly by necking. They were surrounded by parabolic dimples and deep elongated dimples, most of which deflect toward the center of fracture surface by shearing and tearing of internal crack propagation. Also, the shear-lips located at the outside edge of fracture surface, which were formed by internal crack connecting with the pre-crack through shear banding, indicate the final rupture position [17]. In general, the experimental results are in good agreement with the FEA results.

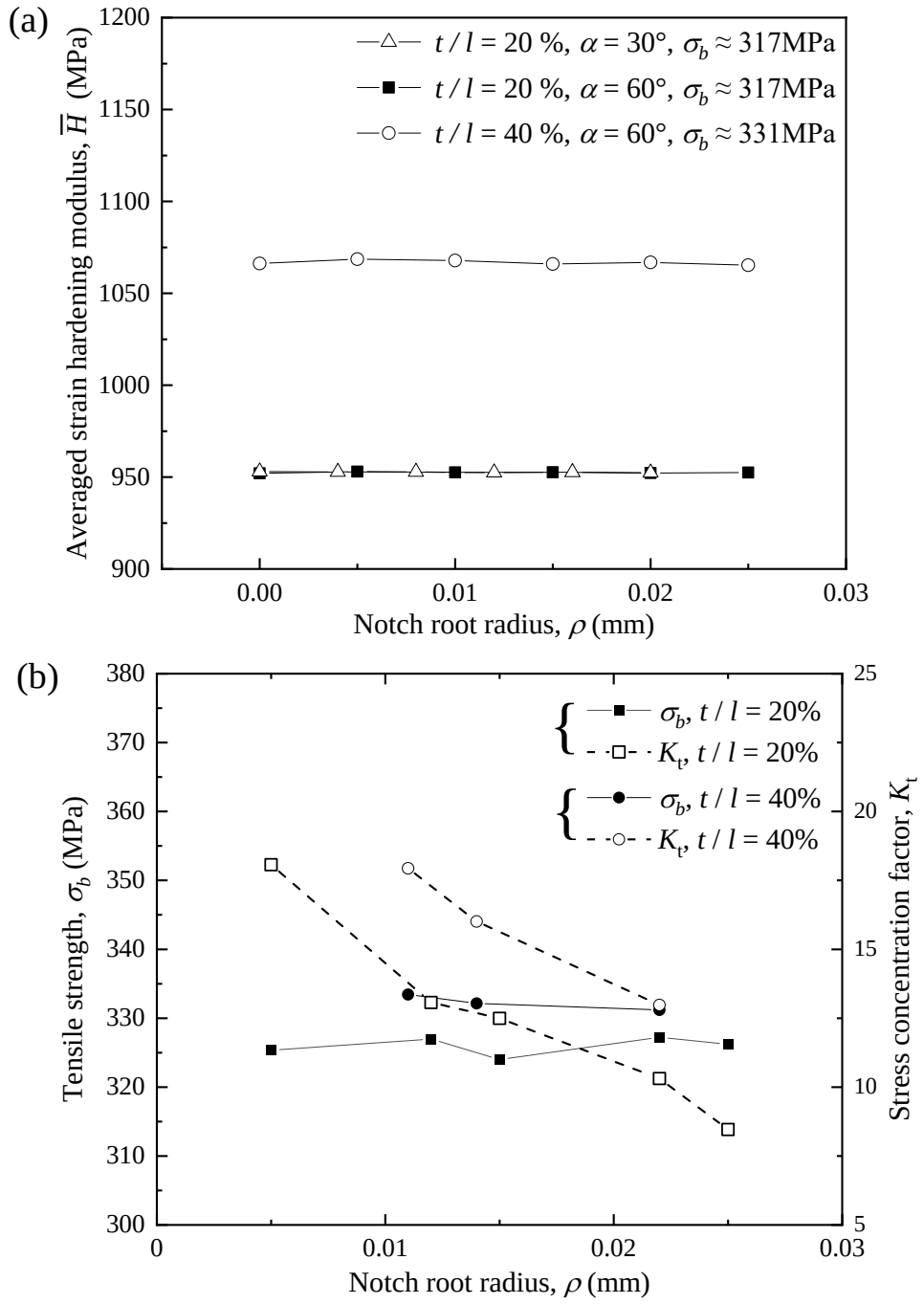

Fig. 2.7 (a) Overall work hardening in notched/pre-cracked sections quantified by averaged strain hardening modulus, $\overline{H}$, obtained by FEA. (b) Tensile strength, σ_b, of notched specimens with same normalized notch depth, t/l, and opening angle, α = 60°, but different root radius, ρ < 0.025 mm, plotted against (elastic) stress concentration factor, K_t.

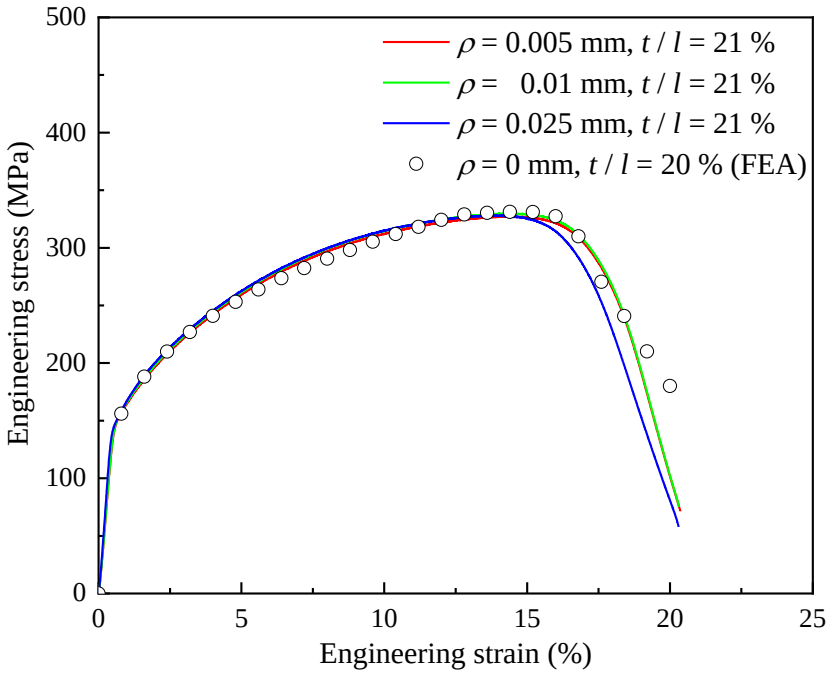

Fig. 2.8 Engineering stress-strain curves of notched specimens obtained by experiment comparing with that of pre-cracked specimen obtained by FEA.

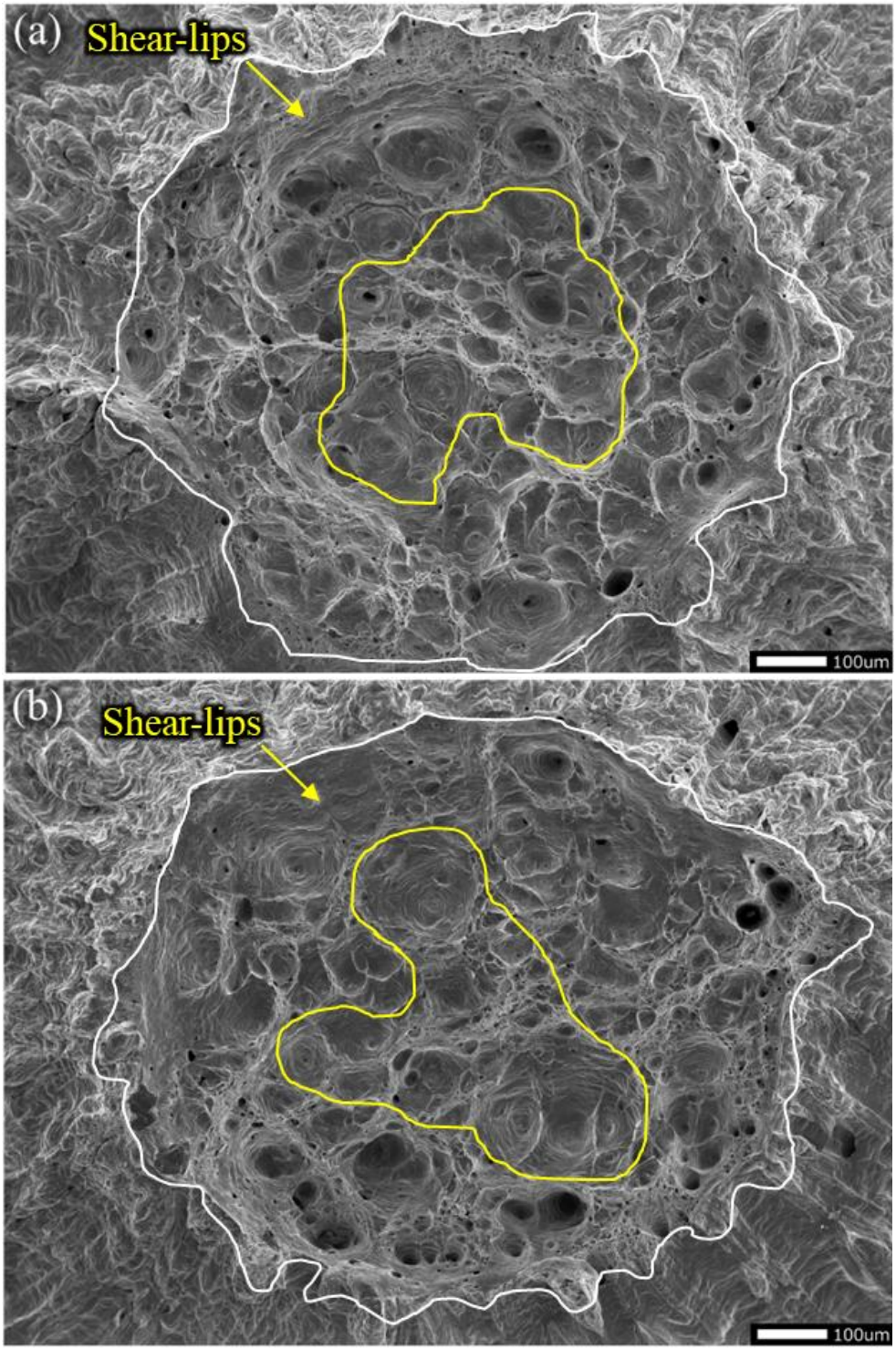

Fig. 2.9 Fractography with same failure mode of plastic instability generating internal crack initiation (yellow line shows the equiaxed round dimples; white line shows the notch root line) : (a) t/l = 21%, ρ = 0.005 mm, α = 60.6°, (b) t/l = 21%, ρ = 0.025 mm, α = 60.1°.

2. 3 Discussion

The results confirmed the validity of the assumption that the overall work hardening conditions in the notched and pre-cracked cross-sections are identical. Hence, if the structural strength is governed by plastic instability, a shallow crack-like notch may exist. An effective method to ensure the same overall work hardening is to assess the convergence between the elastoplastic fields of the notched cross-section and those of the pre-cracked section. In other words, when the structural strength is independent of the notch geometry, except for the notch depth, the shallow crack-like notch can be identified using asymptotic analysis of the elastoplastic fields. In addition, how much percentage of the convergent elastoplastic fields occupying the notched and pre-cracked cross-sections can be called “broadly convergent” is also an important issue before the practical application of the concept of identifying shallow crack-like notch proposed by this study. According to the results of this study, the “broadly convergent” of the elastoplastic fields at least is 80% in ligament with 5% discrepancy. However, it is suggested that “broadly convergent” should base on the design requirements of shallow crack-like notches, which deserve more analysis and discussions in practical applications.

This proposed concept of identifying shallow crack-like notch is suitable for shallow notched structures made of general power strain-hardening material, whose strain-hardening rate decreases with the increase of plastic deformation, because the strain-hardening property of these material combined with the gradient of elastoplastic fields is the fundamental reason for the identical overall work hardening in the shallow notch and shallow pre-cracked specimens. The work hardening exponent is critical not only for the onset of plastic instability [41,54] but also for the gradient of elastoplastic fields

near the geometric discontinuity [17,87,88]. It thus can significantly influence the overall work hardening condition in one yield notched/pre-cracked section. In consequence, the concept of shallow crack-like notches in this study is invalid to the ideal elastic or plastic materials, and the work hardening exponent prospectively becomes a critical material property for assessing whether shallow crack-like notches exist.

The discussion on the overall work hardening condition in notched and pre-cracked cross-sections according to FEA results is based on the precondition of the plastic instability governing the structural strength. This condition typically results in an internal crack initiation by the void formation and subsequent propagation to the exterior. However, it should be noted that the decrease in notch root radius may also induce failure mode transition, such as from ductile failure to brittle failure [31]. Hence, another requirement for crack-like notches should be added; specifically, the failure mode of the pre-crack should be the same because comparing the notched and pre-cracked structure with two different types of failure modes (e.g., voids formation and cleavage) is unreasonable. After determining the geometry of a shallow crack-like notch by FEA, it is necessary to experimentally check the failure mode with some critical values of the notch root radius for scientific rigor. For instance, if the notched root radius, ρ, smaller than a critical value, ρ_c, is the necessary condition for shallow crack-like notches according to the FEA results, then one can check the failure mode at $\rho = \rho_c$ and $\rho \ll \rho_c$.Additionally, the results presented in Fig. 2.5 reveal that a shallow crack-like notch exists when its root radius and opening angle are smaller than critical values determined by the sensitivity of the overall work hardening to the geometry variation. The tensile strength is independent of the notch opening angle in the wide range of 0° to 90°. Similarly, deep crack-like notches are also insensitive to the variation

of the opening angle [62]. This is attributed to the notch opening angle smaller than 90° generally has a minor effect on (elastic) stress concentration under tension [84], which can influence the future plasticity development regardless of the deep pre-cracked structure governed by fracture instability or the shallow pre-cracked structure governed by plastic instability. Typically, the practical crack-like notch introduced in the specimens cannot have such a great opening angle. Hence, the notch opening angle is not a critical factor for shallow crack-like notches compared with the notch root radius. In this study, the critical notch root radius is not considered as an intrinsic material property because the overall work hardening naturally depends on the entire notched section instead of a small area at the front of the notch root. Moreover, the ligament is considered to be more significant than that of a deep pre-cracked structure of the small-scale yielding assumption, because it does not only determine the magnitude of elastoplastic field disturbance caused by notch root radius variation, but also is the carrier of the work hardening development during the stretching process. What percentage of the convergent elastoplastic fields occupying the ligaments can be called "broadly convergent" is also an essential issue in applicating the concept of shallow crack-like notch identification proposed by this study. According to Fig. 2.6, when t = 0.5 mm and r = 3 mm, namely, t/l = 20%, the "broadly convergent" of the elastoplastic fields at least should occupy 80% of ligaments within less than 5% discrepancy in elastoplastic fields to maintain the same overall work hardening condition at the onset of plastic instability. However, the above results cannot be used as a general conclusion because they are not constants of material plastic properties in general yielding conditions and also can be influenced by geometric properties of notches and structures. Hence, "broadly convergent" presently should base on the practical design requirements of shallow crack-like notches and the calculation of

overall work hardening conditions by FEA. From the engineering viewpoint, it is more intuitive to obtain a general quantitative definition of "broadly convergent." A potential solution is correlating the elastoplastic field gradients dominated by material and geometric properties to the index of plastic strain localization. The abovementioned important influential factors for the identification of shallow crack-like notches will be investigated in detail in future studies.

2. 4 Chapter conclusions

The emphasis of this study is a new concept for identifying the shallow crack-like notches with the pre-condition of plastic instability, such as necking, occurring before the pre-crack propagation. This condition may readily take place in shallow pre-cracked structures made of strain-hardening materials. Generally, the overall work hardening in one yield cross-section determines the onset of plastic instability. Hence, the existence of shallow crack-like notches is attributed to the overall work hardening in notched cross-section is insensitive to the notch geometric variation (excepting the notch depth). Such physical reasoning corresponds to that of the conventional deep crack-like notches requiring a condition that the fracture process is insensitive to the notch geometric variation. This study extended the idea of crack-like notched from the fracture instability range to the plastic instability range. The following conclusions were drawn from this study:

1. A shallow crack-like notch may exist when structural strength is governed by plastic instability.
2. When the plastic instability governs the structural strength of strain-hardening materials, a crack-like notch should satisfy the following requirements:

(1) The structural strength should be independent of the notch geometry, except for the notch depth;

(2) The elastoplastic fields in the notched cross-section should be broadly convergent to those in the pre-cracked cross-section such that the overall work hardening is identical;

(3) The failure mode should be the same.

3. The material work hardening exponent, notch root radius, and ligament size may exert relatively significant influences on the identification of shallow crack-like notches.

CHAPTER 3. Shallow crack effect on evaluation of residual tensile strength: harmless and stable cracks in finite-sized structure made of ductile metals

3. 1 Introduction

Cracks or crack-like defects are widely believed to weaken engineering structures [7,9,10,44] while achieving flawlessness is impracticable. Hence, the residual strength [2,8,12], which reflects the practical load-carrying capacity of pre-cracked structures, is always a critical concern in fail-safe designs [3,5,6,11]. With the assistance of fracture mechanics, conventional considerations of residual strength mainly focus on cracks deeply embedded in structures [2,3,7–12,44]. However, as technology advances, most pre-cracks in engineering structures nowadays become very shallow. Such shallow cracks [40], whose plastic zone size is usually comparable to the crack depth or even structure dimensions [45,46], have been recognized to have distinct mechanical properties [47,48] and may result in anti-commonsense phenomena, such as the shallow (or short) crack problem in fatigue [49].

Nevertheless, previous studies have rarely involved the residual strength issue of shallow pre-cracked structures, neither the physical meaning of residual strength nor the corresponding damage characteristic has been clarified, let alone reasonable

evaluations and predictions. As mentioned in CHAPTER 1, the increase of fracture instability toughness with the decrease of pre-crack depth can result in plastic instability appearing prematurely and make the physical meaning of residual strength vague. Meanwhile, the of notch strengthening study indicate that the localized deformation near the notch root combined with the triaxial stress state can resist yielding process [68] and a cracked structure should also has a similar phenomenon when plastic instability dominates the structural strength. However, experiences of notched structures probably cannot be directly applied to residual strength issue due to different definitions of strength. Therefore, investigation of shallow crack effect on residual strength is still required.

This chapter focuses on understanding the trends, physical meanings, and damage characteristics of residual strength of shallow pre-cracked structures. The trends of residual strength with shallow pre-crack depth were obtained by monotonically stretching cylinder specimens with shallow crack-like circumferential notches. Next, the physical meaning of residual strength and the corresponding damage characteristics were investigated using a scanning electron microscope (SEM) with an electron backscatter diffraction (EBSD). The effects of plastic strain localization combined with stress triaxiality on local failure (fracture at crack tips) and global failure (cross-sectional plastic instability) were dissertated based on finite element analysis (FEA). According to elastic-plastic field responses to pre-crack depth variations, the pre-cracked section was divided into three partitions, namely, cross-sectional reduction (by pre-crack) partition, near crack-tip partition, and remote crack-tip partition. These partitions assisted the clarification of negative and positive influences of pre-cracks on the load-carrying capacity of pre-cracked sections. Then, the concept of shallow crack effect in residual strength issue was proposed and its universality was discussed.

3. 2 Experimental and analytical methods

3.2.1 Material and testing

The chemical composition of IF steel is listed in Table 2.1. The atoms of C and N are fixed by Ti (CN) to ensure that the content of interstitial solute atoms is extremely low [89]. The raw material was treated by annealing to improve the ductility and reduce the anisotropy. It was kept in a furnace at 750 ℃ for two hours and then cooled down to room temperature. After annealing, its hardness and average grain size were adjusted to 65 HV and 52.3 μm, respectively.

Circumferential pre-cracks on cylinder specimens can well satisfy the plane strain condition, but their geometric symmetry and depth measurability are hardly guaranteed by fatigue pre-cracking. An alternative method is circumferentially grooving a crack-like notch (V-shape) in the middle of the gage, as explained in CHAPTER 2. The design dimensions of specimens are illustrated in Fig. 3.1(a). The variation of notch opening angle, α, in the range of 0 to 90° has little influence on mechanical properties [62,84,90] compared with the notch root radius, ρ, and notch depth, t. Besides, it can be regarded as an initial opening angle of pre-crack. Hence, α was set at 60° for the convenience of machining and polishing. The buff polish was applied to the gage with 0.05 μm alumina. The final dimensions of the notched specimens are listed in Table 3.1.

Table 3.1 Final dimension of circumferential notch (notch depth, t, notch root radius, ρ, radius of intact section, r, and ligament of notched section, l), stress concentration factor, K_t, yield strength, $\sigma_{0.2}$ (0.2% proof stress), residual strength, σ_R, gage elongation, λ, and reduction of area after rupture, ψ.

No.	t/l (%)	t (mm)	r (mm)	ρ (mm)	$\sigma_{0.2}$ (MPa)	σ_R (MPa)	λ (%)	ψ (%)	Note
0	0	0	3.01	0.000	116.1	246.4	62.6	97.7	Smooth specimen
Continuous test:									
1	0.7	0.02	3.02	0.011	112.9	245.4	57.0	97.8	Ruptured in post-necking elongation
2	1.0	0.03	3.00	0.011	104.8	242.2	56.7	97.7	
3	2.0	0.06	3.01	0.010	106.3	245.0	56.1	97.7	
4	3.8	0.11	3.02	0.012	105.7	244.5	55.3	97.9	
5	4.5	0.13	3.02	0.013	109.9	243.2	46.4	97	
6	6.0	0.17	3.01	0.011	110.3	240.2	45.9	96.8	
7	20.3	0.51	3.03	0.005	107.7	228.1	28.8	95.9	
8	22.8	0.56	3.02	0.012	102.6	220.7	28.3	96.1	
9	21.2	0.53	3.03	0.025	104.1	223.8	28.9	96	
10	30.1	0.70	3.03	0.012	102.7	205.0	21.3	95.8	
11	35.4	0.79	3.02	0.012	101.9	180.9	16.0	95.4	
12	51.6	1.03	3.03	0.012	102.9	150.9	11.0	95.8	
Interrupting test:									
13	2.7	0.08	3.02	0.012	103.2	—	4.9	—	Terminated at σ^{nom} = 160 MPa
14	4.6	0.13	2.97	0.011	103.9	—	4.8	—	
15	19.8	0.50	3.02	0.012	101.4	—	4.8	—	
16	50.5	1.01	3.01	0.013	100.3	—	6.4	—	Terminated at $\sigma^{nom} \approx \sigma_R$ = 150 MPa

Different from the notch strength evaluation usually depending on the net cross-section [54,67,68], residual strength evaluation was based on the intact cross-section in this study. That is, the residual strength was derived by the nominal cross-sectional stress, σ^{nom}, and notch tensile strength was derived by the net cross-sectional stress, σ^{net}, as followings:

Nominal cross-sectional stress: $\sigma^{nom} = \frac{P}{A^{int}} = \frac{P}{\pi r^2}$ (3-1)

Net cross-sectional stress: $\sigma^{\mathrm{net}} = \frac{P}{A^{\mathrm{net}}} = \frac{P}{\pi l^2}$ (3-2)

where P is the load, A^{int} the initial area of intact cross-section, and A^{net} the initial area of net cross-section reduced by the presence of notch/crack. In this study, residual strength, σ_{R}, and yield strength (0.2% proof strength), σ_{Y}, were calculated by Eq. (3-1).

The specimens were stretched at room temperature with an initial strain rate of 1×10^{-3} /s. A digital camera was used to monitor the gage elongation and cross-sectional reduction (The method of strain measurement was changed from this chapter because some data in this chapter would be compared to that of CHAPTER 4 obtained in hydrogen environment, where the extensometer cannot be applied. Obviously, the strain data calculated by video record has a lower confidence compared to that obtained by extensometer in CHAPTER 2. However, the strain train data is only a reference value for the rest of the thesis, and it will not significantly affect the trend analysis of the residual strength and the magnitude of plastic strain localization). The fundamental mechanical property of IF steel was obtained by averaging the tensile results of two smooth specimens (No. 0 in Table 3.1) to reduce scatters. The specimens (No. 7 to 9) with the same t but different ρ were used to evaluate the dependence of σ_{R} on ρ, and served for the following identification of shallow crack-like notches. Additionally, four specimens were manually terminated at σ^{nom} = 160 MPa in the pre-necking elongation (No. 13 to 15) and σ^{nom} = 150 MPa $\approx \sigma_{\mathrm{R}}$ (No. 16) to investigate the pre-crack propagation, secondary crack initiation and plastic strain localization by microstructure observations.

Microstructure observations were performed on a scanning electron microscope (SEM) with an electron backscatter diffraction (EBSD) accessory to analyze damage phenomena and plastic strain distributions of post-testing specimens. The latter is

represented by the kernel average misorientation (KAM), which quantitatively relates to the density of geometrically necessary dislocation (GND) in lattice altered by plastic deformation [91–93]. The preparation of the longitudinal section of gage followed the process shown in Fig. 3.1(b). The SEM and EBSD were operated at 15 kV, and by a beam step size of 5 μm at 15 kV, respectively.

3.2.2 Implementation of finite element analysis

The material model used for elastic-plastic FEA was isotropic nonlinear and rate-independent hardening. Hence, the true stress-strain curve of the smooth specimen (No. 0 in Table 3.1), as plotted in Fig 3.2(a), was directly used as the strain hardening curve. For the elastic elongation, Young's modulus, E = 198.75 GPa, and Poisson's ratio, v = 0.30. The FEA results fitted well with the experimental data, as shown in Fig. 3.2(b). The FEA model was established in ANSYS Workbench 18.2. As shown in Fig. 3.3(a), the specimen was simplified to an axisymmetric model, which was a quarter of the gage projecting on the O-*xy* plane with 2D Cartesian coordinates. The *y*-axial displacement, U_y, was fixed at $[0 \leq x \leq \mathrm{l}, y = 0]$. For the smooth specimen, the top-end of the model was cemented to an additional rigid grip to generate necking [94]. The value of P was calculated by the force reaction of U_y at $[0 \leq x \leq r, y = H/2]$. The axisymmetric and large deflection options were selected. The model was meshed (Quadratic dominant) by a higher order 2D, 8-node element (PLANE183) [81]. Element refinements were applied to areas near notch roots/crack tips and ligaments. Meshing examples of the notch root/crack tip are shown in Fig. 3.4(b). The minimum element size was optimized to 0.1 μm to guarantee the following FEA results were independent of the element size within the precision of two decimals.

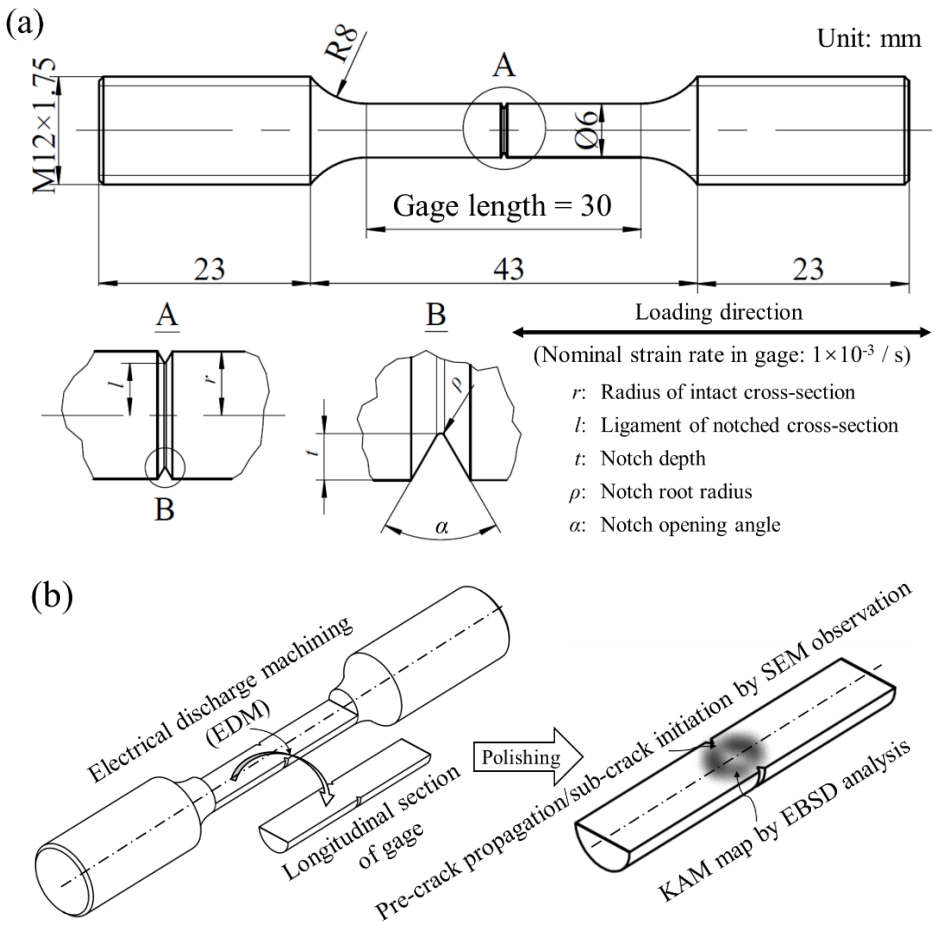

Fig.3.1 (a) Geometry of circumferentially notched specimen. (b) Preparation of longitudinal section of gage.

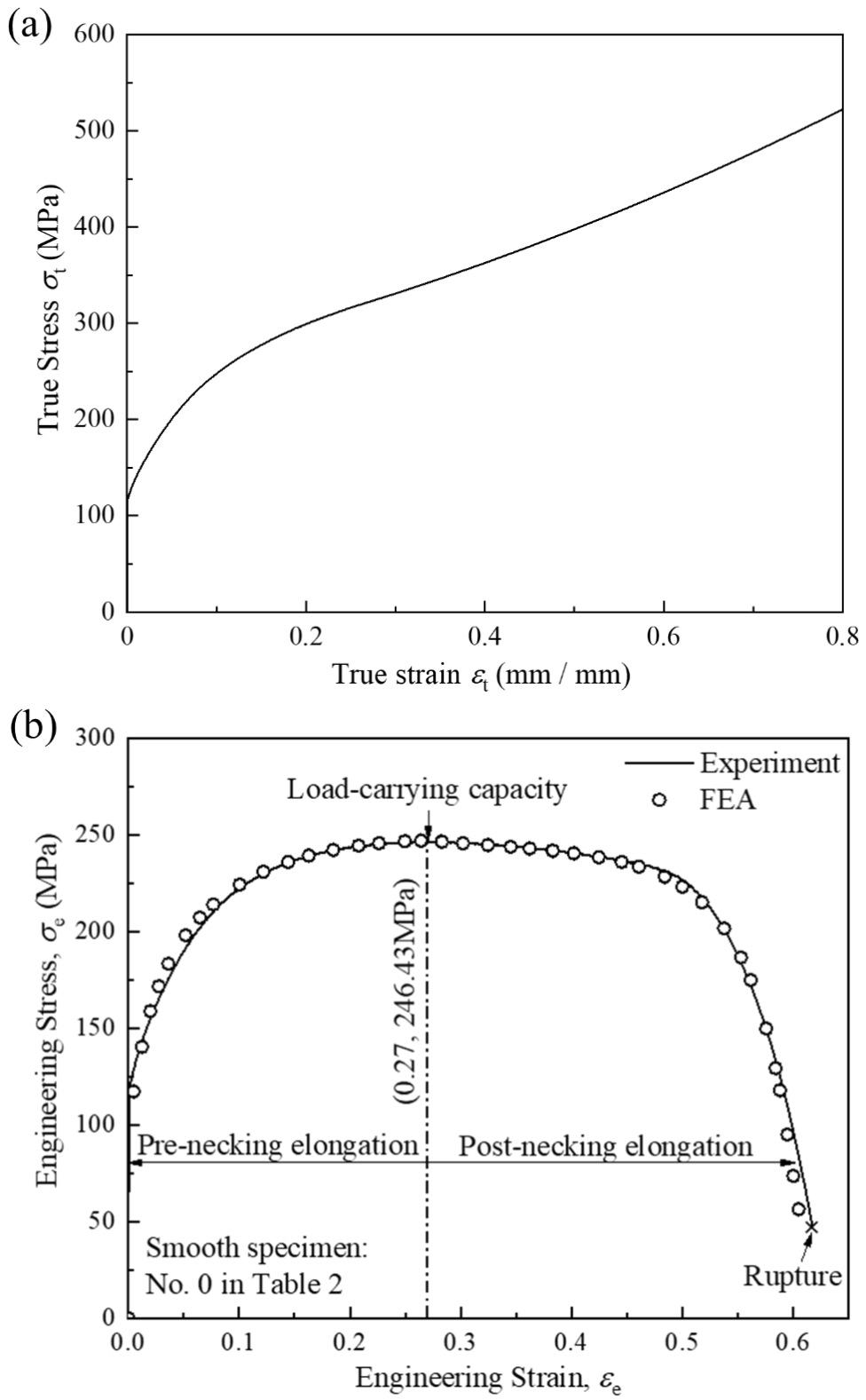

Fig. 3.2 (a) True tress-strain curve of smooth specimen obtained by experiment. (b) Engineering stress-strain curve of smooth specimen obtained by experiment and finite element analysis.

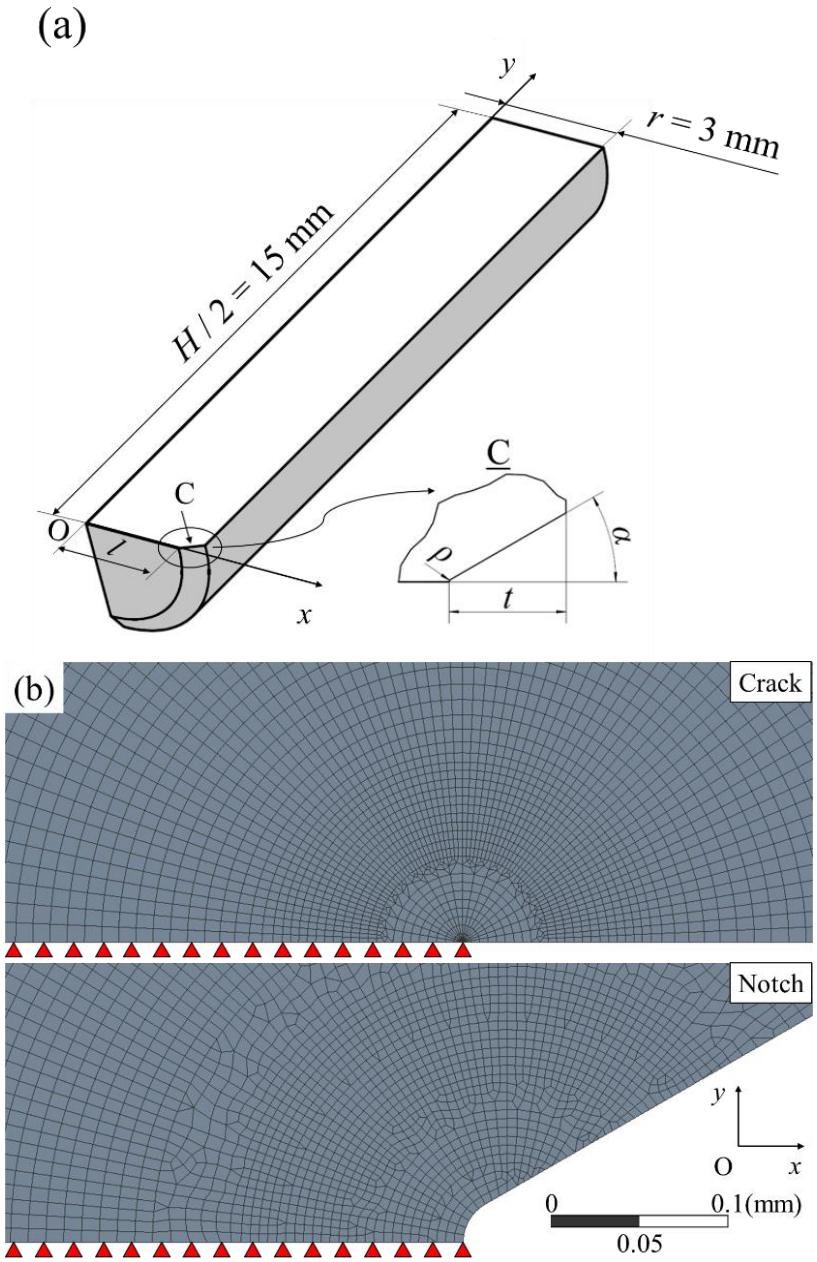

Fig. 3.3 Simplified model for finite element analysis: (a) geometry in 2D Cartesian coordinates; (b) examples of meshing near notch root and crack tip.

3. 3 Results

The mechanical properties measured by the experiment were summarized in Table 3.1 (For detailed information on engineering stress-strain curves of tested specimens, see Appendix A3). The gage elongation, λ, dramatically degraded with the increase of normalized notch depth, t/l, indicating that the structural ductility was sensitive to the

presence of geometrical discontinuities. When σ_{R} was plotted against t/l, as shown in Fig. 3.4(a), an apparent plateau of the 'IH' segment, which equaled to the tensile strength of smooth specimens, existed until a significant decreasing trend in the 'HT' segment. This plateau of σ_{R} was initially supposed to be caused by notch strengthening phenomenon. However, when the net cross-sectional strength, σ_b^{net}, was plotted against t/l, as shown in Fig. 3.4(b), the notch strengthening existed in the full range of t/l because σ_b^{net} increased with t/l almost smoothly. Besides, in Fig. 3.4(a), the measured trends of σ_{R} seem to have a distinct physical transition point of 'H,' because the necking and rupture of specimens in the plateau of 'IH' segment (No. 1 to 5 in Table 3.1) even occurred in the intact cross-section of the gage, see the example of No. 2 in Fig. 3.4(a). It conflicted with the commonsense that the geometric discontinuity, as a stress concentrator, would generate the failure and confine the fracture locus. Additionally, all specimens of continuous tests invariably ruptured in the post-necking elongation. Hence, plastic instability should occur under loading but whether it is the physical meaning of σ_{R} still needs the latter microscopic analysis.

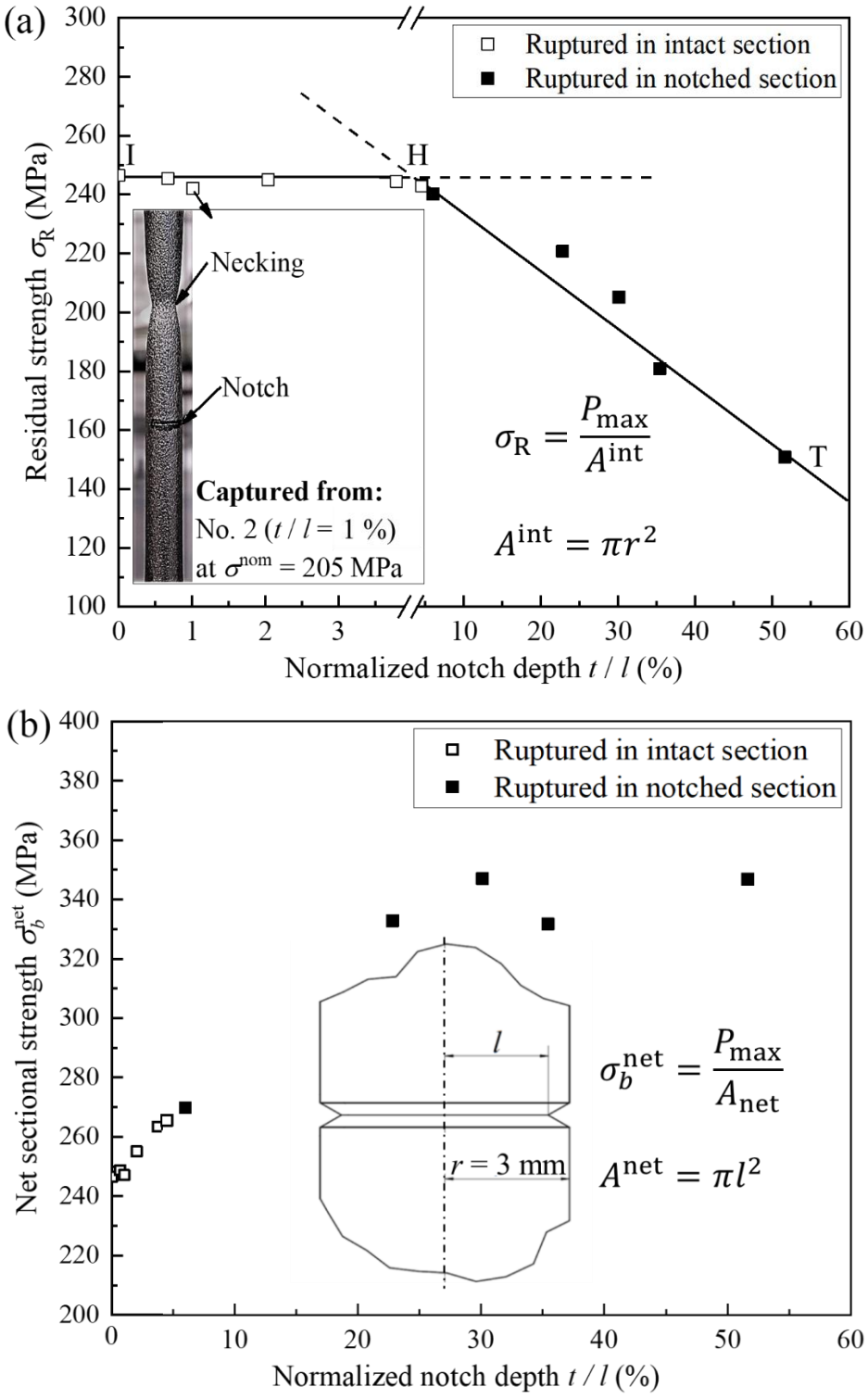

Fig. 3.4 Responses of (a) residual strength, σ_R, and (b) net sectional strength, σ_b^{net}, to variation of notch depth, t, with a constant radius of intact section r = 3 mm.
(Note: the straight segment in Fig. 3.4(a) were drawn for dividing different response of σ_R to t, they do not represent the precise trends of σ_R)

Fig. 3.5 shows the dependences of σ_R on ρ obtained by experiments and FEA. The results of t/l = 20 % indicate that σ_R were independent of ρ = 0.005 to 0.025 mm. This trend was also valid for other configurations of t/l in the range of 0.5 % < t/l < 55 % (including the shallowest and the deepest notches). Besides, the case of ρ = 0 denotes a real crack that has α = 0 (see the 'crack example' in Fig. 3.3(b)). It again proved that α = 60° is insignificant for identifying crack-like notches in this study. The results here only aimed to state that the notches in Table 3.1 were equivalent to cracks. Hence, no consideration was further placed on the size effect on shallow crack-like notches. Therefore, hereinafter, the notches listed in Table 3.1 are regarded as cracks, and then t directly denotes pre-crack depths. Additionally, the authors believe that a systematic discussion about the equivalence between the shallow notch and shallow crack could be of great significance for experimental and engineering designs. This issue may be solved in future studies.

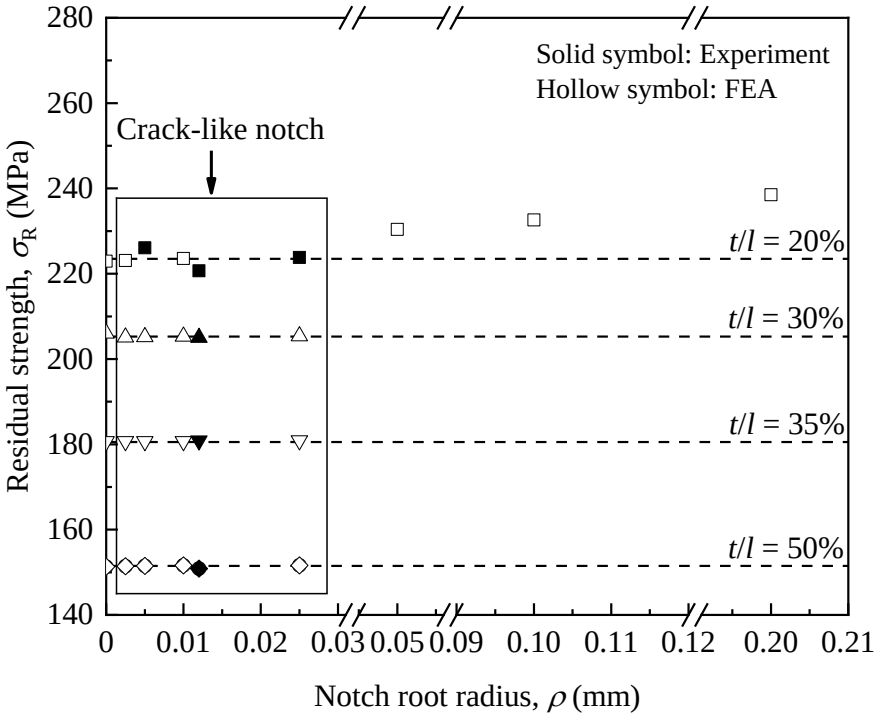

Fig. 3.5 Notch root radius ρ influences on residual strength, σ_R.

The fractographs of ruptured specimens with representative damage characteristics are shown in Fig. 3.6. The smooth specimen (No. 0 in Table 3.1) exhibits a typical ductile failure with the cup-and-cone appearance, which was caused by the internal crack initiation (see the fibrous zone with large equiaxed dimples [17,31,95]) and final intersection with the outer surface of the specimen (see the shear-lips [17,96]) in the post-necking elongation. The specimens (No. 1 to 5) in the plateau of 'IH' segment in Fig. 3.4(a) that were ruptured in the intact cross-sections have a similar damage pattern compared with the smooth specimen, so they are not presented here. However, when ruptures moved to pre-cracked cross-sections, see Figs. 3.6(b) to (d), an apparent deviation of internal crack initiation from the cross-sectional center shown in Figs. 3.6(b) and (c) to the outer (near the pre-crack tip) shown in Figs. 3.6(d) occurred. It is inferred that the increase in pre-crack depth changes the damage characteristics by increasing plastic strain localization, which may correspond to the trends of σ_R.

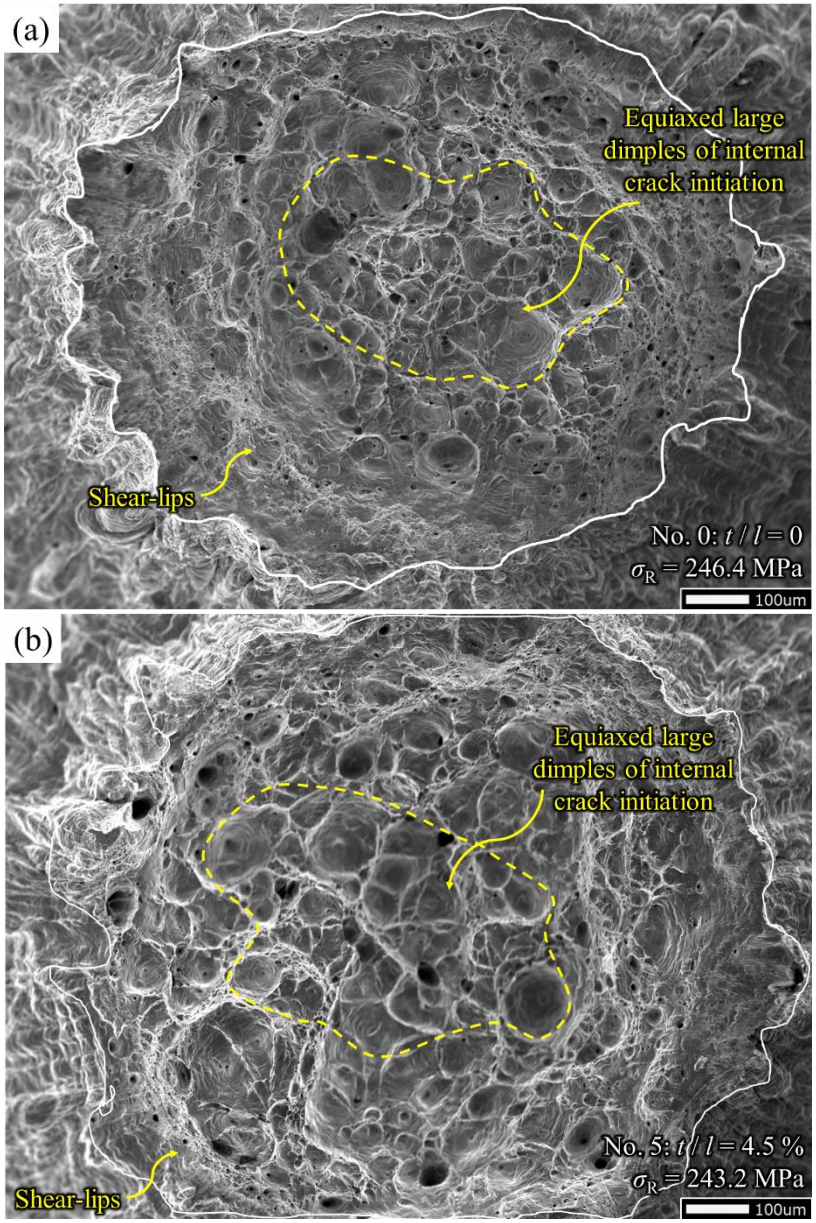
(a)
Equiaxed large dimples of internal crack initiation
Shear-lips
No. 0: $t / l = 0$
$\sigma_R = 246.4$ MPa
100um
(b)
Equiaxed large dimples of internal crack initiation
Shear-lips
No. 5: $t / l = 4.5$ %
$\sigma_R = 243.2$ MPa
100um

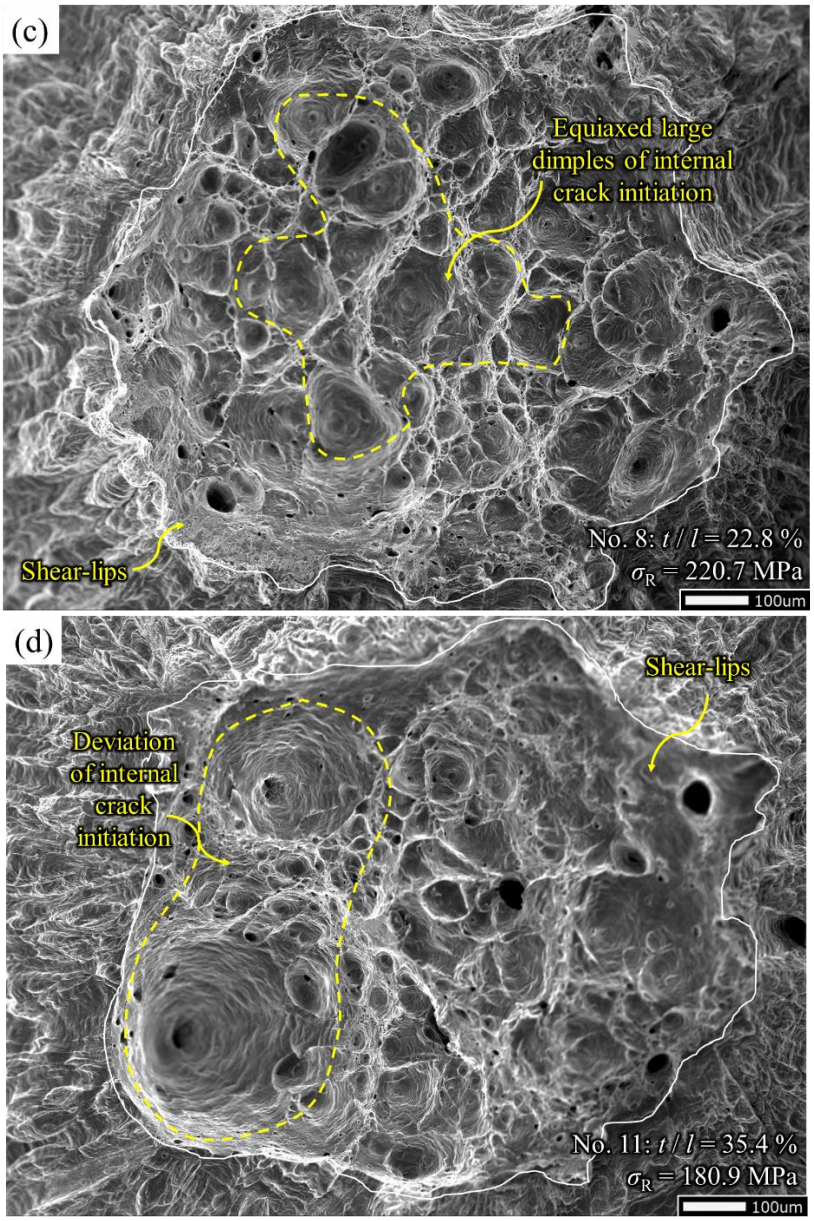

Fig. 3.6 Fractographs of ruptured specimens with representative damage patterns (white solid line shows initial pre-crack tip; yellow dash line shows large equiaxed dimples of internal crack initiation): (a) t/l = 0 (No.0: smooth specimen), (b) t/l = 4.5% (No. 5), (c) t/l = 22.8% (No. 8), and (d) t/l = 35.4% (No. 11).

Fig. 3.7 shows the representative enlarged views in the vicinity of pre-crack tips: Fig. 3.7(a) represents the specimens ruptured in intact cross-sections in continuous tests; Fig. 3.7(b) represents the specimens terminated in pre-necking elongation and would rupture in pre-cracked cross-sections according to continuous tests; and Fig. 3.7(c) represents specimens terminated at σ_R and would rupture in pre-cracked cross-sections according to continuous tests. All pre-crack tips in Fig. 3.7 were blunted severely but neither the pre-crack propagation nor the secondary crack initiation was observed in the vicinity of pre-crack tips, even for Fig. 3.7(c) of deepest pre-crack (No. 16 in Table 3.1) terminated at σ_R. Consequently, for all specimens listed in Table 3.1, pre-cracks remained non-propagating before the onset of plastic instability. That is, the physical meaning of σ_R is plastic instability instead of fracture instability. This also supports the assumption of FEA implementation without considering the damage initiation.

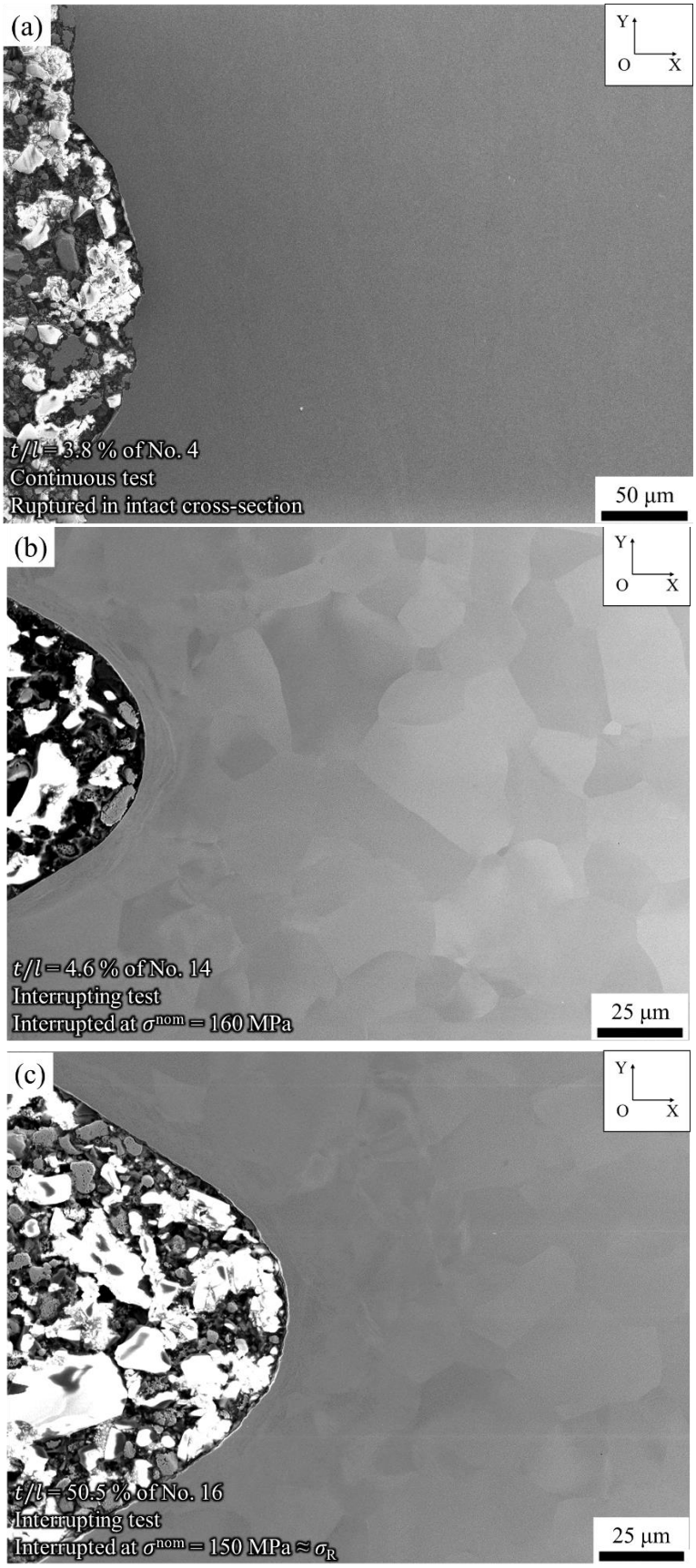

Fig. 3.7 Representative enlarge views in vicinity of blunted pre-crack tips for inspection of pre-crack propagation and sub-crack initiation: (a) t/l = 3.8% - ruptured in smooth section; (b) t/l = 4.6% - interrupted at σ^{nom} = 160MPa; (c) t/l = 50.5% - interrupted at $\sigma^{\mathrm{nom}} \approx \sigma_{\mathrm{R}}$ = 150 MPa.

It is remarkably interesting why transition point 'H' in Fig. 3.4(a) distinguishes two different damage characteristics but with the same physical meaning of σ_{R}. There should be two individual elastoplastic responses to the variation of t/l in the pre-cracked cross-section. Fig. 3.8 (a-K) (b-K) (c-K) show the KAM maps of specimens (No. 13 to 15 in Table 3.1) interrupted at σ^{nom} = 160 MPa. As the increase of t/l, a clear trend of plastic strain localization in front of the pre-crack tip can be seen. Additionally, another plastic strain localization site occurs near the specimen central axis in Fig. 3.8 (c-K) when t/l = 19.8%. Figs. 3.8 (a-P) (b-P) (c-P) show the normal axial plastic strain, ε_{ii}^{pl}, along ligament obtained by FEA. The normal y-axial plastic strain, ε_{yy}^{pl}, which is parallel to the loading direction, occupied the majority area of the ligament. Particularly, it proves that the plastic strain localization site near the specimen central axis in Fig. 3.8 (c-K) is due to the intensified ε_{yy}^{pl} occurs in the center axis when t/l = 19.8%. Figs. 3.8 (a-F) (b-F) (c-F) show the counters maps of ε_{yy}^{pl} normalized by that of the smooth specimen, $\bar{\varepsilon}_{yy}^{pl}$. The expansions of the high crack-tip plastic strain is resisted by the contiguous enclave of low plastic strain, which is conjectured to be caused by the high stress triaxiality.

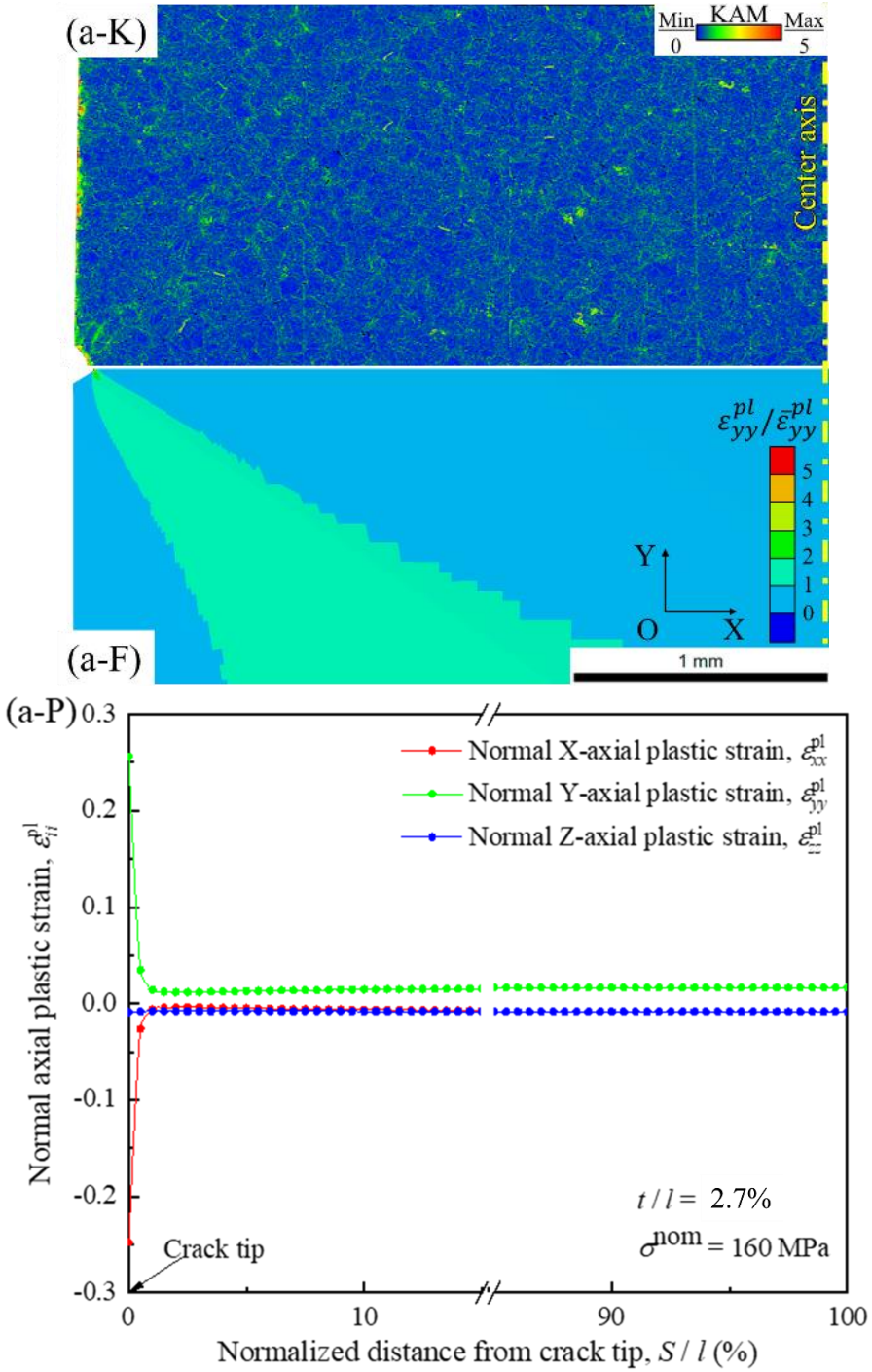
(a-K)
Min
KAM
Max
0
5
Center axis
$\varepsilon_{yy}^{pl}/\bar{\varepsilon}_{yy}^{pl}$
5
4
3
2
1
0
Y
O
X
(a-F)
1 mm
(a-P)
Normal X-axial plastic strain, ε_{xx}^{pl}
Normal Y-axial plastic strain, ε_{yy}^{pl}
Normal Z-axial plastic strain, ε_{zz}^{pl}
Normal axial plastic strain, ε_{ii}^{pl}
0.3
0.2
0.1
0.0
-0.1
-0.2
-0.3
t/l = 2.7%
σ^{nom} = 160 MPa
Crack tip
0
10
90
100
Normalized distance from crack tip, S/l (%)

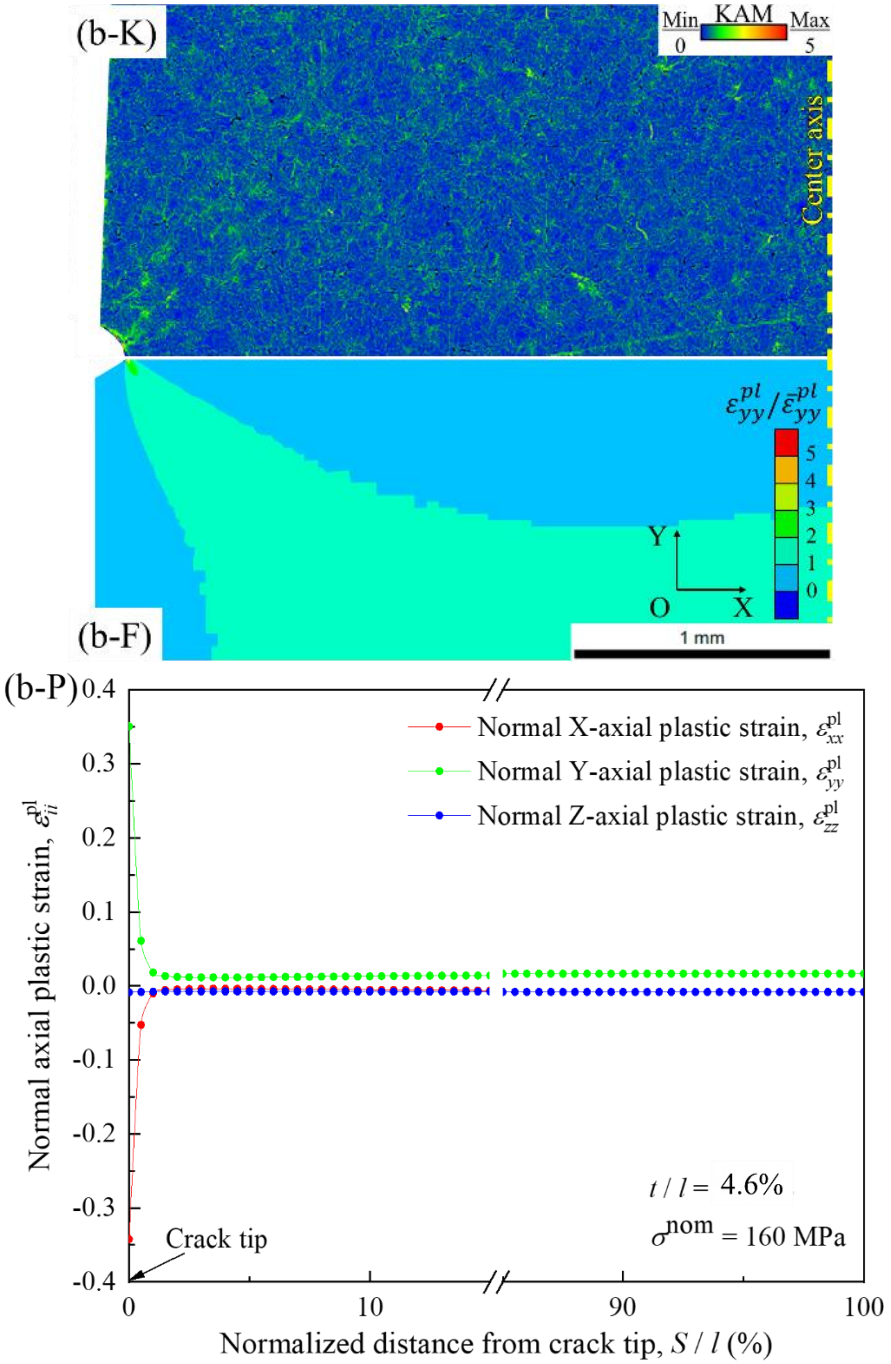
(b-K)
Min
KAM
Max
0
5
Center axis
$\varepsilon_{yy}^{pl}/\bar{\varepsilon}_{yy}^{pl}$
5
4
3
2
1
0
Y
O
X
(b-F)
1 mm
(b-P)
Normal X-axial plastic strain, ε_{xx}^{pl}
Normal Y-axial plastic strain, ε_{yy}^{pl}
Normal Z-axial plastic strain, ε_{zz}^{pl}
Normal axial plastic strain, ε_{ii}^{pl}
0.4
0.3
0.2
0.1
0.0
-0.1
-0.2
-0.3
-0.4
t / l = 4.6%
σ^{nom} = 160 MPa
Crack tip
0
10
90
100
Normalized distance from crack tip, S / l (%)

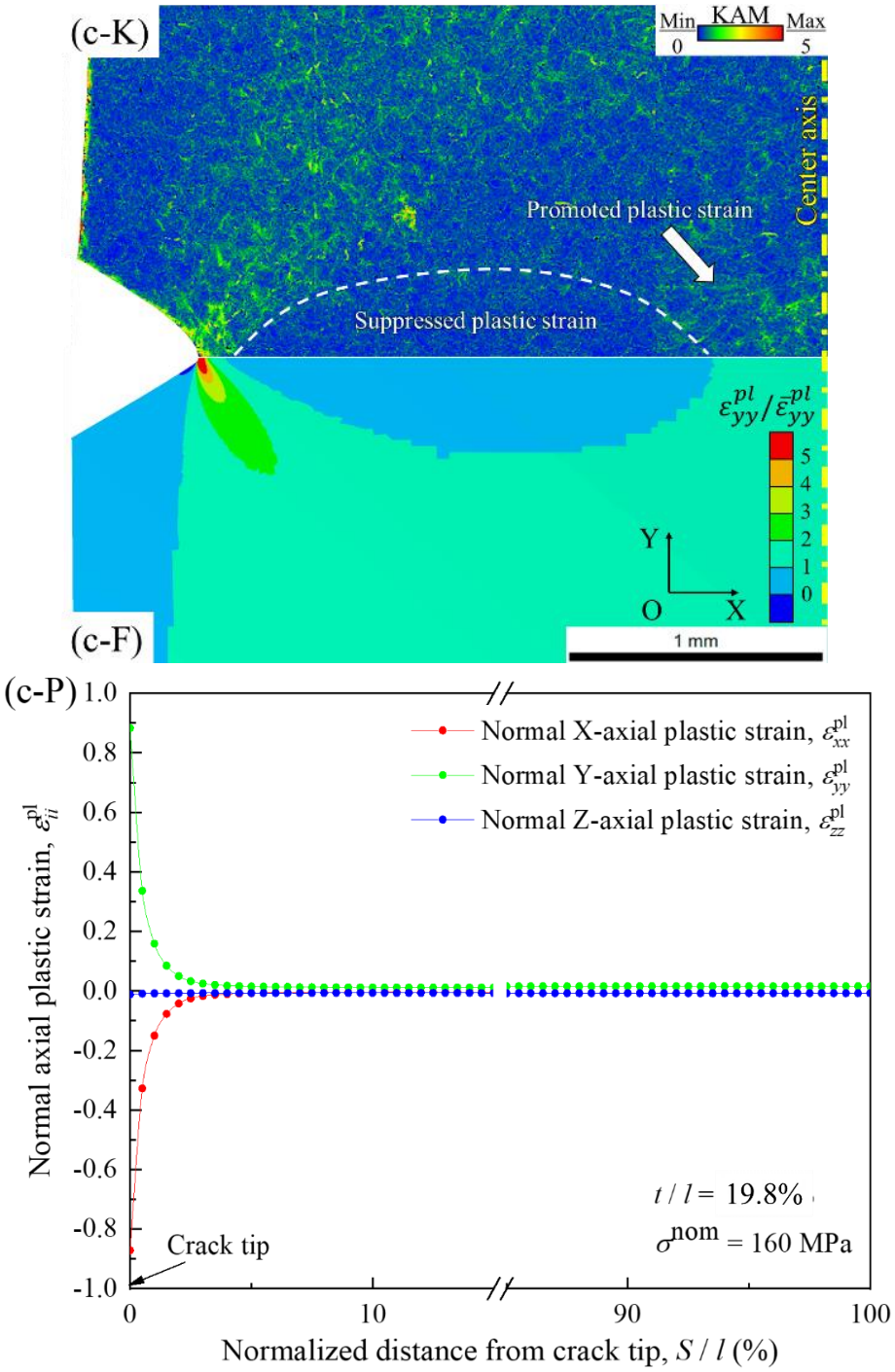

Fig. 3.8 Plastic strain distribution represented by: (a-K)(b-K)(c-K) KAM map by EBSD; (a-P) (b-P) (c-P) Normal axial plastic strain, ε_{ii}^{pl}, along ligament by FEA; and (a-F) (b-F) (c-F) Counters map of normal Y-axial plastic strain deviator, ε_{yy}^{pl}, by FEA normalized by that of smooth specimen, $\bar{\varepsilon}_{yy}^{pl}$.

3. 4 Discussion

3.4.1 Shallow crack effect in residual strength issue and its general applicability

Previous studies of residual strength of pre-cracked structures are one-sided because the loss of load-carrying capacity is not only determined by fracture instability but also by geometric instability or plastic instability [12,38,97]. Geometric instability, such as bucking and bulging [41–43], limits the load-carrying capacity as a result of the dramatic geometric variation deviating the deformation path from the original loading path. The cylinder specimens under in-plane tension naturally prevent the deformation path straying from the tensile direction in the pre-necking elongation. Therefore, this study only needs to consider fracture instability and plastic instability in pre-cracked cross-sections.

The competition between fracture instability and plastic instability in dominating the residual strength is illustrated in Fig. 3.9. As the pre-crack depth decreasing, *R*-curve rises due to the loss of plastic constraint [31,98–100]. When the load threshold of fracture instability is higher than that of plastic instability, the trace of *R*-curves will be cut off, as the cross marks on *R*-curves of t_a and t_b in Fig. 3.9. The cut-off point may exist in the crack blunting stage, like the results in this study, or in the stable crack propagation stage. The following situations in pre-cracked cross-sections can be recognized:

1. Plastic instability occurs before the pre-crack propagation, as the case of t_a at $\sigma^{\mathrm{nom}} = \sigma'_{t_a}$, which is applicable to all pre-cracked specimens tested in this study;

2. Plastic instability occurs with stable pre-crack propagation, as the case of t_b at $\sigma^{\text{nom}} = \sigma'_{t_b}$;

3. Fracture instability occurs before plastic instability, as the case of $t = t_c$ at $\sigma^{\text{nom}} = \sigma_{t_c}$ (the conventional considerations of deep pre-cracked structures).

Evidently, the residual strength in the first and second cases has the same physical meaning so they can be integrated into one condition. That is, shallow pre-cracks remained non-propagating or stable propagating until at least the onset of plastic instability. This condition was used to distinguish shallow and deep cracks for the convenience of the following discussions.

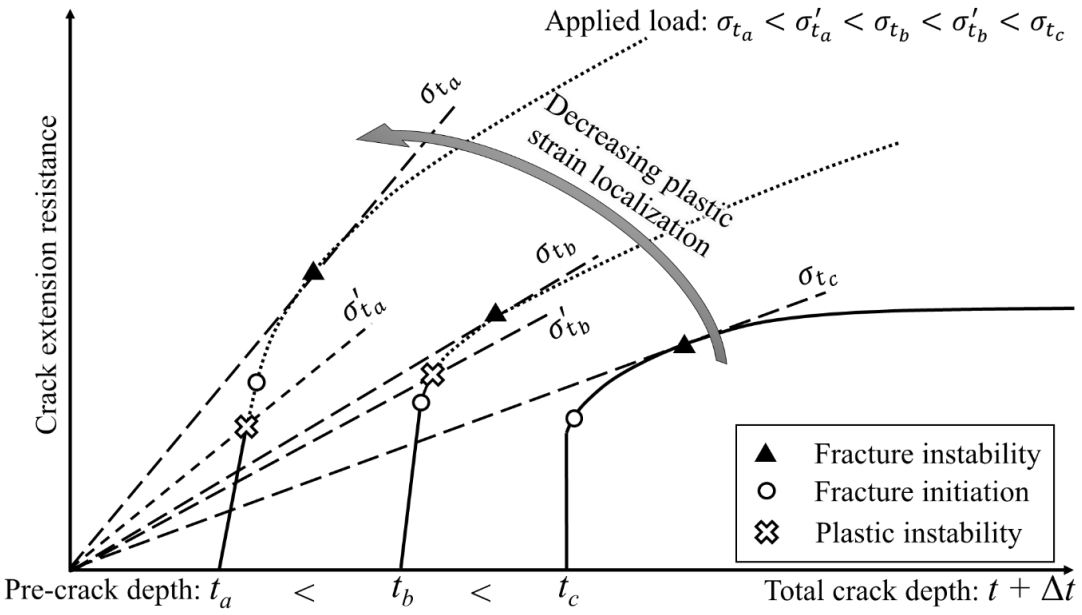

Fig. 3.9 Competition between fracture instability and plastic instability in dominating residual strength of pre-cracked structures (σ_{t_a}, σ'_{t_a}, σ_{t_b}, σ'_{t_b}, and σ_{t_c} and σ_{t_d} are represented by nominal stress, σ^{nom}, in this study).

3.4.2 Mechanism of shallow crack effect

The increases of plastic strain localization and stress triaxiality with the deep crack depth can stimulate the fracture instability. However, results in this study showed that the presence of shallow pre-cracks might not weaken the structures (see the 'IH' plateau in Fig. 3.4(a)), thereby inferring plastic strain localization coupled with stress triaxiality has a distinct influence on plastic instability. Fig. 3.10 plots the distributions of plastic strain deviation, ε_{yy}^{pl}, and stress triaxiality, η, in the ligaments of pre-cracked sections during pre-necking elongation. η is written as [31]:

$$\eta = \frac{\sigma_h}{\sigma_{eq}} = \frac{\sqrt{2}(\sigma_1+\sigma_2+\sigma_3)}{3\sqrt{(\sigma_1-\sigma_2)^2+(\sigma_2-\sigma_3)^2+(\sigma_1-\sigma_3)^2}} \tag{3-3}$$

where σ_h and σ_{eq} are hydrostatic stress and von Mises equivalent stress, respectively. As shown in Fig. 3.10(a), ε_{yy}^{pl} increased with t/l near crack tips, but decreased in the remote place, indicating the plastic strain localization is proportional to t/l. Correspondingly, η increased in the remote place, as shown in Fig. 3.10(b), but it formed a parabola in the vicinity of crack tips, as shown in Fig. 3.10(b). Namely, a larger t/l resulted in a lower η at the crack tip but induced a higher peak of η. Notably, the suppressed plastic strain with the increased stress triaxiality that resists the yielding occupied the majority part of the ligament. Hence, the main effect of the plastic strain localization coupled with stress triaxiality is hindering plastic instability. This effect became significant with the increase of shallow crack depth according to the trends of ε_{yy}^{pl} and η in the remote places of pre-crack tips in Fig. 3.10.

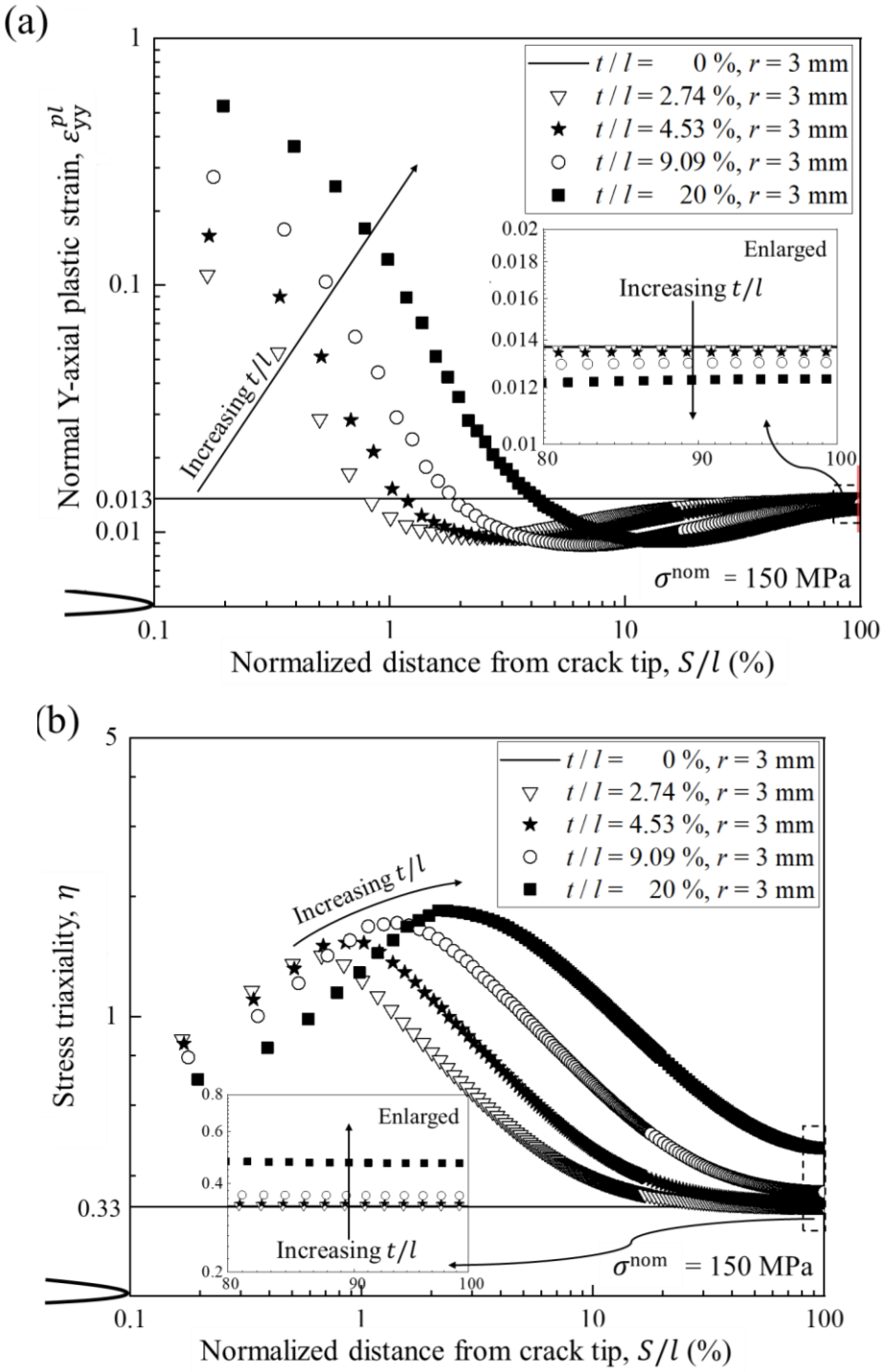

Fig. 3.10 Distributions of plastic strain deviation, ε_{yy}^{pl}, and stress triaxiality, η, in ligaments of pre-cracked sections during pre-necking elongation.

Although the increases in plastic strain localization and stress triaxiality probably can enhance the load-carrying capacity, the trends of σ_R obtained by experiment showed another case. To further clarify when the presence of shallow crack is negative

or positive, the pre-cracked section was divided into three partitions, as shown in Fig. 3.11. The red color denotes the cross-sectional reduction, which always has a negative effect on the load-carrying capacity. The green color denotes the near crack-tip portion that has intense plastic strain and stress triaxiality. The blue color denotes the remote crack-tip portion that, which is always positive for the load-carrying capacity because of suppressed plastic strain and moderate stress triaxiality hindering the onset of plastic instability. Hence, if the negative influence of the cross-sectional reduction can be offset by the combined influences of the remote crack-tip portion and the near crack-tip portion, the residual strength would not decrease and even the pre-cracked cross-section can be strengthened. However, the influence of the near crack-tip portion is not immutable. It depends on the damage initiation controlled by the magnitude of plastic strain localization and stress triaxiality. With a low magnitude of plastic strain localization, if there is no apparent fracture in the near crack-tip portion, such as pre-crack propagation and secondary crack initiation, the strain-hardening by intense plastic strain combined with stress triaxiality can provide an additional positive influence on the load-carrying capacity. Hence, the existence of pre-crack is harmless, and the rupture occurs in the intact cross-section, just like the case of the 'IH' plateau of σ_R in Fig. 3.4(a).

In summary, shallow crack effect in residual strength issue resulted from the following factors: 1. The fracture toughness of shallow cracks were so high that the main impact of the plastic strain localization coupled with stress triaxiality changed from stimulating fracture instability at crack tip to hindering cross-sectional plastic instability; 2. The presence of shallow pre-cracks resulted in both negative and positive influences on load-carrying capacity in different partitions of the pre-cracked cross-section. It has general applicability. First, most ductile ferrite steels have the strain

hardening mechanisms that give rise to a decreasing first derivative of σ_t vs. ε_t [35]. Thus, plastic instability does occur in many cases. Second, there is no absolutely perfect engineering component. Although various shallow cracks or crack-like flaws exist in/on the engineering components, their local failure behaviors and disturbances to elastic-plastic fields seem not to affect the overall mechanical properties. Therefore, shallow crack effect in residual strength issue is not the result of a case study with some unique materials or under exceptional test conditions. Instead, it is a general result in the case of low plastic strain localization that did not cause enough attention in previous studies.

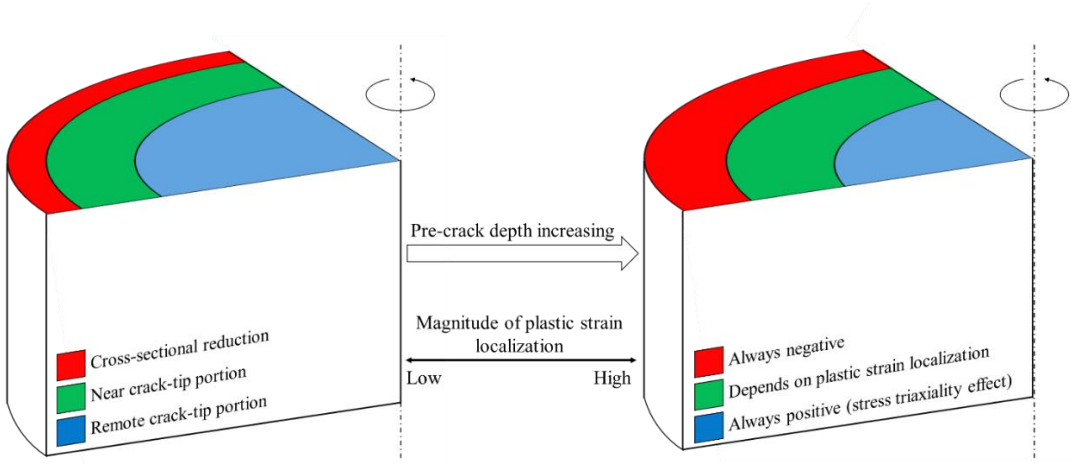

Fig. 3.11 Schematic of partitions and their effects on load-carrying capacity in pre-cracked cross-section.

3. 5 Chapter conclusions

The present work focused on the residual tensile strength of shallow pre-cracked structures that were rarely considered in the previous literature. Results showed that the residual strength of shallow pre-cracked specimens was preferentially governed by plastic instability instead of fracture instability because shallow pre-cracks remained non-propagating or stable propagating until at least the onset of plastic instability during

monotonic tension. Furthermore, when shallow pre-crack depths were shorter than a critical value, the rupture occurred in the intact cross-section, and the residual strength was identical to the tensile strength of smooth specimens. Based on macroscopic observation and FEA, the following conclusions can be drawn:

1. Shallow cracks have the following effect on residual strength evaluation.
    a. The fracture toughness of shallow cracks is so high that the main impact of the plastic strain localization coupled with stress triaxiality changed from stimulating fracture instability at crack tip to hindering cross-sectional plastic instability.
    b. The presence of shallow pre-cracks resulted in both negative and positive influences on load-carrying capacity in different partitions of the pre-cracked cross-section.
2. The physical meaning of residual strength changes with the pre-crack depth due to the different magnitudes of plastic strain localization and can be reflected in the variation of the damage characteristics.

CHAPTER 4. Residual strength prediction of shallow cracked structures

4. 1 Introduction

Predicting the residual strength [10,12] of the pre-cracked structure is in great significance for engineering safety consideration. Generally, there are two kinds of engineering predictions. That is, the qualitative prediction that usually base on the trend analysis, and qualitative prediction that can be addressed by both analytical solution and numerical solution. Qualitative prediction is popular in material selection and environmental effect analysis. For instance, the plastic strain localization can promote fracture instability while hinder plastic instability, so one can choose the appropriate material and working environment based on their effects on the plastic strain localization and physical meaning of mechanical properties. For the residual strength issues, since the physical meaning has been proved to alter with the pre-cracks in CHAPTER 3, a novel failure assessment diagram (FAD) correlating to physical meanings of residual strength and corresponding damage characteristics was resuggested for qualitative predicting the trends of residual strength from the perspective of plastic strain localization. Then, the intrinsic factors of material property and extrinsic factors of geometry, load, and environment that may affect the residual strength by influencing the plastic strain localization were discussed. of the pre-cracked structure is in great significance for engineering safety consideration. Generally, there are two kinds of engineering predictions. That is, the qualitative prediction that usually

base on the trend analysis, and quantitative prediction that can be addressed by both analytical solution and numerical solution. Qualitative prediction is popular in material selection and environmental effect analysis. For instance, the plastic strain localization can promote fracture instability while hinder plastic instability, so one can choose the appropriate material and working environment based on their effects on the plastic strain localization and physical meaning of mechanical properties. For the residual strength issues, the physical meaning has been proved to alter with the pre-crack depth in CHAPTER 3, but previous experiences about trend analysis of residual strength are almost based on analyzing the fracture instability responding to influential factors. Hence, a new evaluation criterion required to include the range of shallow cracks.

For quantitative prediction, the primary task conventionally is providing a confident value of residual strength. It is unrealistic to fully reproduce the actual and complex working conditions in the prediction. Hence, the qualitative prediction usually requires a simplified model, which depends on correctly determining the dominant factor of predicted target. In chapter 3, the pre-cracked section was divided into partitions, namely, cross-sectional reduction partition, near crack-tip partition, and remote crack-tip partition. It is interesting to know which partition is the dominated factor for residual strength prediction of shallow pre-cracked structures. Also, how to generate the correct damage phenomenon, such as the necking away from the intact cross-section, is also meaningful because it helps engineers perceive the inflection point of residual strength in the range of shallow cracks.

In this chapter, a novel failure assessment diagram (FAD) correlating to physical meanings of residual strength and corresponding damage characteristics was suggested for qualitative predicting the trends of residual strength from the perspective of plastic strain localization. Then, the intrinsic factors of material property and extrinsic factors

of geometry, load, and environment that may affect the residual strength by influencing the plastic strain localization were discussed. The quantitative prediction was expected to be numerical and phenomenological because engineers can easily find out when the prediction method fails. It was implemented by finite element analysis based on continuum mechanics. Then, whether the local mechanism of damage initiation and plastic flow property in the near crack-tip partition can influence the prediction results was evaluated.

4. 2 Qualitative trend prediction of residual strength

4.2.1 Novel failure assessment diagram and classification of pre-cracks for predicting residual strength variation

The decrease of the pre-crack depth not only results in increasing fracture instability toughness but also alters the physical meaning of residual strength. Meanwhile, the residual strength is not always inversely proportional to the increase of pre-crack depth. To remind this problem in design, a novel FAD considering physical meanings of residual strength and damage characteristics was supposed. As shown in Fig. 4.1, the residual strengths in Regions I and II are dominated by plastic instability, while those in Regions III and IV are dominated by fracture instability. Therefore, Regions I and II belong to the shallow crack category, and Regions III and IV belong to the deep crack category. The decreasing trends of residual strength in Regions II to IV were considered to own an exponential curve because both work hardening in Regions I to II and crack propagating driving force are the exponential functions to crack depth [17,54].

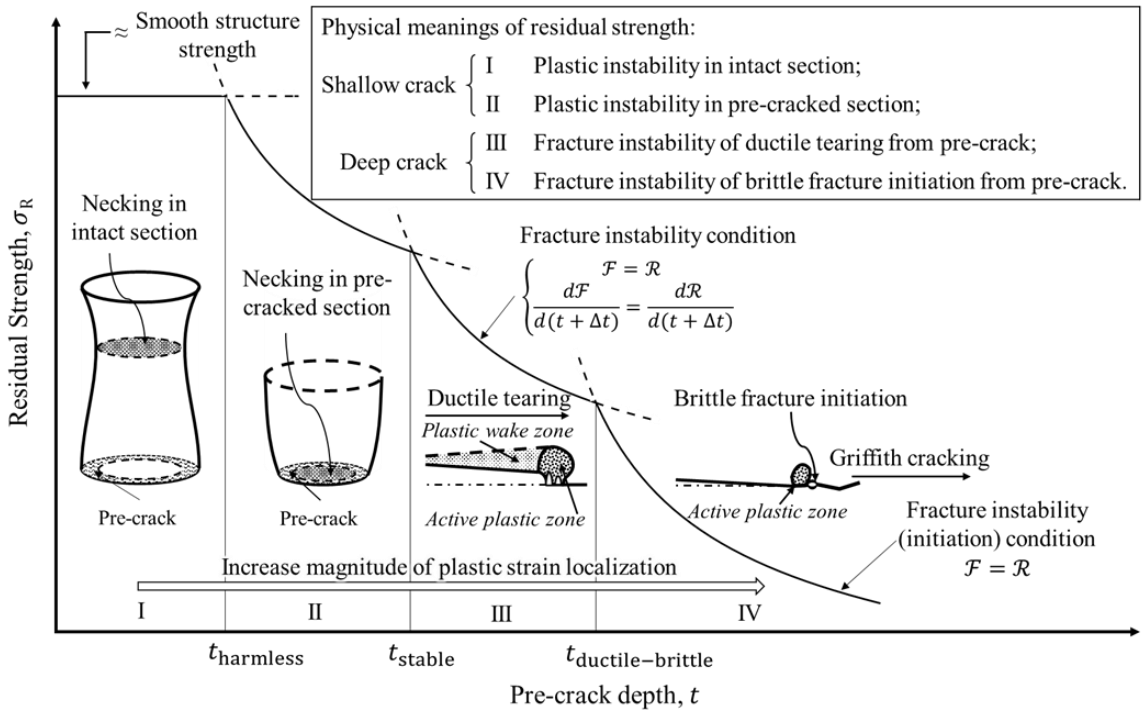

Fig. 4.1 Residual strength diagram considering physical meaning of residual strength and corresponding damage characteristic

For Region I of $t < t_{\text{harmless}}$, the pre-crack does not propagate and has a positive influence on load-carrying capacity because the plastic strain localization coupled with the stress triaxiality can totally offset the negative influence of cross-sectional reduction. Pre-cracks with depths located in this region is named as 'harmless crack.' Although the residual strength cannot be higher than the tensile strength of smooth specimens because the rupture occurs in intact cross-sections, the increases of plastic strain localization and stress triaxiality will expand the border of harmless crack.

For Region II of $t_{\text{harmless}} < t < t_{\text{stable}}$, the pre-crack also does not propagate or at least remains a stable propagation until the onset of plastic instability. Hence, pre-cracks with depths located in this region is named as 'stable crack.' However, the increase of pre-crack depth makes the negative influence of cross-sectional reduction is too significant to be offset by other partitions of pre-cracked sections, so the residual strength is decreased. The increase of plastic strain localization and stress triaxiality can

increase the residual strength in region II because their increases provide more positive influences in the pre-cracked section to offset the negative influence of cross-sectional reduction. Additionally, excessively high plastic strain localization and stress triaxiality promote the physical meaning of residual strength transforming from plastic instability to fracture instability, thereby shrinking the border of Region II.

For the deep crack category, the onset of unstable crack extension occurs before the plastic instability. For the ductile failure, the increasing plastic constraint state usually results in a gentler *R*-curve, so the residual strength is reduced gradually by the increase of t. The residual strength is limited by a rising load required by the stable crack extension until the onset of fracture instability of ductile fracture. Therefore, the pre-crack in Region III of $t_{\text{stable}} < t < t_{\text{ductile-brittle}}$ is named as the 'ductile crack.' Besides, if the structure size is large enough for t increasing, another critical point of $t_{\text{ductile-brittle}}$, which governs the ductile-brittle transition, can be anticipated. For Region IV of $t > t_{\text{ductile-brittle}}$, the plastic strain is constrained in a tiny zone so the high elastic potential energy can readily induce the onset of brittle failures, such as cleavage or intergranular cracking. The unstable crack extension almost occupies the entire crack extension procedure, which indicates that the crack initiation toughness limits the residual strength. The residual strength decreases with $1/\sqrt{t}$, resulting in a flaw-sensitive structure [101]. Therefore, the pre-crack in Region IV of $t > t_{\text{ductile-brittle}}$ can be named as the 'brittle crack'.

This FAD supplied a possibility to qualitatively estimate the trends of residual strength from the perspective of plastic strain localization. One can judge the fluctuation of residual strength according to the different main function of plastic instability in Regions I to IV. It can contribute to material selections in design. Also, this FAD

closely relates to the physical meaning of residual strength and corresponding damage characteristics. It helps with identifying whether pre-cracks are harmless or not through the phenomenological analysis of the damage.

4.2.2 Influential factors on shallow crack effect in residual strength issue

From the above discussion, the plastic strain localization significantly influences the physical meaning of residual strength and the corresponding damage phenomenon. Hence, any factors that can affect plastic strain localization may also change the effect of pre-crack on the residual strength. In this section, the influence of intrinsic and extrinsic factors on microscopic plastic strain localization at the crack tip and macroscopic plastic strain localization in one yield section are simply enumerated.

If the influence of extrinsic factors is neglected, the yield strength and the hardening exponent of elastic-plastic determine the development of plastic deformation [102]. Because the plasticity of metal is mainly realized by the dislocation motion, the factors that can affect or interact with the dislocation motion may change the condition of plastic strain localization in the pre-cracked structure. The level of Peierls stresses and the dislocation line orientation determines the lattice resistance to dislocation motion, which depends on the crystal type, dislocation type, and corresponding slip system [54]. Large lattice resistance can provide high yield strength to result in high plastic constraint easily but can delay the onset of plastic instability. The macroscopic plastic strain localization is inversely proportional to the number of barriers for dislocation motion, such as grain boundary in addition to the ultrafine crystal (Hall-Petch effect)

[103], substructure, phase (participation or diffusion particle and fiber) and inclusion [35]. Because the influence of material intrinsic factors on plastic strain localization is too complex to be listed, they will not be expanded in detail here — the relative Refs. [35,104] can provide more information. However, it still can conclude that the material generating a substantial microscopic plastic strain localization at the crack tip may provide high residual strength for a structure containing harmless or stable crack due to the low magnitude of plastic strain localization in the entire pre-cracked section.

The extrinsic factors, such as loading configuration, structure geometry, and circumstance, also have significant influences on plastic strain localization by changing the local stress-strain state or thermodynamic conditions. Load configuration includes the strain rate and loading types such as tension, bending, and torsion. It may significantly influence the local stress-strain state near the crack tip, thereby changing the magnitude of plastic strain localization. For a certain t, the increase in l is helpful to obtain the shallow pre-crack and general yielding condition [105]. However, a limitation should exist for t/l to distinguish the shallow pre-crack and deep crack as t_{stable} shown in Fig. 4.1. For $t < t_{\text{stable}}$, the increase in l can enlarge the uniform plastic deformation area in the pre-cracked section, which is helpful to suppress the gross of magnitude of plastic strain localization to delay the onset of plastic instability. In contrast, if l is infinite or large enough, the plastic strain emitting from the pre-crack never causes the entire pre-cracked section to yield until the onset of fracture instability of pre-crack, similar to the case of $t > t_{\text{stable}}$. Hence, the classification of different pre-cracks should cautiously consider the structural size effect. In addition, the conditions of circumstance, such as temperature [106] and hydrogen [107], can affect the mobility of dislocation during the formation of plastic deformation. For example, low temperatures may increase the microscopic plastic localization but decrease the

macroscopic plastic localization because Peierls stress is usually sensitive to temperature in BCC metal, and hydrogen may also have the similar influence through enhancing the localized plasticity in some metals.

It should be noted that the intrinsic and extrinsic factors mentioned above may have a particular case for the residual strength evaluation of shallow-cracked structure. Additionally, the detailed influences of those factors on plastic strain localization have still not been described for residual strength governed by plastic instability. These problems will be studied in the future.

4. 3 Quantitative prediction of residual strength

4.3.1 Numerical modeling

Form the mechanical viewpoint, the presence of a crack can generate a triaxial stress state and accelerate the local strain near the crack tip. Both of them may influence the work hardening condition in the pre-cracked cross-section and then determine the residual strength governed by global plastic instability [54,103]. In order to clarify their significance to the prediction of harmless crack and judge the dominate partition of pre-cracked cross-section, two prediction models were established. If the stress-triaxiality in pre-cracked cross-section was assumed to govern the harmless crack depth independently, namely, the remote partition dominating the residual strength prediction, the load-carrying capacity of the pre-cracked section should initially increase with the pre-crack depth and then decreases, as shown in Fig. 4.2. Hence, an artificial reference defect, which is always smaller in size compared with the pre-crack and also can be regarded as a material defect, was placed in the center of an intact cross-section far

away from the pre-cracked cross-section. The artificial reference defect has two functions: 1. Generating an increase of stress triaxiality that can vary with load in the center of specimen that corresponding to the remote crack-tip partition; 2. representing a competition between material internal defects and pre-cracks. The FEA geometric modeling and meshing were the same as those in CHAPTER 2 and CHAPTER 3. During the prediction by FEA, the size of the artificial reference defect increased with the pre-cracked depth, but it is always 80% of the pre-crack depth to ensure the stress triaxiality generated by artificial reference defect is always smaller than that generated by pre-cracks in the specimen center. The artificial reference defect was placed at the surface of the top-edge of Fig. 2.3 (a) by eliminating some elements (element size of 5 μm). Then the load-carrying capacity of the pre-cracked cross-section and intact cross-section with an artificial reference defect can be compared. Although this comparison cannot deal with the load-carrying capacity of the pre-cracked section that is higher than the intact section but has a decreasing trend, an aggressive numerical prediction combined with the correct phenomenological approach can still be accepted by engineering.

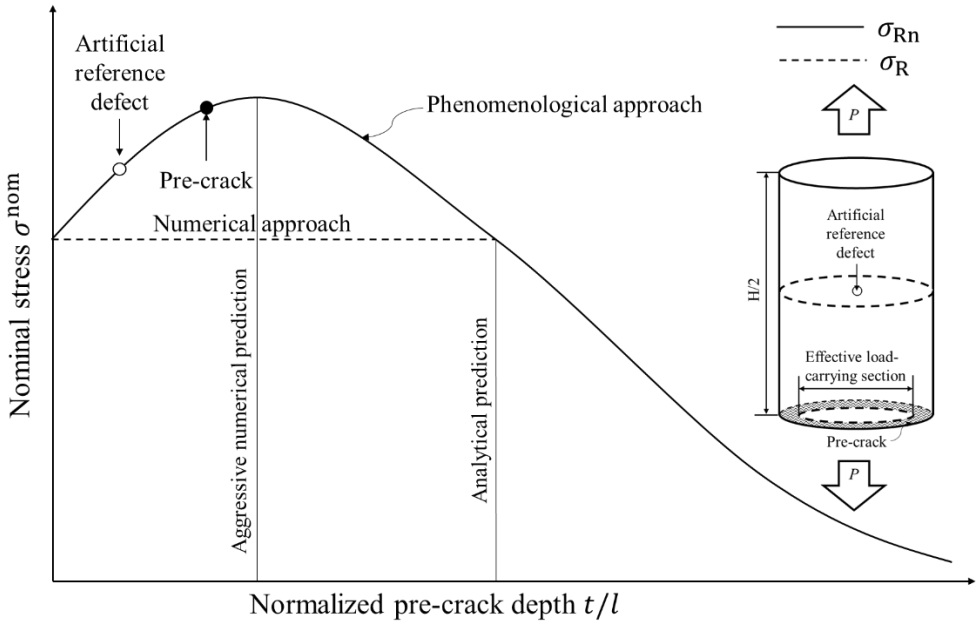

Fig. 4.2 Diagrammatic sketch of prediction model that assumes stress triaxiality independently controlling harmless crack depth.

Another prediction model aimed to judge whether the local effect in the near crack-tip partition was necessary for residual strength prediction. Here, the local strain-rate effect near the crack tip was chosen as the representation because the strain hardening property of IF steel was found sensitive to the strain rate according to the true stress-strain curve in the post-necking elongation, as illustrated in Fig. 4.3(a). To highlights the local effect in the near crack-tip partition, no artificial reference defect was placed in the intact cross-section. The model should be based on a rate-dependent strain hardening model, which is different from the previous prediction model that assumes the strain hardening is independent of strain rate. In this study, the base strain-hardening property of IF steel was measured at 10^{-3} /s according to ASTM E8M standard (6 mm in diameter and 30 mm in gage) [83]. The chemical composition of IF steel is listed in Table 2.1. Before machining, the average grain size and hardness were respectively adjusted to 66μm and 65HV by annealing. The true stress-strain curve was plotted in Fig. 4.3(a), and it is clear that the strain-hardening property in post-necking elongation was influence by strain-rate variation in the necked section. The tensile constants of IF

steel were listed in Table 4.1. The rate-independent strain hardening for prediction model shown in Fig. 4.1 was described by Hollomon's equation:

$$\sigma_t = K\varepsilon_t^n \tag{4-1}$$

where σ_t is the true stress, ε_t is the true strain, K = 432 MPa is the strength coefficient, and n = 0.27 is the work hardening exponent.

Table 4.1 Value of tensile constants for Interstitial-free steel.

E	v	σ_Y	σ_b
200 GPa	0.3	117 MPa	246MPa

The rate-dependent strain hardening for prediction was assumed as the Johnson-Cook model, which is purely empirical and takes into account the effects of isotropic strengthening, kinematic strengthening, temperature variation and the associated variation in yield strength. According to this model, the stress is determined by the formula

$$\sigma_Y = \left(A + B{\varepsilon_p}^n\right)\left(1 + C\ln\varepsilon_p^*\right)\left(1 - {T_H}^m\right) \tag{4-2}$$

where ε_p is the effective plastic strain, ε_p^* is the normalized effective plastic strain rate, and T_H is the homologous temperature = 0 (for normal laboratory experiment):

$$T_H = \frac{T - T_{\text{room}}}{T_{\text{melt}} - T_{\text{room}}} \tag{4-2}$$

A, *B*, *C*, *n* and *m* are material constants, as listed in Table 4.2. They were obtained by fitting according to the data in Fig. 4.3. The tensile property of IF steel at higher strain rates shown in Fig. 4.3(b) comes from the isothermal data of Ref. [108], whose material chemical composition and microstructure of IF steel is similar to this study.

Table 4.2 Value of constants for Johnson–Cook model.

Name	Symbol	Units	Value
Initial yield stress	*A*	MPa	117

Hardening constant	B	MPa	432
Hardening exponent	n		0.4
Strain rate constant	C		0.04
Thermal softening exponent	m		0.5

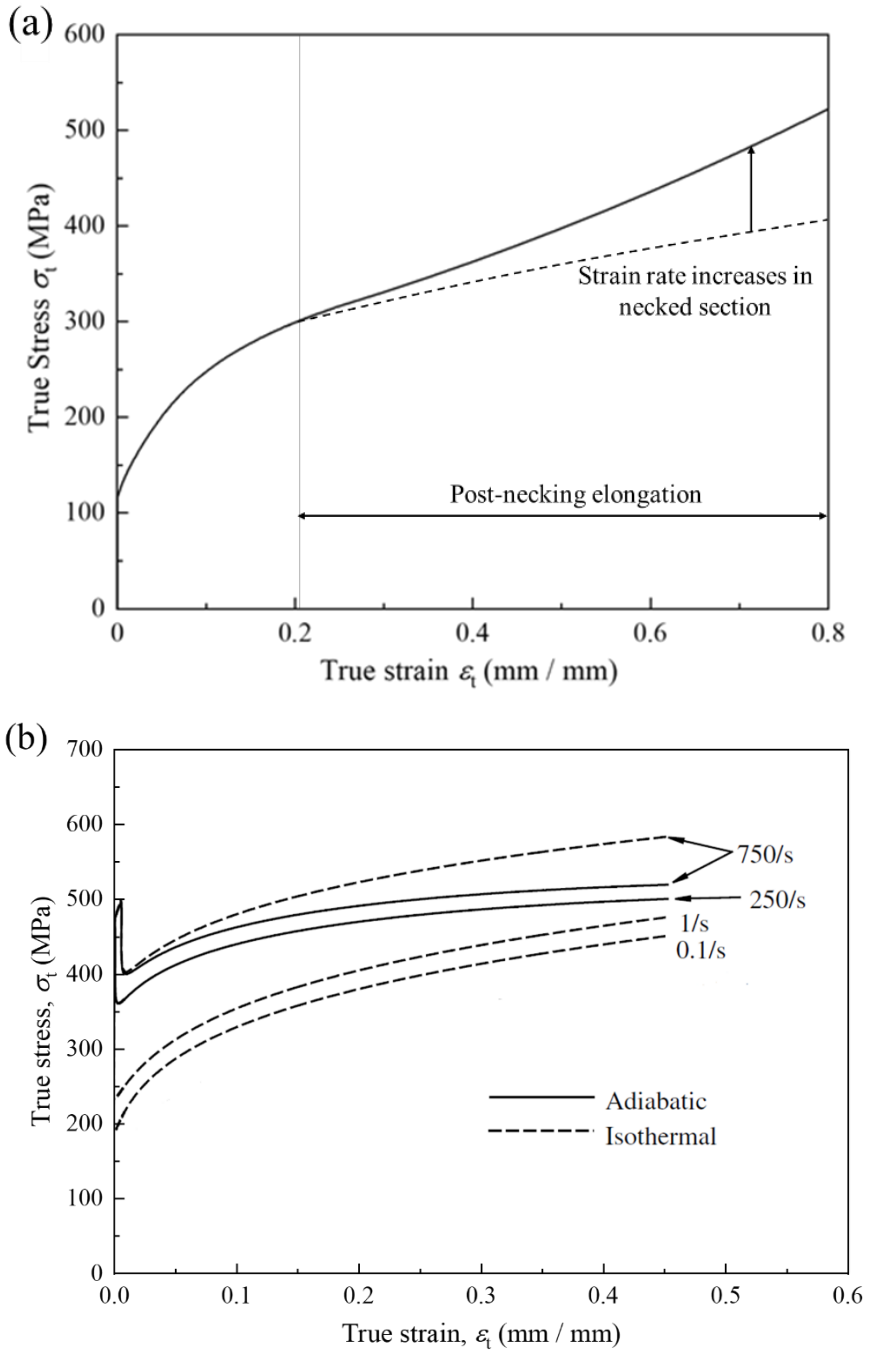

Fig. 4.3 (a) True stress-strain curve of IF steel measured at 10^{-3} /s by experiment. (b) Strain-rate effect on engineering stress-strain curves of IF steel measured at various strain rates from Ref. [108].

4.3.2 Results and discussion

Fig. 4.4 shows the residual strength varying with pre-crack depth predicted by the FEA. In Fig. 4.4 (a), residual strength various with the pre-crack depth smoothly, decreasing form the value identical to the structural strength of the smooth specimen. It indicates that continuum mechanics is still valid to predict the residual strength if the influence of stress triaxiality is considered. That is, the remote crack-tip partition can dominate the value of residual strength. However, users may have less confidence to determine an exact depth for harmless crack because of the smooth transition of residual strength without any physical phenomenon. When the local plastic flow property affected by the presence of pre-crack is considered, this problem can be solved, as shown in Fig. 4.4 (b). The variation of local plastic flow property obviously mainly happened in near crack-tip partition with large gradients of elastoplastic fields, as shown in Fig. 3.10. Hence, a valid and explicit prediction should also consider the effects of pre-crack on local plastic properties in the near crack-tip partition.

Admittedly, this local characteristic should not be limited to the strain rate. The local damage initiation, such as damage by micro voids that can be solved by Gurson-Tvergaard-Needleman model [109], may also provide additional variation in the stress triaxiality and local plastic property. The user can choose an FEA model coupled with damage mechanics base on the practical needs.

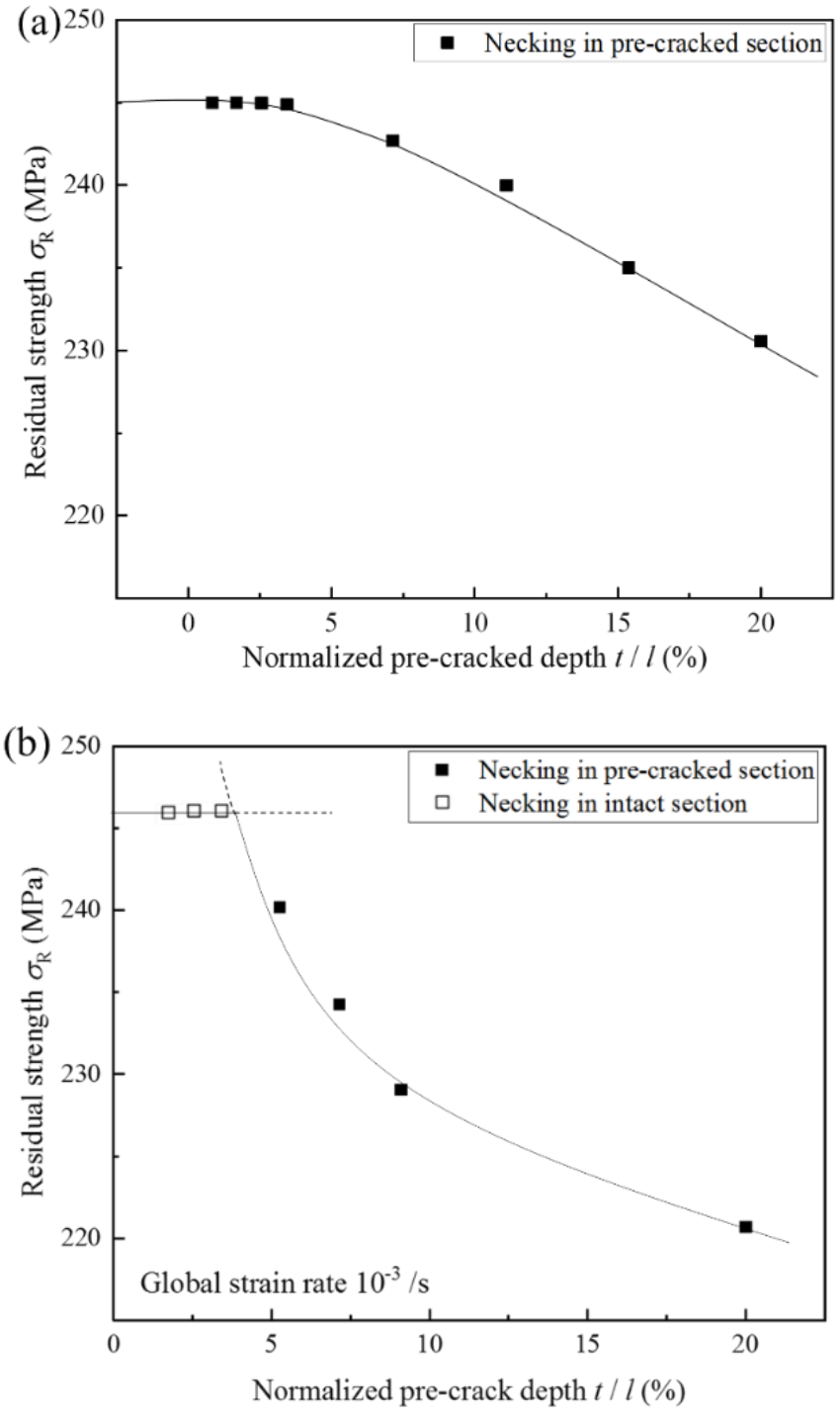

Fig. 4.4 Prediction of harmless crack based on (a) triaxiality effect without strain-rate effect, and (b) triaxiality coupled with strain-rate effects.

4. 4 Chapter conclusions

1. The trends of residual strength in the shallow crack category can be qualitatively estimated from the perspective of plastic strain localization.
2. The shallow crack effect is not a material intrinsic property, and all factors that can influence the magnitude of plastic strain localization are significant for shallow pre-crack structures.
3. The continuum mechanics is suitable for numerical prediction of residual strength of shallow pre-cracked structures. However, it should consider the local plastic flow property influenced by the presence of pre-crack to induce the correct damage phenomenon, namely, the necking away from the pre-cracked section
4. The remote crack-tip partition dominates the value of residual strength while the near crack-tip partition dominates generating the correct damage phenomenon.

CHAPTER 5. Distinguishing geometric and metallurgic hydrogen-embrittlement susceptibilities in pre-cracked structures made of interstitial-free steel under monotonic tension

5.1 Introduction

Pre-cracks in engineering components are almost inevitable with current technology. They are significant local stress intensifiers that promote the formation of the plastic zone in the vicinity of crack tips under loading. As the primary conductor of plastic deformation, dislocation emitting from crack-tips can interact with hydrogen and result in the hydrogen-embrittlement (HE) phenomenon [110–112], which manifests degradations in the mechanical properties of various HE-sensitive materials due to hydrogen-assisted cracking (HAC) [113–117]. Hydrogen is a clean energy source with abundant potential applications [118,119], but the existence of HE resists the practical application of hydrogen in engineering [120–122]. Hence, there is an increasing need for investigations of HE effects on pre-cracked structures.

Investigations into the hydrogen-assisted failure of pre-cracked structures have

mainly focused on the mechanical properties governed by cracking behaviors, often referring to the crack propagation accelerated by different HAC mechanisms [113,117,123,124], such as the stress-induced hydride formation and cleavage [125], hydrogen-enhanced localized plasticity (HELP) [126] and the hydrogen-enhanced decohesion (HEDE) [127]. Ultimate tensile strength (UTS) is a vital mechanical property of pre-cracked structures that may be decreased dramatically by the unstable crack propagation taking place prematurely in the hydrogen environment [110]. However, it is governed not only by the unstable crack propagation but also by the plastic instability in one yield section [25]. The latter may occur in a structure with a shallow pre-crack because of the exceedingly-high fracture instability toughness [30,128]. As technology advances, engineering components rarely contain very deep pre-cracks. Nevertheless, few investigations report the UTS of shallow pre-cracked structures governed by plastic instability in the hydrogen environment.

This study aims to investigate HE coupled with the effects of shallow crack on the UTS of structures governed by plastic instability. The specimens were made of interstitial-free (IF) steel, which represents a standard microstructure of ferritic steel. Its properties include excellent ductility, simple metallurgical microstructure, and significant HE susceptibility due to the high diffusivity and permeation rate of hydrogen in the ferrite [70,129]. Fully electrochemical hydrogen pre-charged cylinder specimens (also with the in-situ charging during monotonic tension to maintain the hydrogen saturation) ware experimentally and microscope-analytically compared with uncharged specimens (without in-situ charging). After clarifying the trend of UTS with a shallow pre-crack, the corresponding physical meaning of UTS was analyzed, and then the underlying reasons were discussed. Also, its general applicability and merit to fail-safe design were discussed.

5.2 Experimental Procedure

5.2.1 Material and specimen

The chemical composition of IF steel used in this study was shown in Table 2.1. The interstitial C and N were completely trapped in Ti-containing precipitates [130] so that there were no interstitial solute atoms. The IF steel was heat-treated by 2 h annealing at 750° and then furnace cooled to room temperature to reduce anisotropy. The average grain size and hardness were 52 μm and 62 HV, respectively.

Figure 5.1 shows the dimensions of the cylinder specimens. It was expected that the UTS (the maximum load divided by the initial area of intact cross-section) was governed by plastic instability, so the pre-crack depths should be very shallow to ensure an exceedingly-high fracture instability toughness [30]. However, such shallow pre-cracks with certain depths cannot be introduced to cylinder specimens by fatigue methods due to the immeasurability of circular fatigue cracks. Hence, the pre-cracks were introduced by grooving crack-like notches in the middle of gages using the method of Refs. [131,132]. The verification of crack-like notches was conducted in the normal environment because hydrogen promoted the stable crack propagation (this will be proved by results) at the shallow notch root so all the notches with hydrogen were identical to cracks in this study. Table 5.1 lists the dimensions of the shallow pre-cracks (shallow crack-like notches, and hereinafter, will be directly called as shallow pre-cracks for convenience) after polishing and cleaning. Since the pre-crack depth can be reduced by polishing, a margin on the specimen gage was left after machining. Then, the radius of the specimen gage, as well as the pre-crack depth, was polished to

approach the designed size. All the surfaces of the specimen gages were polished with emery papers to a No. 2000 grit finish and then buff-polished using 50 nm alumina particles.

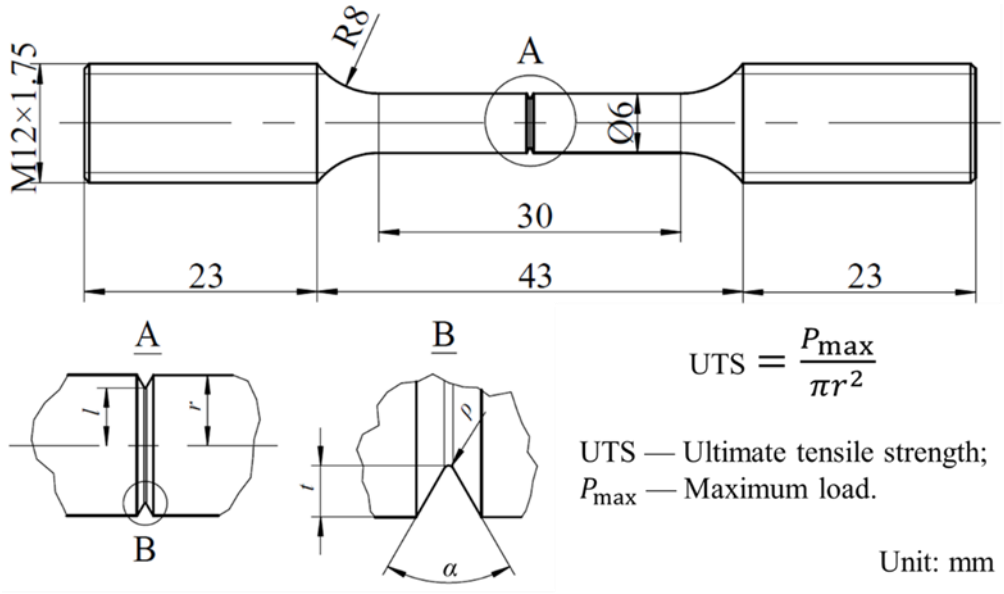

Fig 5.1. Dimensions of shallow pre-cracked (shallow crack-like notched) specimens.

Table 5.1 Dimensions of pre-cracks (shallow crack-like notches).

	t (mm)	ρ (mm)	α (°)	Note
A	0.011	0.005	60	Pre-charged specimen stretched to rupture in hydrogen environment
B	0.030	0.005	60	
C	0.094	0.005	60	
D	0.660	0.005	60	
E	0.980	0.005	60	
F	0.028	0.005	60	Pre-charged specimen stretched and interrupted at UTS in hydrogen environment
G	0.024	0.005	60	Uncharged specimen stretched to rupture in normal environment

5.2.2 Hydrogen charging

The electrochemical hydrogen charging [133] was adopted in this study, as

schematically shown in Fig. 5.2. A working condition of pre-cracked engineering components continuously exposed to hydrogen was assumed. Hence, the pre-cracked specimens were fully pre-charged in 3% NaCl aqueous solution with 3g/L NH_4SCN with a constant current of 10 mA/cm^2 at 25 ℃. The diffusion coefficient of hydrogen in the ferrite under these conditions (10 mA/cm^2 at 25 °C) was reported to be 5.8×10^{-8} m^2/s [134,135], which indicates that the hydrogen was saturated in gage of $\Phi 6 \times 30$ mm within 1 h [110,136,137]. Although it has also been reported that titanium hydride formation in the ferritic matrix can reduce hydrogen diffusivity [129], the low content of Ti in IF steel used in this study will not have a significant impact. Hence, the pre-charging time was universally set to 2 h to ensure that hydrogen was saturated in the specimens.

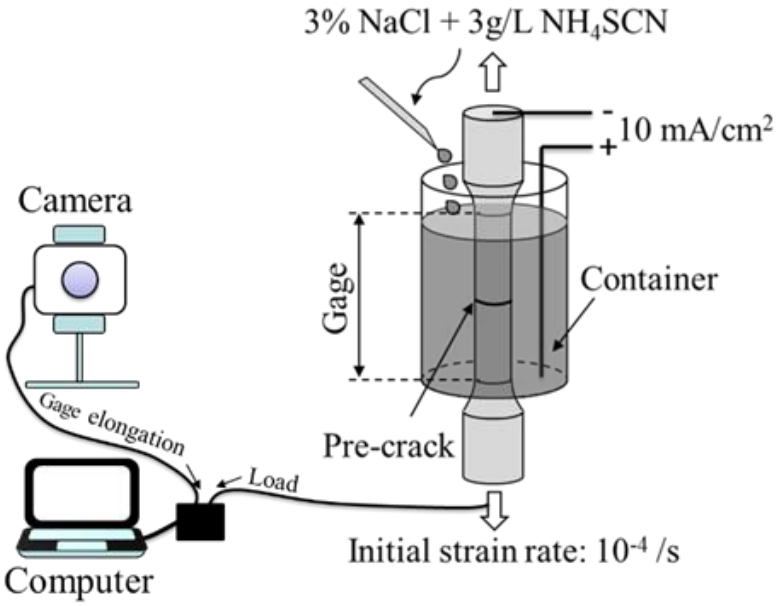

Fig. 5.2 Schematic of electrochemical hydrogen charging for monotonic tensile tests: 1 h pre-charging followed by in-situ charging during stretching.

5.2.3 Monotonic tensile tests

Pre-charged specimens (A to F in Table 5.1) were stretched at a constant nominal strain rate of 10^{-4} /s, which was achieved by controlling the gage elongation increment. The gage elongation and sectional reduction were monitored by a camera, as shown in Fig. 5.2. To keep the gage below the liquid level, the solution was continuously dripped into the container, as shown in Fig. 5.2. By contrast, an uncharged specimen (G) was stretched at the same initial strain rate as the pre-charged specimens. Additionally, one of the pre-charged specimens (F) was manually interrupted at the UTS, and then it was longitudinally cut and polished. It was used for determining the physical meaning of the UTS and observation of hydrogen assisted fracture. The microscopic analysis was conducted by scanning electron microscope (SEM) with electron backscatter diffraction (EBSD) at 15 kV.

5.3 Results

Figure 5.3 shows the tensile stress-displacement curves of pre-cracked specimens with different pre-crack depth. An apparent degradation of ductility in the presence of hydrogen indicates that pre-cracked specimens were sensitive to HE. However, for specimens with $t \approx 0.03$ mm (B, F, and G in Table 1), the interaction of hydrogen with pre-cracks had no influence on the UTS. Additionally, their UTS was identical to that of the crack-free specimen in the normal environment (the center line in Fig. 5.3). This identity is shown more clearly in the plot of UTS vs. pre-crack depth in Fig. 5.4. Figure 5.4 also shows that the UTSs of pre-cracked specimens with hydrogen are higher than those without hydrogen when pre-crack depth is greater than a critical value (Although this critical value was not experimentally obtained in this study, its existence is

predictable).

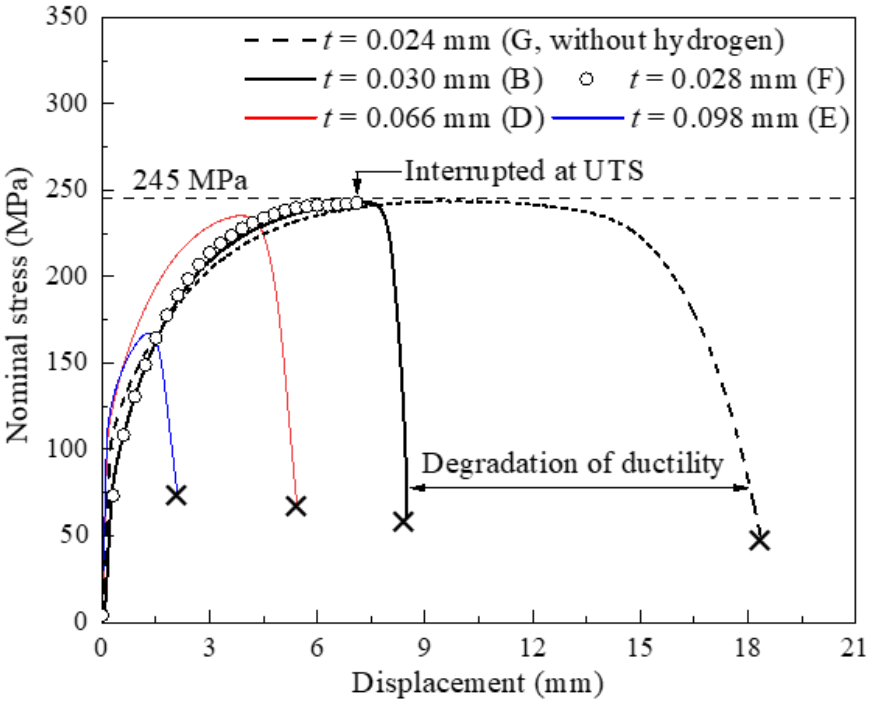

Fig. 5.3 Tensile stress-displacement curves of pre-cracked specimens.

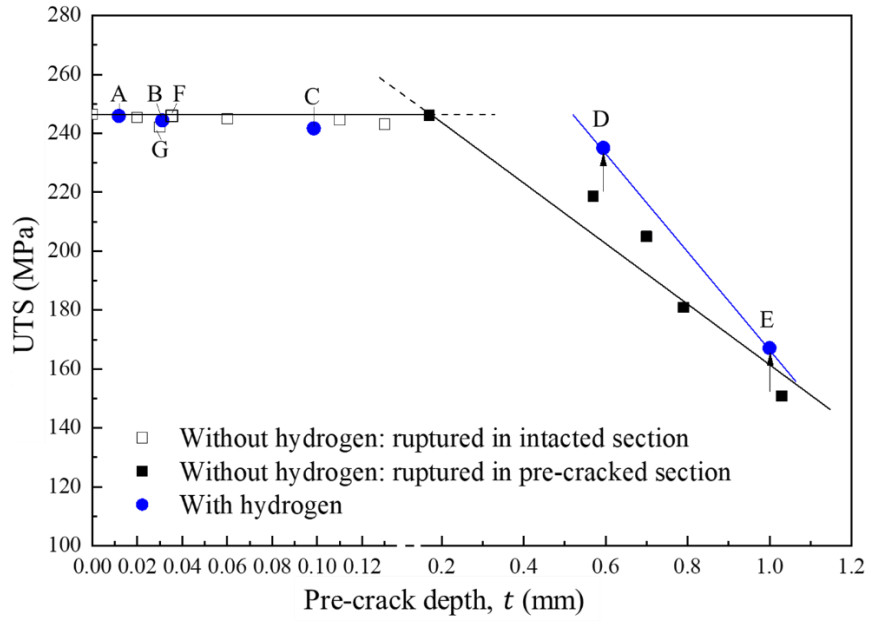

Fig. 5.4 Response of UTS to pre-cracked depth (data from Ref. [138] except the pre-cracks listed in Table 5.1; F is interrupted test with hydrogen).

Figure 5.5(a) shows the fracture surface of the uncharged specimen with t = 0.024

mm (G in Table 5.1) in the normal environment. It presents a ductile failure with a cup-and-cone appearance, which typically originates from the internal crack initiation by void initiation, growth, and coalescence after necking [17,31]. Moreover, the final rupture occurs in the intact cross-section so that the pre-crack should have an exceedingly-high fracture instability toughness [138]. Therefore, the failure of the pre-cracked specimen in the normal environment was governed by plastic instability.

The pre-cracked specimens with hydrogen have a different appearance, as shown in Fig. 5.5(b) and Fig. 5.6. The pre-crack propagated, and the final rupture moved to the pre-cracked cross-section, as shown in Fig. 5.6(a). There are two kinds of damage patterns in the fracture surface, namely, the quasi-cleavage mixed with intergranular fracture, as shown in Figs. 5.6 (b) and (c), and the dimple area located in the specimen center, as shown in Figs. 5.6 (a) and (d). The transition between the two kinds of damage patterns is considered as the onset of unstable crack propagation, because the accelerating local strain rate at an unstable crack tip can suppress the susceptibility to HE [110]. Hence, compared to the uncharged specimen shown in Fig. 5.5(b), HE effect is significant in the pre-charged specimens as exemplified in Fig. 5.6.

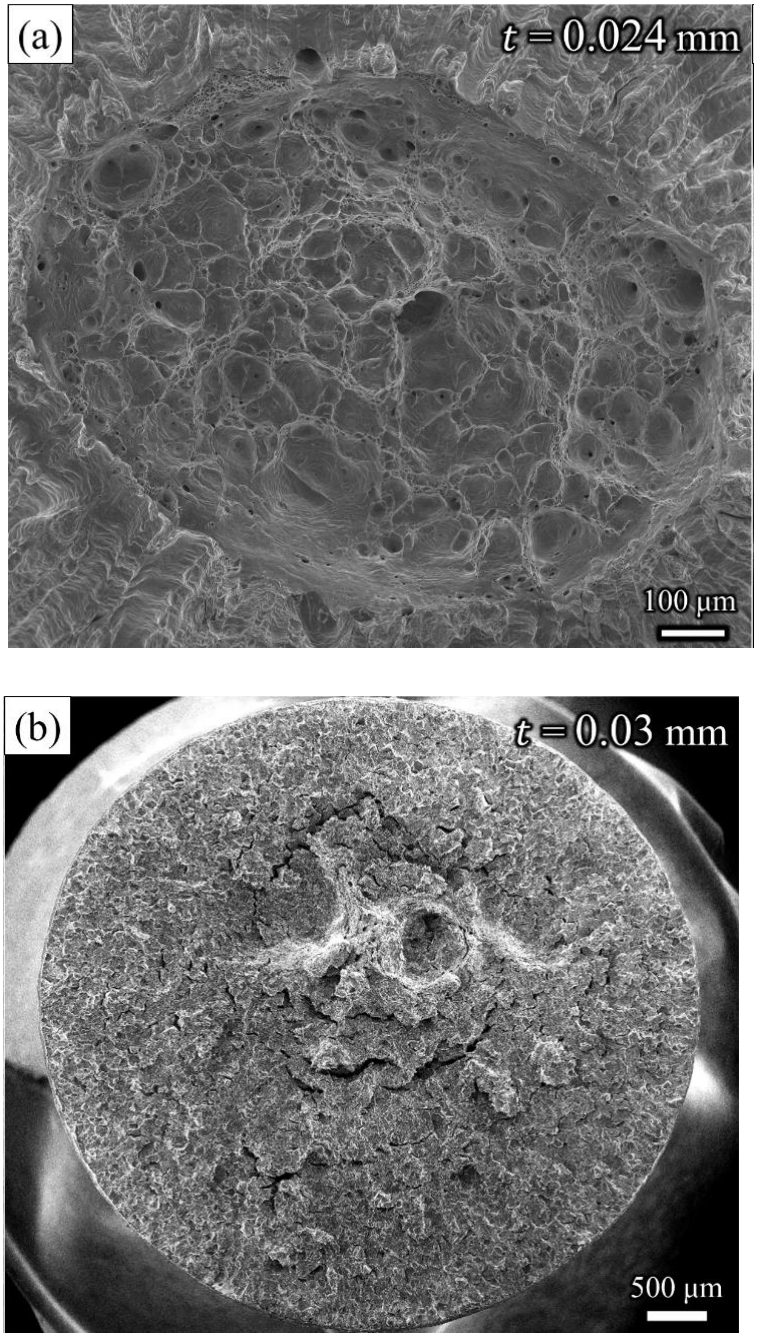

Fig. 5.5 Fracture surface of pre-cracked specimens with $t \approx 0.03$ mm (a) in normal environment with cup-and-cone appearance, and (b) in hydrogen environment.

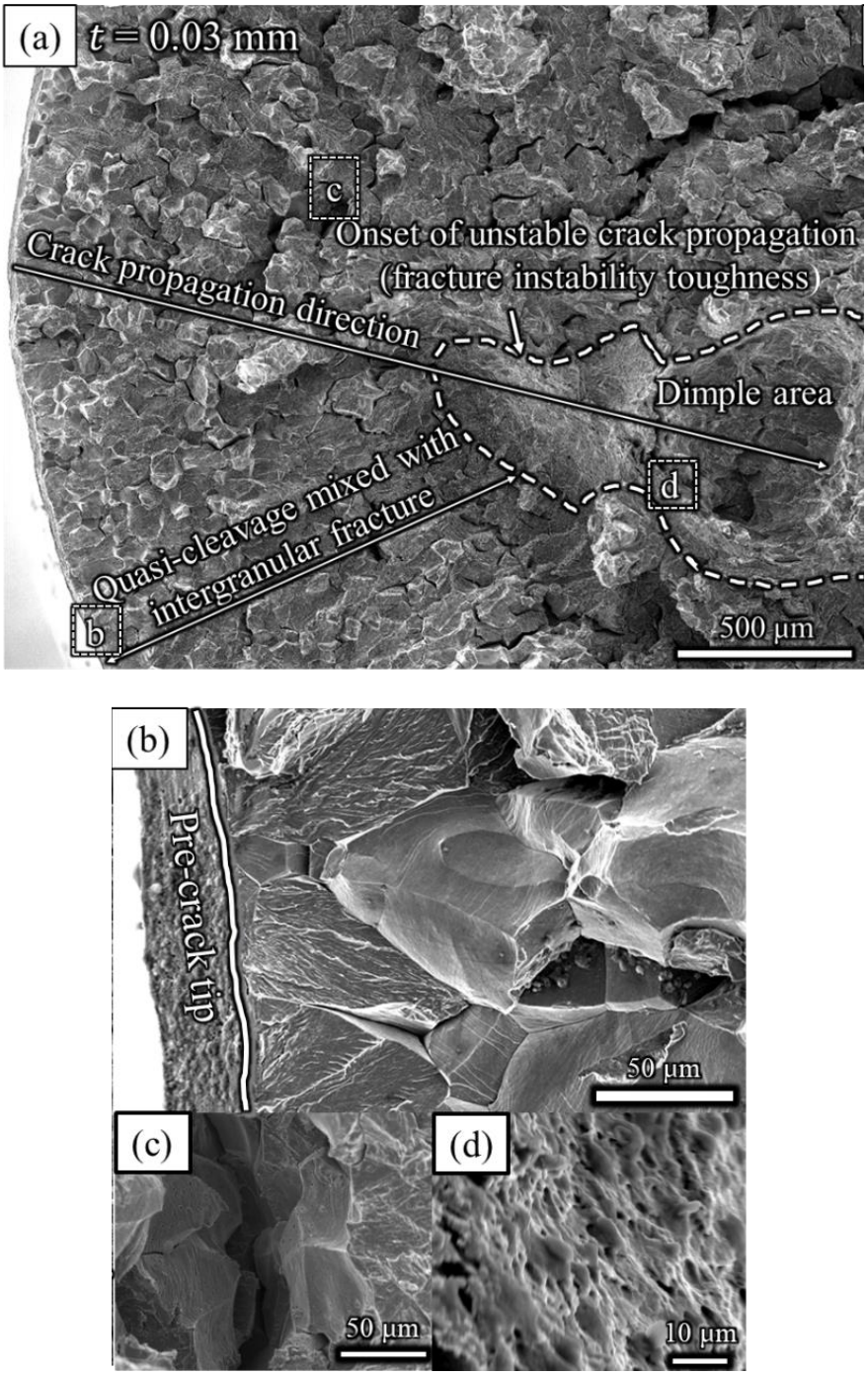

Fig. 5.6 Representative damage patterns on fracture surfaces of pre-cracked specimens in hydrogen environment.

Figure 5.7 shows the microscopic observations of the pre-charged specimen with t = 0.028 mm (F in Table 5.2) interrupted at the UTS in the hydrogen environment. The pre-crack advancing at UTS in Fig. 5.7(a) is much shorter than that at the boundary

between the quasi-cleavage mixed with intergranular fracture and the dimple area in Fig. 5.6(a). The initiation of secondary cracks as the form of intergranular fracture was almost homogenous in the specimen, as shown in Figs. 5.7(a) and (b). Moreover, the striation-like pattern [139] on the intergranular fracture surface in Fig. 5.7(c) and the high value of kernel average misorientation (KAM) in Fig. 5.7(d) near the void initiating along the grain boundary demonstrate that the intergranular fracture was caused by high plastic deformation related to HELP rather than the decohesion mechanism (HEDE). This result coincided with the conclusion of Ref. [140]. Hence, secondary cracks were probably initiated by extensive plasticity before the pre-crack propagates to their locations. These facts indicate that the pre-crack propagation, which has a form of secondary crack initiation and progressive coalescence with the pre-crack, was still stable at the UTS so that the physical meaning of the UTS is plastic instability even in the hydrogen environment. In addition, as shown in the modified Fig. 5.3, the post necking trends of nominal stress-displacement curves of specimens in hydrogen are similar to each other. Even for the specimen with the largest pre-crack depth of t = 0.098 mm, its nominal stress-displacement curves in post necking decreases gradually. Therefore, the physical meaning of UTS for tested specimens is plastic instability instead of fracture instability.

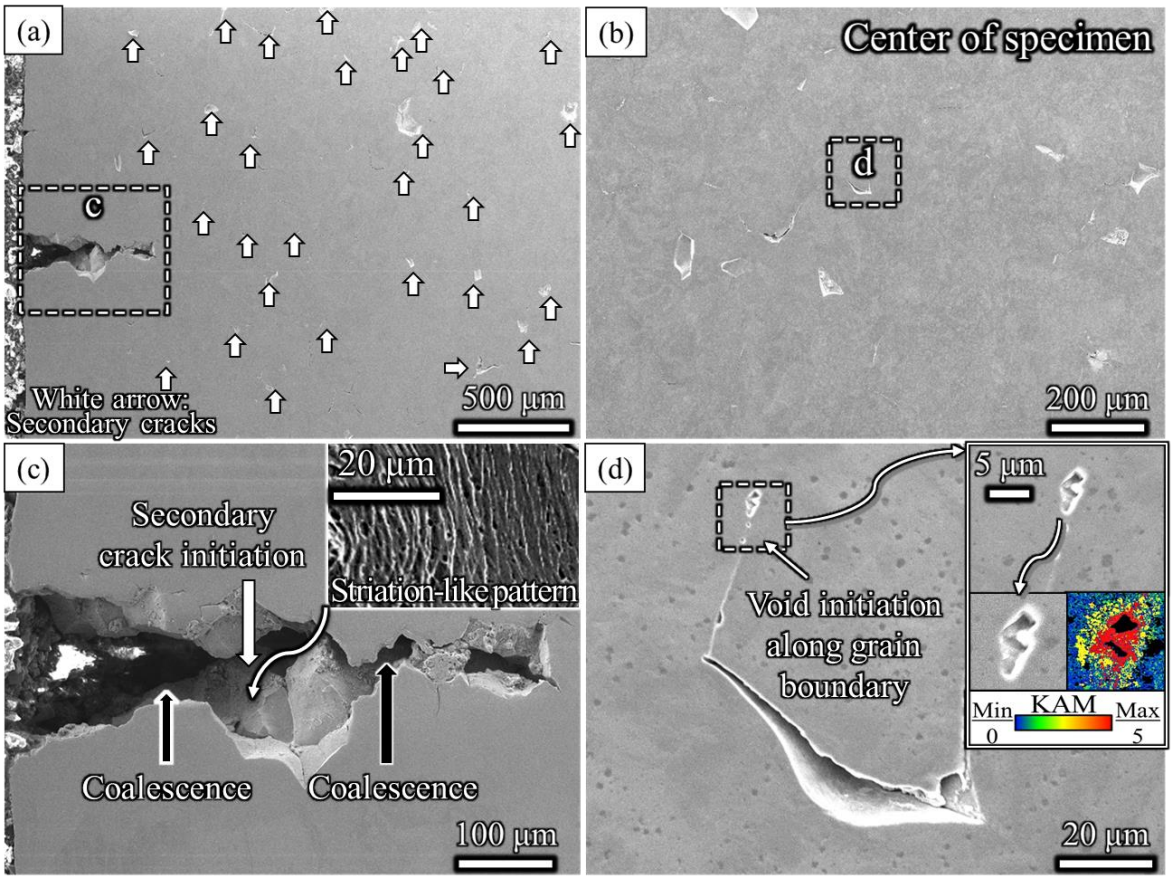

Fig. 5.7 Microscopic observations of the pre-cracked specimen (t = 0.028 mm) interrupted at UTS in hydrogen environment.

5.4 Discussion

These results show that the crack effect coupled with the hydrogen effect does not necessarily degrade the UTS governed by plastic instability. Both the crack effect and the HE effect (especially for HELP in ferrite [140]) stimulate the plastic strain localization at the crack tip or microscopic trapping sites. However, in this study, plastic instability in one yield cross-section is a macroscopic failure that occurs only if the work hardening increment is insufficient to offset the rising load. The plastic strain localization caused by crack and HE effects naturally competes with the macroscopic failure of plastic instability. Because hydrogen assisted the plastic strain mainly localized in the vicinities of pre-crack and secondary cracks, so the plastic strain in the

rest part of the pre-cracked cross-section is reduced. Besides, if the pre-crack and secondary cracks can remain stable due to exceedingly-high fracture toughness, some local anti-yielding mechanisms in the vicinity of crack-tip can provide additional resistance for yielding. For instance, larger strain gradients caused by HELP increase the local stress triaxiality and strain rate, requiring higher stress to produce further yielding Hence, for very shallow pre-cracks, the crack and HE effects may resist the onset of plastic instability so that the UTS does not decrease.

Such a phenomenon of crack effect coupled with the hydrogen effect becoming favorable to the UTS is considered to have broad applicability in engineering applications. First, the fracture instability toughness of shallow crack is not a material intrinsic property [30,31]. It strongly depends on the geometric configuration, such as the pre-crack depth and structure size, particularly for structures made of ductile materials [30]. Second, the onset of plastic instability is determined by the work hardening condition, which is strongly dependent on the stress and strain fields in one yield cross-section. Naturally, stress and strain fields are sensitive to geometric variation whether due to design or damage. Therefore, if a pre-cracked structure is made of ductile strain-hardening materials, which includes most commercial metals [54], a positive hydrogen effect in shallow pre-cracked structures probably exists. It should be noted that although the allowable stress for shallow cracks under fatigue load is usually lower than that under static load, the UTS still has significant meaning for safety consideration. The UTS of monotonic loading indicates the ability of a pre-cracked structure to absorb energy before the load-carrying capacity decreases. A crack can propagate gradually by fatigue load, but no one can guarantee that there will be no overload in the next cycle. Hence, a positive hydrogen effect provides an additional guarantee for safety. Besides, the UTS also can be a design reference for low-cycle

fatigue with heavy cyclic loading [141]. Of course, speculation above needs further systematic study.

Additionally, the anti-common-sense influence of hydrogen determined in this study calls into question the general applicability of conventional investigation of HE susceptibility that mainly focuses on the variation of fracture characteristic. Form the metallurgic viewpoint, the material properties were degraded because the ductility, as shown in Fig. 5.3, and fracture characteristic, as shown in Fig. 5.5, were sensitive to hydrogen. However, from the mechanical viewpoint, the load-carrying capacity was not decreased by hydrogen; in fact, hydrogen slightly enhanced the UTS as the case of specimens D and E, as shown in Fig. 5.4. These facts indicate that only considering HE susceptibility of materials occasionally fails to make a correct prediction of the effect of hydrogen on the structural strength. For instance, fracture surfaces with HE appearance of shallow cracked structure may not conclusively show that the crack effect coupled with the hydrogen effect is the origin of the UTS degradation. Hence, subdividing HE susceptibility is suggested to understand the conditions under which plastic strain localization caused by HE susceptibility is beneficial for the UTS of pre-cracked structures in fail-safe design.

Figures 5.8 shows the subdivision of HE susceptibility overlaid on the failure assessment diagram of residual strength. The base diagram comes from our previous study [138] and the definition of residual strength is identical to that of UTS in this study. For the shallow crack region (Regions I and II in Fig. 5.8), the residual strength is governed by plastic instability and shows a strong dependence on geometric properties. The plastic strain localization generated by pre-crack can resist the onset of plastic localization. The HE of fully ferritic steels was mainly ascribed to the HELP effect [140]. Hence, plastic strain localization enhanced by the presence of hydrogen

for sallow cracks can provide additional load-carrying capacity. Although the hydrogen cannot increase the UTS of pre-cracked structures above that t of the smooth structure in the normal environment probably due to the promoted pre-crack propagation and secondary crack initiation, it can delay the decrease of residual strength especially in Region II, as indicated by the blue solid line in Fig. 5.8. The HE susceptibility of shallow pre-cracked structures is not mainly controlled by the material properties but is dominated by geometric properties (such as pre-crack depth), so it is named as geometric HE susceptibility. When pre-crack becomes deep and fracture instability dominates the residual strength (UTS), the HE susceptibility coincides with the conventional investigations [129] and can be termed as metallurgic HE susceptibilities. Ductile fracture can be triggered at low-stress levels by hydrogen-assisted dislocation emission [110]. The stable crack propagation in Region II can be shortened, while the initial part of brittle fracture in Region IV can be transformed to ductile fracture at a lower strength. Hence, Region III will enlarge to compress Regions II and IV in the presence of hydrogen, as the solid blue line in Fig. 5.8 shows.

Since the definition of UTS in this chapter is identical to that of the residual strength in the other chapters of this study, the results, discussion, and conclusions of this chapter can be directly applied to residual strength issues. Therefore, in the remaining content of this chapter, the UTS will be replaced by residual strength.

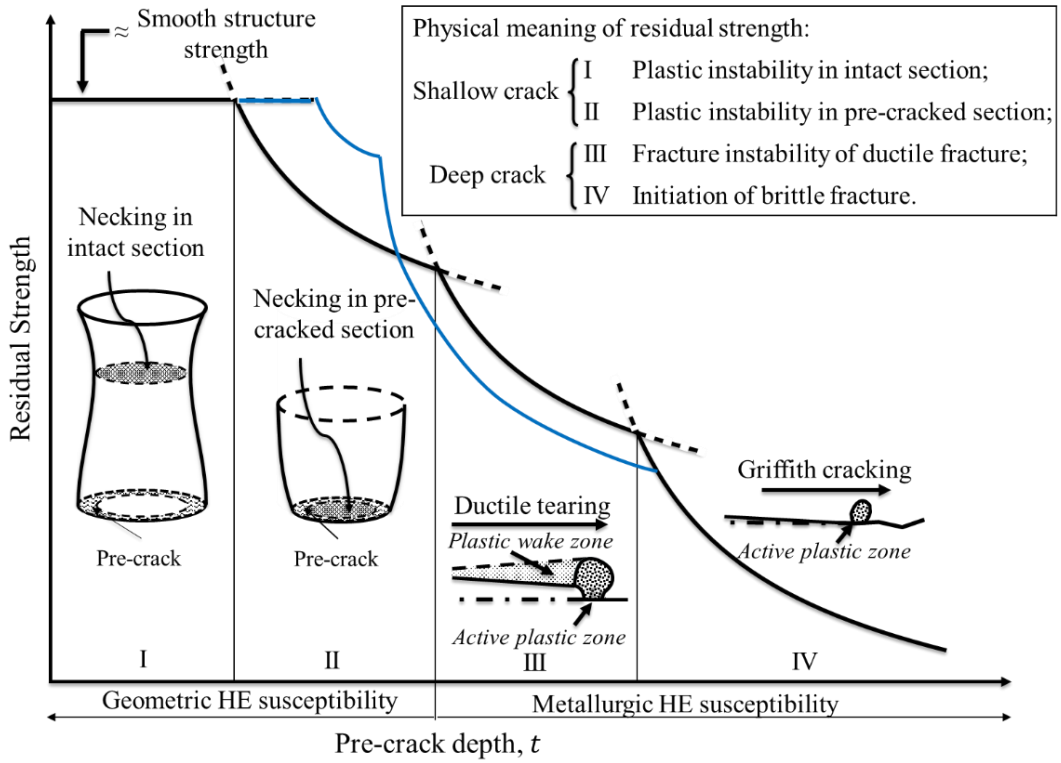

Fig. 5.8 A subdivision of HE susceptibility plotted in failure assessment diagram of residual strength (identical to UTS in this study) [138] (Blue solid line shows the prediction of residual strength with hydrogen from the perspective of plastic strain localization).

5.5 Chapter conclusions

Fully electrochemical hydrogen pre-charged cylinder specimens (also with in-situ charging during monotonic tension to maintain the hydrogen saturation) were experimentally and microscope-analytically compared with uncharged specimens (without in-situ charging). The results showed that shallow cracks with HE did not weaken the residual strength governed by plastic instability. The underlying reason is that crack propagation assisted by HELP is stable before the onset of plastic instability; meanwhile, the plastic strain localization at crack-tips even resists the onset of plastic instability. The influence of hydrogen on pre-cracked structures is contrary to the common-sense understanding of it, and we discussed the previous understanding of HE

susceptibility in light of our results. The following conclusions can be obtained:

1. Shallow cracks with HE may not weaken the residual strength governed by plastic instability.
2. The residual strength influenced by the interaction of crack effect and hydrogen effect depends not only on the material properties but also on the geometric properties.
3. Geometric HE susceptibility is the main contributor to HE susceptibility for shallow pre-cracked structures, whereas metallurgic HE susceptibility dominates for deep pre-cracked structures.
4. Subdividing HE susceptibility can define the conditions under which plastic strain localization caused by HE susceptibility is beneficial for residual strength in fail-safe design.

CHAPTER 6. General conclusions

A shallow crack-like notch may exist when structural strength is governed by plastic instability. When the plastic instability governs the structural strength of strain-hardening materials, a crack-like notch should satisfy the following requirements:1. The structural strength should be independent of the notch geometry, except for the notch depth; 2. The elastoplastic fields in the notched cross-section should be broadly convergent to those in the pre-cracked cross-section such that the overall work hardening is identical; 3. The failure mode should be the same. The material work hardening exponent, notch root radius, and ligament size may exert relatively significant influences on the identification of shallow crack-like notches.

Shallow cracks have the following effect on residual strength evaluation: 1. The fracture toughness of shallow cracks is so high that the main impact of the plastic strain localization coupled with stress triaxiality changed from stimulating fracture instability at crack tip to hindering cross-sectional plastic instability; 2. The presence of shallow pre-cracks resulted in both negative and positive influences on load-carrying capacity in different partitions of the pre-cracked cross-section. The physical meaning of residual strength changes with the pre-crack depth due to the different magnitudes of plastic strain localization and can be reflected in the variation of the damage characteristics.

The trends of residual strength in the shallow crack category can be qualitatively estimated from the perspective of plastic strain localization. The shallow crack effect is not a material intrinsic property, and all factors that can influence the magnitude of plastic strain localization are significant for shallow pre-cracked structures. The

continuum mechanics is suitable for numerical prediction of residual strength of shallow pre-cracked structures. However, it should consider the local plastic flow property influenced by the presence of pre-crack to induce the correct phenomenon, namely, the necking away from the pre-cracked section.

Shallow cracks combined with the hydrogen effect also may not weaken the residual governed by plastic instability. The residual strength influenced by the interaction of crack effect and hydrogen effect depends not only on the material properties but also on the geometric properties. Geometric hydrogen-embrittlement susceptibility is the main contributor to hydrogen-embrittlement susceptibility for shallow pre-cracked structures, whereas metallurgic hydrogen-embrittlement susceptibility dominates for deep pre-cracked structures.

Appendix

A1. Microstructure of IF steel and measurement of grain size

The simple for microstructure observation was extracted from the center of the material raw treated by 2h annealing (750℃). After buff polishing, the surface of simple was etched in 2% nital solution for 10s. The representative microstructure of IF steel is shown in Fig. A1.1. The average grain size was measured according to ASTM E112 - 12 [142]. Fig. A1.2 shows the histogram of grain size by accounting for 200 grains.

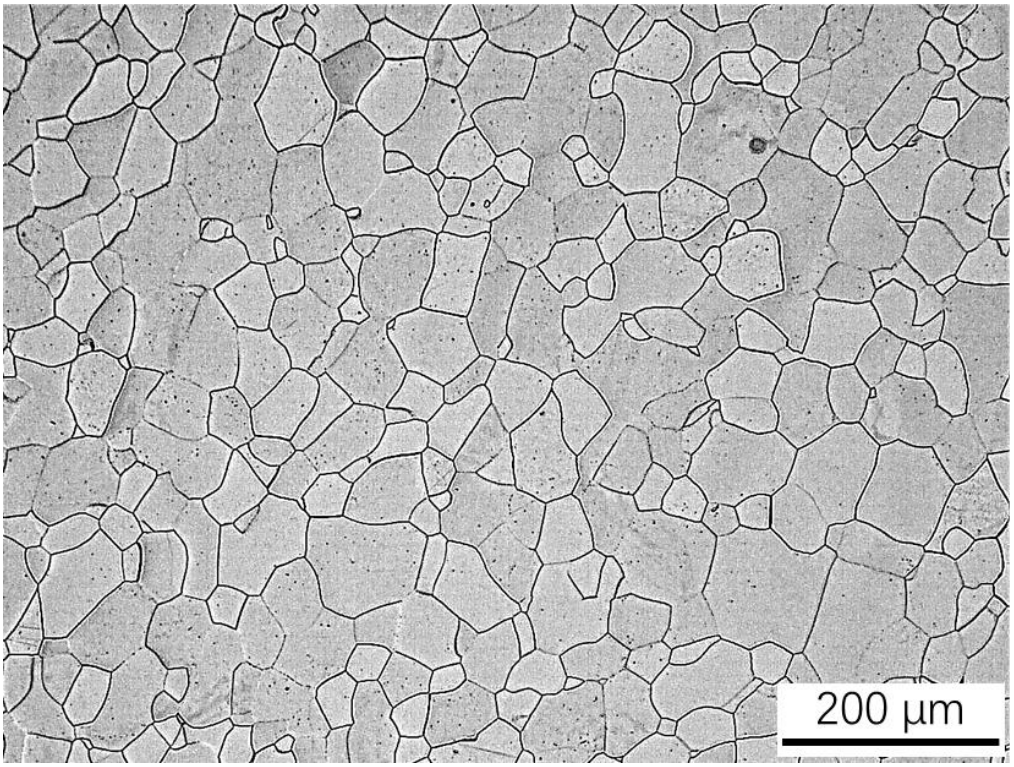

Fig. A1.1 Microstructure of IF steel after 2 h annealing (750 ℃) and then cooling at room temperature.

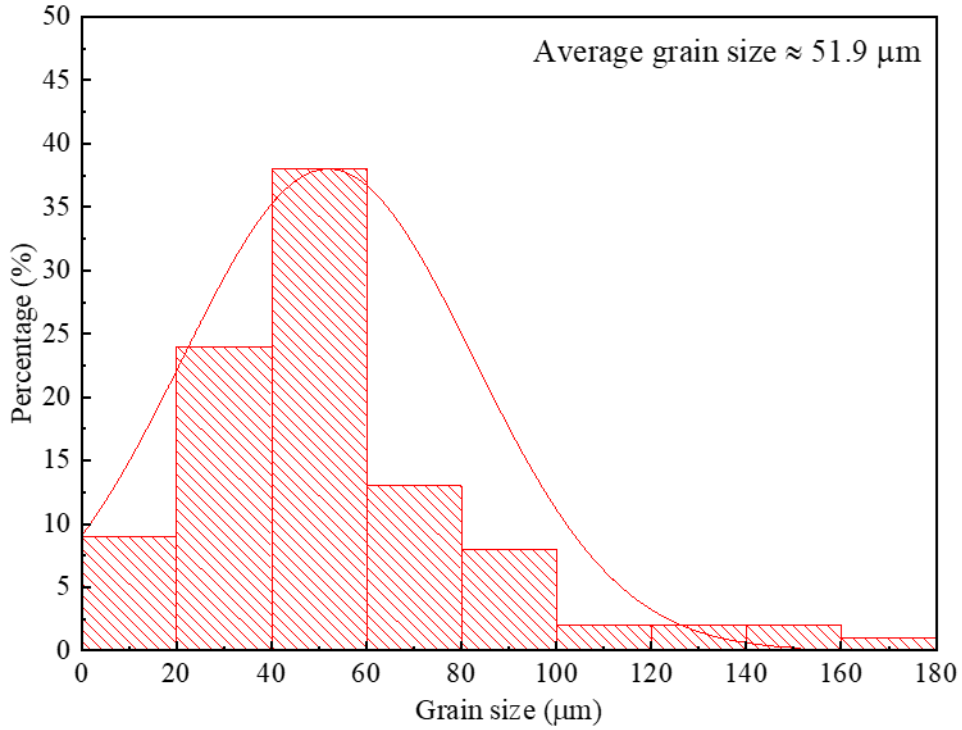

Fig. A1.2 Histogram of grain size by accounting 200 grains.

A2. Measurement of notch dimensions

The measurement of notch dimensions, such as notch depth, root radius, and opening angle, was assisted by SEM, as shown in Fig. A2.1. After machining, the notch dimensions and symmetry were checked initially. As illustrated in Fig. A2.2, four checking points with intervals of 90° were selected for the measurement. Meanwhile, the margin on the specimen gage left after machining also should be verified. Then, the radius of the specimen gage and the pre-crack depth was polished to approach the designed size. Eventually, the final dimensions of notches were rechecked by SEM and were averaged by data measured at four checking point illustrated in Fig. A2.2.

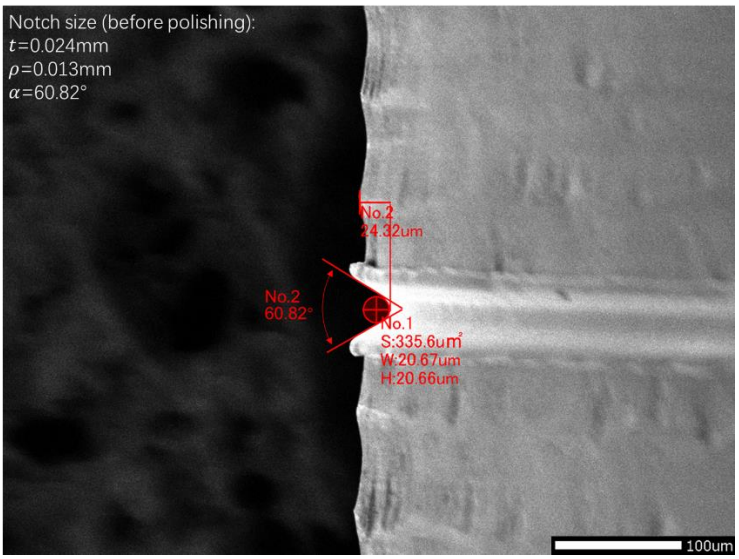

Fig. A2.1 Example of notch dimensions measured by SEM

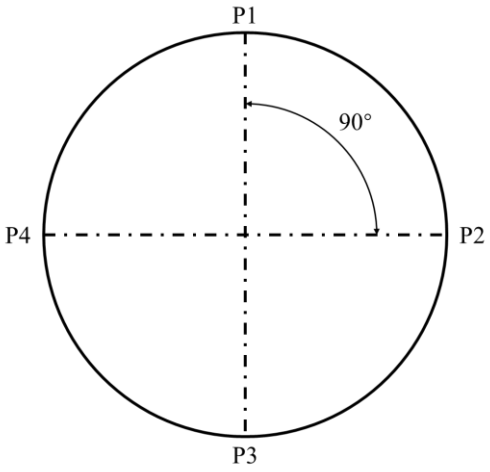

Fig. A2.2 Skemetic of four checking points for notch dimension measurement on pre-cracked cross-section.

A3. Stress-strain curves for specimens of continuous tests listed in Table 3.1

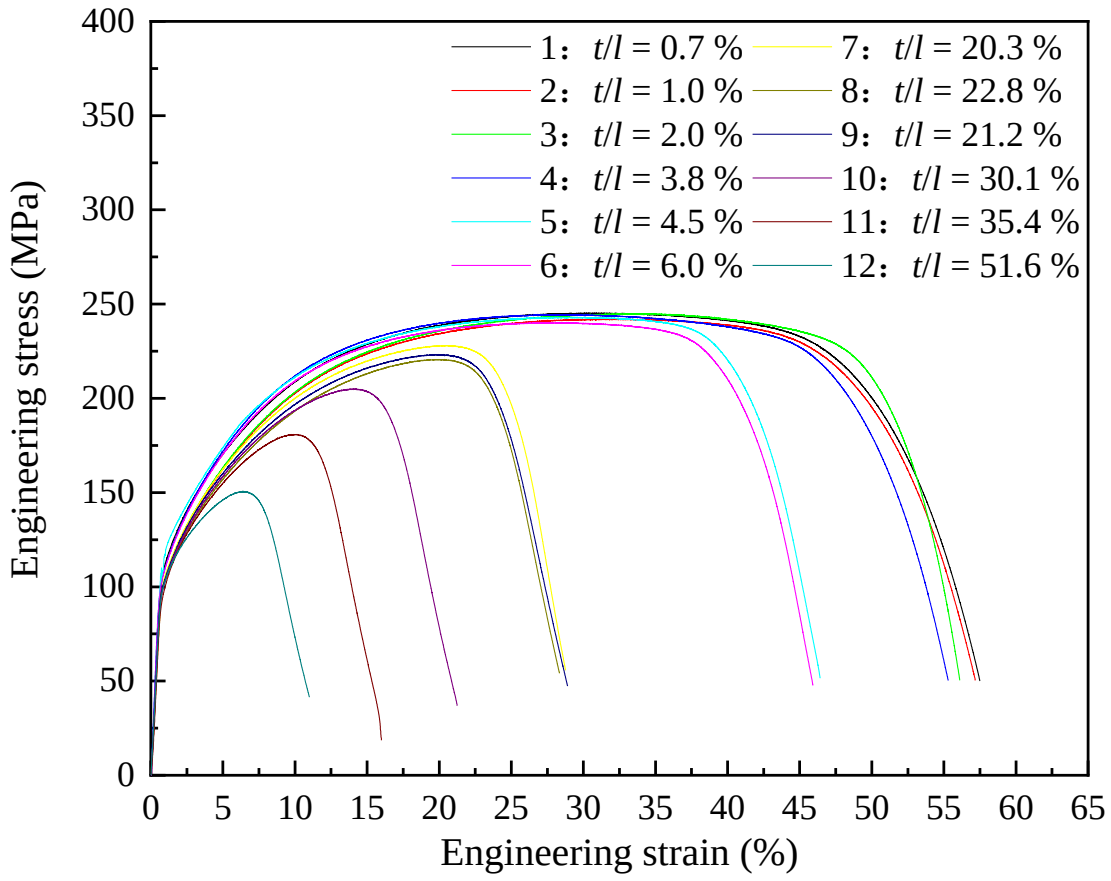

Fig. A3 Engineering stress-strain curves for specimens of continuous tests listed in Table 3.1.

References

[1] J.P. Gallagher, F.J. Giessler, A.P. Berens, USAF Damage Tolerant Design Handbook: Guidelines for the Analysis and Design of Damage Tolerant Aircraft Structures, United States Air Force Flight Dynamics Laboratory, Dayton, OH, 1979.

[2] B. Farahmand, M. Aliabadi, Fracture Mechanics of Metals, Composites, Welds, and Bolted Joints: Application of LEFM, EPFM, and FMDM Theory, Appl. Mech. Rev. 55 (2002) B71. doi:10.1115/1.1483354.

[3] P. Kuhn, Residual tensile strength in the presence of through cracks or surface cracks, Hampton, VA, 1970.

[4] D.A. Sukeerth, G. Thammaiah, Damage Tolerance Evaluation for Wing Structure with Large Cutout, Int. J. Mech. Eng. Res. 4 (2014) 48–57.

[5] J.. Newman, D.. Dawicke, B.. Seshadri, Residual strength analyses of stiffened and un-stiffened panels—Part I: laboratory specimens, Eng. Fract. Mech. 70 (2003) 493–507. doi:10.1016/S0013-7944(02)00133-9.

[6] B.R. Seshadri, J.C. Newman, D.S. Dawicke, Residual strength analyses of stiffened and unstiffened panels—Part II: wide panels, Eng. Fract. Mech. 70 (2003) 509–524. doi:10.1016/S0013-7944(02)00134-0.

[7] F. Wang, W.C. Cui, Cracked structures and residual strength, in: Cond. Assess. Aged Struct., Elsevier, 2008: pp. 186–230. doi:10.1533/9781845695217.3.186.

[8] G. Benedetto, I. Generoso, L. Mauro, M. Marco, S. Fabio, Residual strength validation of a composite stiffened panel virtually impacted, Procedia Eng. 88 (2014) 242–254. doi:10.1016/j.proeng.2014.11.151.

[9] C.-S. Chen, P.A. Wawrzynek, A.R. Ingraffea, Crack growth simulation and residual strength prediction in airplane fuselages, NASA Langley Research Center, Hampton, VA, 1999.

[10] C. Feddersen, Evaluation and prediction of the residual strength of center cracked tension panels, in: Damage Toler. Aircr. Struct. ASTM STP 486, ASTM International, West Conshohocken, PA, 1971: pp. 50–78. doi:10.1520/STP26673S.

[11] K.-H. Schwalbe, A Modification of the COD Concept and Its Tentative Application to the Residual Strength of Center Cracked Panels, in: Fract. Mech. 12th Conf. ASTM STP700, ASTM International, West Conshohocken, PA, 1980: pp. 500–512. doi:10.1520/STP36988S.

[12] C.-S. Chen, P.A. Wawrzynek, A.R. Ingraffea, Elastic-plastic crack growth simulation and residual strength prediction of thin plates with single and multiple cracks, in: T.L. Panontin, S.D. Sheppard (Eds.), Fatigue Fract. Mech. 29th Vol. ASTM STP 1332, ASTM International, West Conshohocken, PA, 1999: pp. 97–113. doi:10.1520/STP14945S.

[13] I. Scheider, W. Brocks, Residual strength prediction of a complex structure using crack extension analyses, Eng. Fract. Mech. 76 (2009) 149–163. doi:10.1016/j.engfracmech.2008.06.035.

[14] A.A. Griffits, The phenomena of rupture and flow in solids, Philos. Trans. R. Soc. London. A (1921) 163–198. doi:10.1098/rsta.1921.0006.

[15] G.R. Irwin, Analysis of Stresses and Strains near the End of a Crack Traversing a Plate, J. Appl. Mech. 24 (1957) 361–364.

[16] J.R. Rice, A Path Independent Integral and the Approximate Analysis of Strain Concentration by Notches and Cracks, J. Appl. Mech. 35 (1968) 379. doi:10.1115/1.3601206.

[17] T.L. Anderson, Fracture Mechanics: Fundamentals and Applications, 3rd ed., CRC Press, Boca Raton, 2005.

[18] J.F. Knott, Fundamentals of Fracture Mechanics, Butterworth & Co Ltd, London, 1973.

[19] T. Kobayashi, Strength and Toughness of Materials, Springer Japan, Tokyo, 2004. doi:10.1007/978-4-431-53973-5.

[20] M.F. Ashby, Materials Selection in Mechanical Design, 4th ed., Butterworth-Heinemann, Burlington, MA, 2011. doi:10.1016/C2009-0-25539-5.

[21] Volpe National Transportation Systems Center, Damage Tolerance: Assessment Handbook. Volume 2: Airframe Damage Tolerance Evaluation, (1993) 196.

[22] BS 7910, BSI Standards Publication Guide to methods for assessing the acceptability of flaws in metallic structures, BSI Stand. Publ. (2015) 490.

[23] API, ASME, Fitness-For-Service, ASME, 2016.

[24] I. Vamsi, R.A. Kumar, Y.S. Reddy, Analysis of Crack in Riveted Joints with the Help of Fracture Mechanics, Int. J. Eng. Sci. 5 (2016) 79–85.

[25] G.C. Sih, Isoenergy density theory: exchange of surface and volume energy, in: G.C. Sih (Ed.), Mech. Fract. Initiat. Propag. Surf. Vol. Energy Density Appl. as Fail. Criterion, Springer Netherlands, Dordrecht, 1991: pp. 307–403. doi:10.1007/978-94-011-3734-8_9.

[26] M. Irfaee, H. Mahmoud, Mixed-Mode Fatigue and Fracture Assessment of a Steel Twin Box-Girder Bridge, J. Bridg. Eng. 24 (2019) 04019056. doi:10.1061/(ASCE)BE.1943-5592.0001424.

[27] B. O'Neill, Preventing Passenger Vehicle Occupant Injuries by Vehicle Design—A Historical Perspective from IIHS, Traffic Inj. Prev. 10 (2009) 113–126. doi:10.1080/15389580802486225.

[28] B. Barényi, Motor vehicles, in particular for the transportation of people, DE854157, 1952. https://www.dpma.de/ponline/erfindergalerie/patente/de854157.pdf.

[29] Euro NCAP, Crash & Safety Tests of Nissan Juke, 2019. https://www.euroncap.com/en/results/nissan/juke/39679.

[30] X.K. Zhu, J.A. Joyce, Review of fracture toughness (G, K, J, CTOD, CTOA) testing and standardization, Eng. Fract. Mech. 85 (2012) 1–46. doi:10.1016/j.engfracmech.2012.02.001.

[31] A. Pineau, A.A. Benzerga, T. Pardoen, Failure of metals I: Brittle and ductile fracture, Acta Mater. 107 (2016) 424–483. doi:10.1016/j.actamat.2015.12.034.

[32] G.R. Irwin, Onset of fast crack propagation in high strength steel and aluminum alloys, Washington DC, 1956.

[33] E. Duncombe, Plastic instability and growth of grooves and patches in plates or tubes, Int. J. Mech. Sci. 14 (1972) 325–337. doi:10.1016/0020-7403(72)90087-2.

[34] I.H. Lin, J.P. Hirth, E.W. Hart, Plastic instability in uniaxial tension tests, Acta Metall. 29 (1981) 819–827. doi:10.1016/0001-6160(81)90124-3.

[35] S.D. Antolovich, R.W. Armstrong, Plastic strain localization in metals: Origins and consequences, Prog. Mater. Sci. 59 (2014) 1–160. doi:10.1016/j.pmatsci.2013.06.001.

[36] D. Broek, The Practical Use of Fracture Mechanics, Springer Netherlands, Dordrecht, 1989. doi:10.1007/978-94-009-2558-8.

[37] G.C. Sih, Mechanics of Fracture Initiation and Propagation, Springer Netherlands, Dordrecht, 1991. doi:10.1007/978-94-011-3734-8.

[38] A. Ibrahimbegovic, Nonlinear Solid Mechanics : Theoretical Formulations and Finite Element Solution Methods, Springer Netherlands, Dordrecht, 2009. doi:10.1007/978-90-481-2331-5.

[39] A. Considére, Memoire sur l'emploi du fer et de l'acier dans les constructions (On the use of iron and steel in construction), Ann Ponts Chauss. 9 (1885) 574–775.

[40] M.G. Dawes, J.R. Gordon, J.R. Gordon, The requirement for shallow crack fracture toughness tests, in: Shallow Crack Fract. Mech. Toughness Tests Appl., Elsevier, 1993: pp. 3–13. doi:10.1533/9780857093226.1.1.

[41] A. Needleman, Continuum mechanics studies of plastic instabilities, Rev. Phys. Appliquée. 23 (1988) 585–593. doi:10.1051/rphysap:01988002304058500.

[42] Y. Tomita, Simulations of Plastic Instabilities in Solid Mechanics, Appl. Mech. Rev. 47 (1994) 171–205. doi:10.1115/1.3111077.

[43] A. Ibrahimbegovic, Geometric and material instabilities, in: A. Ibrahimbegovic (Ed.), Nonlinear Solid Mech., Springer Netherlands, Dordrecht, 2009: pp. 475–530. doi:10.1007/978-90-481-2331-5_8.

[44] H. Vlieger, The residual strength characteristics of stiffened panels containing fatigue cracks, Eng. Fract. Mech. 5 (1973) 447–477. doi:10.1016/0013-7944(73)90033-7.

[45] A.M. Al-Ani, J.W. Hancock, J-Dominance of short cracks in tension and bending, J. Mech. Phys. Solids. 39 (1991) 23–43. doi:10.1016/0022-5096(91)90029-N.

[46] K.J. Miller, The Short Crack Problem, Fatigue Fract. Eng. Mater. Struct. 5 (1982) 223–232. doi:10.1111/j.1460-2695.1982.tb01250.x.

[47] S. Kolitsch, R. Pippan, Crack driving forces for short cracks: The effect of work hardening, Eng. Fract. Mech. 187 (2018) 262–271. doi:10.1016/j.engfracmech.2017.11.028.

[48] W.A. Sorem, R.H. Dodds, S.T. Rolfe, Effects of crack depth on elastic-plastic fracture toughness, Int. J. Fract. 47 (1991) 105–126. doi:10.1007/BF00032572.

[49] Y. Murakami, Metal fatigue: effects of small defects and nonmetallic inclusions, 1st ed., Elsevier, Oxford, 2002. doi:10.1016/B978-0-08-044064-4.X5000-2.

[50] D.A. Skinn, J.P. Gallagher, A.P. Berens, P.D. Huber, J. Smith, Damage tolerant design handbook, Wright Laboratory, Dayton, OH, 1994.

[51] J.R. Rice, Limitations to the small scale yielding approximation for crack tip plasticity, J. Mech. Phys. Solids. 22 (1974) 17–26. doi:10.1016/0022-5096(74)90010-6.

[52] N.P. O'Dowd, C.F. Shih, Family of crack-tip fields characterized by a triaxiality parameter-I. Structure of fields, J. Mech. Phys. Solids. 39 (1991) 989–1015. doi:10.1016/0022-5096(91)90049-T.

[53] N. O'Dowd, C. Shih, Two-Parameter Fracture Mechanics: Theory and Applications, in: Fract. Mech. Twenty-Fourth Vol., ASTM International, West Conshohocken, PA, 1994: pp. 21-21–27. doi:10.1520/STP13698S.

[54] R.W. Hertzberg, R.P. Vinci, J.L. Hertzberg, Deformation and Fracture Mechanics of Engineering Materials, 5th ed., Wiley, 2012.

[55] C.T. Sun, Z.-H. Jin, Crack Tip Plasticity, in: Fract. Mech., 1st ed., Elsevier, Waltham, MA, 2012: pp. 123–169. doi:10.1016/B978-0-12-385001-0.00006-7.

[56] E. Hackett, K.-H. Schwalbe, R. Dodds, eds., Constraint Effects in Fracture, ASTM International, West Conshohocken, PA, 1993. doi:10.1520/STP1171-EB.

[57] M.T. Kirk, The second ASTM/ESIS Symposium on Constraint Effects in Fracture; an overview, Int. J. Press. Vessel. Pip. 64 (1995) 259–275. doi:10.1016/0308-0161(95)98948-6.

[58] M.G. Dawes, B. Cotterell, S.-X. Wu, Y.-W. Mai, PAPER 3 – The effect of constraint on fracture of carbon and low alloy steel, in: Shallow Crack Fract. Mech. Toughness Tests Appl., 1993: pp. 81–90. doi:10.1533/9780857093226.1.78.

[59] Y.J. Chao, P.S. Lam, L. Zhang, Effect of constraint on fracture controlled by stress or strain, Theor. Appl. Fract. Mech. 30 (1998) 75–86. doi:10.1016/S0167-8442(98)00043-3.

[60] X.K. Zhu, J.A. Joyce, J-Resistance curve testing of HY80 steel using SE(B) specimens and normalization method, Eng. Fract. Mech. 74 (2007) 2263–2281. doi:10.1016/j.engfracmech.2006.10.018.

[61] A. Neimitz, I. Dzioba, J. Gałkiewicz, R. Molasy, A study of stable crack growth using experimental methods, finite elements and fractography, Eng. Fract. Mech. 71 (2004) 1325–1355. doi:10.1016/S0013-7944(03)00169-3.

[62] D. Dini, D. a Hills, When does a notch behave like a crack?, Proc. Inst. Mech. Eng. Part C J. Mech. Eng. Sci. 220 (2006) 27–43. doi:10.1243/095440605X32093.

[63] X. Zheng, On an unified model for predicting notch strength and fracture toughness of metals, Eng. Fract. Mech. 33 (1989) 685–695. doi:10.1016/0013-7944(89)90067-2.

[64] B.W. Lee, J. il Jang, D. Kwon, Evaluation of fracture toughness using small notched specimens, Mater. Sci. Eng. A. 334 (2002) 207–214. doi:10.1016/S0921-5093(01)01804-4.

[65] M. Faccoli, C. Cornacchia, M. Gelfi, A. Panvini, R. Roberti, Notch ductility of steels for automotive components, Eng. Fract. Mech. 127 (2014) 181–193. doi:10.1016/j.engfracmech.2014.06.007.

[66] G.E. Dieter, D. Bacon, S.M. Copley, C. a Wert, G.L. Wilkes, Mechanical Metallurgy, SI Metric, McGraw-Hill, New York, 1988.

[67] A.M. Agogino, Notch Effects, Stress State, and Ductility, J. Eng. Mater. Technol. 100 (1978) 348. doi:10.1115/1.3443503.

[68] R. Qu, P. Zhang, Z. Zhang, Notch Effect of Materials: Strengthening or Weakening?, J. Mater. Sci. Technol. 30 (2014) 599–608. doi:10.1016/j.jmst.2014.04.014.

[69] S. Keeler, M. Kimchi, P. J. Mooney, Advanced High-Strength Steels Application Guidelines, 6th ed., World Auto Steel, 2017.

[70] M.N. James, Intergranular crack paths during fatigue in interstitial-free steels, Eng. Fract. Mech. 77 (2010) 1998–2007. doi:10.1016/j.engfracmech.2009.12.006.

[71] O. Akourri, M. Louah, A. Kifani, G. Gilgert, G. Pluvinage, The effect of notch radius on fracture toughness JIc, Eng. Fract. Mech. 65 (2000) 491–505. doi:10.1016/S0013-7944(99)00109-5.

[72] M.H. El Haddad, T.H. Topper, K.N. Smith, Prediction of non propagating cracks, Eng. Fract. Mech. 11 (1979) 573–584. doi:10.1016/0013-7944(79)90081-X.

[73] R.A. Smith, K.J. Miller, Prediction of fatigue regimes in notched components, Int. J. Mech. Sci. 20 (1978) 201–206. doi:10.1016/0020-7403(78)90082-6.

[74] D. Taylor, M. O'Donnell, Notch geometry effects in fatigue: A conservative design approach, Eng. Fail. Anal. 1 (1994) 275–287. doi:10.1016/1350-6307(94)90003-5.

[75] D. Taylor, Crack modelling: A technique for the fatigue design of components, Eng. Fail. Anal. 3 (1996) 129–136. doi:10.1016/1350-6307(96)00004-0.

[76] D. Taylor, Geometrical effects in fatigue: a unifying theoretical model, Int. J. Fatigue. 21 (2000) 413–420. doi:10.1016/S0142-1123(99)00007-9.

[77] B. Atzori, P. Lazzarin, Notch Sensitivity and Defect Sensitivity under Fatigue Loading: Two Sides of the Same Medal, Int. J. Fract. 107 (2001) 3–8. doi:10.1023/A:1007686727207.

[78] G.G. Adams, D.A. Hills, Analytical representation of the non-square-root singular stress field at a finite angle sharp notch, Int. J. Solids Struct. 51 (2014) 4485–4491. doi:10.1016/j.ijsolstr.2014.08.024.

[79] L. Tutluoglu, C. Keles, Mode I fracture toughness determination with straight notched disk bending method, Int. J. Rock Mech. Min. Sci. 48 (2011) 1248–1261. doi:10.1016/j.ijrmms.2011.09.019.

[80] P. Antoine, S. Vandeputte, J.B. Vogt, Effect of microstructure on strain-hardening behaviour of a Ti-IF steel grade, ISIJ Int. 45 (2005) 399–404. doi:10.2355/isijinternational.45.399.

[81] H.-H. Lee, Finite element simulations with ANSYS Workbench 18: theory, applications, case studies, Schroff Development Corporation, Mission, KS, 2018.

[82] J. Chakrabarty, Theory of plasticity, Elsevier/Butterworth-Heinemann, 2006. https://www.sciencedirect.com/science/book/9780750666381 (accessed March 15, 2018).

[83] ASTM International, ASTM E8 / E8M - 16a: Standard Test Methods for Tension Testing of Metallic Materials, in: West Conshohocken, PA, 2016. doi:10.1520/E0008_E0008M-16A.

[84] N.A. Noda, Y. Takase, Stress concentration formula useful for all notch shape in a round bar (comparison between torsion, tension and bending), Int. J. Fatigue. 28 (2006) 151–163. doi:10.1016/j.ijfatigue.2005.04.015.

[85] H. Liebowitz, Fracture of Metals, in: Fract. An Adv. Treatise, Academic Press, New York, 1969: p. 513. doi:10.1016/C2013-0-11089-6.

[86] W.T. Becker, Ductile and brittle fracture, in: Princ. Fail. Anal., ASM International, Novelty, OH, 2002.

[87] J.Y. Chen, Y. Wei, Y. Huang, J.W. Hutchinson, K.C. Hwang, The crack tip fields in strain gradient plasticity: The asymptotic and numerical analyses, Eng. Fract. Mech. 64 (1999) 625–648. doi:10.1016/s0013-7944(99)00073-9.

[88] H. Jiang, Y. Huang, Z. Zhuang, K.C. Hwang, Fracture in mechanism-based strain gradient plasticity, J. Mech. Phys. Solids. 49 (2001) 979–993. doi:10.1016/S0022-5096(00)00070-3.

[89] B. Li, M. Koyama, E. Sakurada, N. Yoshimura, K. Ushioda, H. Noguchi, Potential resistance to transgranular fatigue crack growth of Fe–C alloy with a supersaturated carbon clarified through FIB micro-notching technique, Int. J. Fatigue. 87 (2016) 1–5. doi:10.1016/j.ijfatigue.2016.01.003.

[90] D.A. Hills, D. Dini, Characteristics of the process zone at sharp notch roots, Int. J. Solids Struct. 48 (2011) 2177–2183. doi:10.1016/j.ijsolstr.2011.03.023.

[91] S.I. Wright, M.M. Nowell, D.P. Field, A review of strain analysis using electron backscatter diffraction, Microsc. Microanal. 17 (2011) 316–329. doi:10.1017/S1431927611000055.

[92] J. Ast, M. Göken, K. Durst, Size-dependent fracture toughness of tungsten, Acta Mater. (2017). doi:10.1016/j.actamat.2017.07.030.

[93] N. Allain-Bonasso, F. Wagner, S. Berbenni, D.P. Field, A study of the heterogeneity of plastic deformation in IF steel by EBSD, Mater. Sci. Eng. A. 548 (2012) 56–63. doi:10.1016/j.msea.2012.03.068.

[94] A. Le Van, P. Le Grognec, Modeling and numerical computation of necking in round bars using a total Lagrangian elastoplastic formulation, C. - Comput. Model. Eng. Sci. 2 (2001) 63–72.

[95] C.D. Beachem, Electron Fractographic Studies of Mechanical Fracture Processes in Metals, J. Basic Eng. 87 (1965) 299. doi:10.1115/1.3650544.

[96] W.T. Becker, S. Lampman, Fracture appearance and mechanisms of deformation and fracture, Mater. Park. OH ASM Int. 2002. (2002) 559–586. doi:10.1361/asmhba0003537.

[97] S. Govindjee, Engineering Mechanics of Deformable Solids, Oxford University Press, 2012. doi:10.1093/acprof:oso/9780199651641.001.0001.

[98] J.R. Rice, Elastic-plastic models for stable crack growth, in: M.J. May (Ed.), Mech. Mech. Crack Growth, British steel corporation, Cambridge, UK, 1973: pp. 14–39.

[99] J.R. RICE, Elastic–Plastic Crack Growth, in: Mech. Solids, Elsevier, 1982: pp. 539–562. doi:10.1016/B978-0-08-025443-2.50022-7.

[100] T. Pardoen, Y. Marchal, F. Delannay, Thickness dependence of cracking resistance in thin aluminium plates, 1999. doi:10.1016/S0022-5096(99)00011-3.

[101] A. Ridruejo, R. Jubera, C. González, J. LLorca, Inverse notch sensitivity: Cracks can make nonwoven fabrics stronger, J. Mech. Phys. Solids. 77 (2015) 61–69. doi:10.1016/j.jmps.2015.01.004.

[102] J.R. Rice, The localization of plastic deformation, 14th Int. Congr. Theoratical Appl. Mech. (1976) 207–220. doi:10.1.1.160.6740.

[103] M.A. Meyers, K.K. Chawla, Mechanical Behavior of Materials, 2nd ed., Cambridge university press, Cambridge, 2009. www.cambridge.org/9780521866750.

[104] A. Das, M. Ghosh, S. Tarafder, S. Sivaprasad, D. Chakrabarti, Micromechanisms of deformation in dual phase steels at high strain rates, Mater. Sci. Eng. A. 680 (2017) 249–258. doi:10.1016/j.msea.2016.10.101.

[105] S.X. Wu, Y.W. Mai, B. Cotterell, C. Wiet Le, Ductile-brittle fracture transition due to increasing crack length in a medium carbon steel, Acta Metall. Mater. 39 (1991) 2527–2532. doi:10.1016/0956-7151(91)90068-C.

[106] M.R. Gilbert, S. Queyreau, J. Marian, Stress and temperature dependence of screw dislocation mobility in α-Fe by molecular dynamics, Phys. Rev. B - Condens. Matter Mater. Phys. 84 (2011) 1–11. doi:10.1103/PhysRevB.84.174103.

[107] M. Koyama, H. Springer, S. V. Merzlikin, K. Tsuzaki, E. Akiyama, D. Raabe, Hydrogen embrittlement associated with strain localization in a precipitation-

hardened Fe-Mn-Al-C light weight austenitic steel, Int. J. Hydrogen Energy. 39 (2014) 4634–4646. doi:10.1016/j.ijhydene.2013.12.171.

[108] M. Kuroda, A. Uenishi, H. Yoshida, A. Igarashi, Ductility of interstitial-free steel under high strain rate tension: Experiments and macroscopic modeling with a physically-based consideration, Int. J. Solids Struct. 43 (2006) 4465–4483. doi:10.1016/j.ijsolstr.2005.06.076.

[109] V. Tvergaard, Material Failure by Void Growth to Coalescence, in: Adv. Appl. Mech., 1989: pp. 83–151. doi:10.1016/S0065-2156(08)70195-9.

[110] M. Nagumo, Fundamentals of Hydrogen Embrittlement, Springer Singapore, Singapore, 2016. doi:10.1007/978-981-10-0161-1.

[111] N.N. Sergeev, A.N. Sergeev, S.N. Kutepov, A.G. Kolmakov, A.E. Gvozdev, Mechanism of the Hydrogen Cracking of Metals and Alloys, Part I (Review), Inorg. Mater. Appl. Res. 10 (2019) 24–31. doi:10.1134/S207511331901026X.

[112] N.N. Sergeev, A.N. Sergeev, S.N. Kutepov, A.G. Kolmakov, A.E. Gvozdev, Mechanism of the hydrogen cracking of metals and alloys, part II (Review), Inorg. Mater. Appl. Res. 10 (2019) 32–41. doi:10.1134/S2075113319010271.

[113] S.P. Lynch, Hydrogen embrittlement (HE) phenomena and mechanisms, in: Stress Corros. Crack., Elsevier, 2011: pp. 90–130. doi:10.1533/9780857093769.1.90.

[114] M. Koyama, C.C. Tasan, E. Akiyama, K. Tsuzaki, D. Raabe, Hydrogen-assisted decohesion and localized plasticity in dual-phase steel, Acta Mater. 70 (2014) 174–187. doi:10.1016/j.actamat.2014.01.048.

[115] M. Koyama, E. Akiyama, T. Sawaguchi, K. Ogawa, I. V. Kireeva, Y.I. Chumlyakov, K. Tsuzaki, Hydrogen-assisted quasi-cleavage fracture in a single crystalline type 316 austenitic stainless steel, Corros. Sci. 75 (2013) 345–353. doi:10.1016/j.corsci.2013.06.018.

[116] P. Sofronis, I.M. Robertson, Viable mechanisms of hydrogen embrittlement - A review, AIP Conf. Proc. 837 (2006) 64–70. doi:10.1063/1.2213060.

[117] A. Mohammadi, M. Koyama, G. Gerstein, H.J. Maier, H. Noguchi, Hydrogen-assisted failure in a bimodal twinning-induced plasticity steel: Delamination

events and damage evolution, Int. J. Hydrogen Energy. 43 (2018) 2492–2502. doi:10.1016/j.ijhydene.2017.11.177.

[118] N.P. Brandon, Z. Kurban, Clean energy and the hydrogen economy, Philos. Trans. R. Soc. A Math. Phys. Eng. Sci. 375 (2017) 20160400. doi:10.1098/rsta.2016.0400.

[119] L. Peraldo Bicelli, Hydrogen: A clean energy source, Int. J. Hydrogen Energy. 11 (1986) 555–562. doi:10.1016/0360-3199(86)90121-7.

[120] F.F. Dear, G.C.G. Skinner, Mechanisms of hydrogen embrittlement in steels: Discussion, Philos. Trans. R. Soc. A Math. Phys. Eng. Sci. 375 (2017). doi:10.1098/rsta.2017.0032.

[121] E.L. Simpson, M. Patel, Hydrogen in steels: Discussion, Philos. Trans. R. Soc. A Math. Phys. Eng. Sci. 375 (2017). doi:10.1098/rsta.2017.0027.

[122] A. Traidia, E. Chatzidouros, M. Jouiad, Review of hydrogen-assisted cracking models for application to service lifetime prediction and challenges in the oil and gas industry, Corros. Rev. 36 (2018) 323–347. doi:10.1515/corrrev-2017-0079.

[123] B.P. Somerday, M. Dadfarnia, D.K. Balch, K.A. Nibur, C.H. Cadden, P. Sofronis, Hydrogen-assisted crack propagation in austenitic stainless steel fusion welds, Metall. Mater. Trans. A Phys. Metall. Mater. Sci. 40 (2009) 2350–2362. doi:10.1007/s11661-009-9922-1.

[124] D.C. Ahn, P. Sofronis, R. Dodds, Modeling of hydrogen-assisted ductile crack propagation in metals and alloys, Int. J. Fract. 145 (2007) 135–157. doi:10.1007/s10704-007-9112-3.

[125] D.G. Westlake, A generalized model for hydrogen embrittlement, Trans. Am. Soc. Met. 62 (1969) 1000–1006.

[126] H.K. Birnbaum, P. Sofronis, Hydrogen-enhanced localized plasticity—a mechanism for hydrogen-related fracture, Mater. Sci. Eng. A. 176 (1994) 191–202. doi:10.1016/0921-5093(94)90975-X.

[127] R.A. Oriani, P.H. Josephic, Testing of the decohesion theory of hydrogen-induced crack propagation, Scr. Metall. 6 (1972) 681–688. doi:10.1016/0036-9748(72)90126-3.

[128] M.G. Dawes, Shallow crack fracture mechanics, toughness tests and applocations, 1st ed., Woodhead Publishing, Cambridge, UK, 1992.

[129] P.W. Liu, J.K. Wu, Hydrogen susceptibility of an interstitial free steel, Mater. Lett. 57 (2003) 1224–1228. doi:10.1016/S0167-577X(02)00962-X.

[130] P. Ghosh, R.K. Ray, C. Ghosh, D. Bhattacharjee, Comparative study of precipitation behavior and texture formation in continuously annealed Ti and Ti + Nb added interstitial-free high-strength steels, Scr. Mater. 58 (2008) 939–942. doi:10.1016/j.scriptamat.2008.01.056.

[131] H. Liu, T. Chen, V.K. Verma, M. Koyama, S. Hamada, H. Noguchi, Similarity between shallow notch and crack effects on structural strength, in: Japan Soc. Mech. Eng. M M 2019 Mater. Mech. Conf., Fukuoka, 2019.

[132] H. Liu, S. Hamada, M. Koyama, H. Noguchi, Equivalence between shallow notch and shallow crack in structural failure caused by plastic instability, Theor. Appl. Fract. Mech. (2020) 102577. doi:10.1016/j.tafmec.2020.102577.

[133] M. Nagumo, K. Takai, N. Okuda, Nature of hydrogen trapping sites in steels induced by plastic deformation, J. Alloys Compd. 293 (1999) 310–316. doi:10.1016/S0925-8388(99)00322-9.

[134] T.Y. Zhang, Y.P. Zheng, Effects of absorption and desorption on hydrogen permeation - I. Theoretical modeling and room temperature verification, Acta Mater. 46 (1998) 5023–5033. doi:10.1016/S1359-6454(98)00176-1.

[135] N.M. Beylerian, M.Z. Asaturyan, On the mechanism of hydrogen peroxide decomposition in alkaline medium, Oxid. Commun. 27 (2004) 263–274.

[136] I.M. Bernstein, The role of hydrogen in the embrittlement of iron and steel, Mater. Sci. Eng. 6 (1970) 1–19. doi:10.1016/0025-5416(70)90073-X.

[137] W.Y. Choo, J.Y. Lee, C.G. Cho, S.H. Hwang, Hydrogen solubility in pure iron and effects of alloying elements on the solubility in the temperature range 20 to 500° C, J. Mater. Sci. 16 (1981) 1285–1292. doi:10.1007/BF01033843.

[138] H. Liu, S. Hamada, M. Koyama, H. Noguchi, Shallow crack effect on evaluation of residual tensile strength: harmless and stable cracks in finite-sized structure made of ductile metals, Theor. Appl. Fract. Mech. (2020). doi:under review (TAFMEC_2019_760).

[139] M. Koyama, Y. Onishi, H. Noguchi, Characteristics of hydrogen-assisted intergranular fatigue crack growth in interstitial-free steel: role of plastic strain localization, Int. J. Fract. 206 (2017) 123–130. doi:10.1007/s10704-017-0205-3.

[140] T. Neeraj, R. Srinivasan, J. Li, Hydrogen embrittlement of ferritic steels: Observations on deformation microstructure, nanoscale dimples and failure by nanovoiding, Acta Mater. 60 (2012) 5160–5171. doi:10.1016/j.actamat.2012.06.014.

[141] J. Zapletal, S. Věchet, J. Kohout, K. Obrtlík, Fatigue lifetime of ADI from ultimate tensile strength to permanent fatigue limit, Strength Mater. 40 (2008) 32–35. doi:10.1007/s11223-008-0009-9.

[142] ASTM International, Standard Test Methods for Determining Average Grain Size, West Conshohocken, PA, 2012. doi:10.1520/E0112-12.

Acknowledgment

This study was conducted in the Solid Mechanics Laboratory, Department of Hydrogen Energy System, Kyushu University, Japan. Firstly, I am very grateful to my supervisor, Professor Hiroshi Noguchi, for his patient and valuable guidance during the period of my Ph.D. study. He taught me how to study and think, what to innovate and dedicate. He allowed me to make mistakes and gave me opportunities to correct them in research. Under his guidance, I gained not only a wealth of knowledge but also advanced concepts. I also really appreciate the valuable suggestions from Professor Kaneaki Tsuzaki and Professor Hiroyuki Toda for my Ph.D. thesis revision. Meanwhile, I am very grateful to Associate Professor Shigeru Hamada for his help in the analysis and discussion of experimental and numerical results. Additionally, I appreciate Associate Professor Motomichi Koyama for his help in experiment and group discussion. I also want to extend my thanks to Mrs. Masako Kadota, secretary of our lab, for the care and help she gave in my daily study and life.

Besides, I would like to thank my companions and friends in the Solid Mechanics Laboratory, Structural Materials Research Laboratory, and Fatigue and Fracture of Materials Laboratory. Their advice has benefited me a lot in research and daily life. I would especially thank my family for their encouragement, support, and love. Finally, I acknowledge the financial support from the China Scholarship Council (CSC) during the period of my Ph.D. study.